AN IMPEDANCE ANALYSIS OF DOUBLE-STREAM INTERACTION IN SEMICONDUCTORS

by

P. W. Chen
C. H. Durney

July 1, 1972

MICROWAVE DEVICE AND PHYSICAL ELECTRONICS LABORATORY
DEPARTMENT OF ELECTRICAL ENGINEERING

UNIVERSITY OF UTAH
SALT LAKE CITY, UTAH 84112

UTEC MD 72-138

AN IMPEDANCE ANALYSIS OF DOUBLE-STREAM INTERACTION IN SEMICONDUCTORS

by

P. W. Chen
C. H. Durney

July 1, 1972

Microwave Device and Physical Electronics Laboratory

Electrical Engineering Department
University of Utah
Salt Lake City, Utah

ABSTRACT

The electromagnetic waves propagating through a drifting semiconductor plasma are studied generally from a macroscopic point of view in terms of double-stream interaction. The possible existing waves (for instance, helicon waves, longitudinal waves, ordinary waves, and pseudolongitudinal waves) which depend upon the orientation of the dc external magnetic field are derived.

A powerful impedance concept is introduced to investigate extensively the wave behavior of longitudinal (space-charge) waves or pseudolongitudinal waves in a semiconductor plasma. The impedances due to one- and two-carrier stream interactions have been calculated theoretically following the proper procedure.

According to the frequency range of operation, two feasible and practical experimental techniques are proposed. In the microwave frequency range, the standing-wave-ratio measurement is used. The observations of the impedance change due to the pulsed electric field and the relaxation phenomenon due to recombination of excess electrons and holes in InSb material are reported. In the radio frequency range, a sensitive RF bridge measurement is used. The observation of impedance change due to pulsed voltage is reported. By comparison with the theory, the results of the measurement in this RF range indicate the existence of space-charge waves in InSb plasma.

ACKNOWLEDGMENT

The authors acknowledge the support of the National Aeronautics and Space Administration under grant NGR-003-027 during the period from April 1, 1968 to April 30, 1969. Subsequent to that time, the research has been supported by the University of Utah.

TABLE OF CONTENTS

LIST OF ILLUSTRATIONS AND TABLES

I. INTRODUCTION

Research activity in the solid-state plasma effect has grown significantly in recent years. One objective of such research is the possibility of generating high-frequency growing instabilities when the electron-hole plasma is drifted.

Pines and Schrieffer[1] proposed the conditions for existence of plasma wave instabilities in the plasma formed by the electrons and holes in semiconductors. The work of Larrabee and Hicinbotham[2] gave inspiration and courage to the researcher in this area by observing microwave emission from InSb at 77° K when the sample was subjected simultaneously to applied electric and magnetic fields. They reported threshold values of the magnetic and electric field of about 3 kG and 200 V/cm, respectively. Buchsbaum, Chynoweth and Feldmann[3] reported microwave emission from InSb under experimental conditions similar to those of Larrabee and found the threshold magnetic field to be 1.5 kG and the threshold electric field to be only about 12 V/cm. Ancker-Johnson[4] observed microwave emission

---

[1] D. Pines and J. R. Schrieffer, "Collective Behavior in Solid-State Plasma," *Physical Review*, Vol. 124, December 1961, pp. 1387-1400.

[2] R. D. Larrabee and W. A. Hicinbotham, "Observation of Microwave Emission from Indium Antimonide," *Proceedings of the Symposium on Plasma Effects in Solids*, Paris, France, 1964; published by Dunod, Paris, 1965, pp. 181-187.

[3] S. J. Buchsbaum, A. G. Chynoweth, and W. L. Feldmann, "Microwave Emission from InSb," *Applied Physics Letters*, Vol. 6, February 1965, pp. 67-69.

[4] B. Ancker-Johnson, "Microwave Emission from Magnetic Field-Free Electron-Hole Plasmas," *Applied Physics Letters*, Vol. 10, May 1967, pp. 279-280.

from magnetic-field-free P-type InSb plasmas under special conductance conditions. Suzuki[5] reported instabilities under transverse magnetic field also.

The first attempted theory was the well-known helicon-wave instability studied by Bok and Nozieres.[6] It is, however, difficult to find any reasonable connection between the low frequencies at which helicon instabilities occur and the observed high-frequency spectrum of the noise emission. The investigations of Bok and Nozieres were generalized by Vural and Steele[7] who made a study of double-stream interaction with TEM and TM waves in a cylindrical semiconductor with the magnetic and electric field along the cylindrical axis. Their results predicted a value of the threshold magnetic field in good agreement with the experiment value ($B_o \geq 1.5$ kG) but did not give any information on the electric field and its dependence on the magnetic field. Also, the theory of Vural and Steele is essentially valid in the high frequency limit ($\omega > \nu$) and their interpretation is essentially in terms of two-stream instabilities of the type that exist in a collisionless medium (i.e., the electron beam case). In their description collisions act only as a perturbation which reduces

---

[5] K. Suzuki, "The Generation of Microwave Radiation from InSb," *Japanese Journal of Applied Physics*, Vol. 4, January 1965, pp. 42-52.

[6] J. Bok and P. Nozieres, "Instabilities of Transverse Waves in a Drifted Plasma," *Journal of Phys. Chem. Solids*, Vol. 24, 1963, pp. 709-714.

[7] B. Vural and M. C. Steele, "Possible Two-Stream Instabilities of Drifted Electron-Hole Plasmas in Longitudinal Magnetic Fields," *Physical Review*, Vol. 139, July 1965, pp. A300-A304.

the growth rates of the various instabilities, which is incorrect since InSb is a collision-dominant case with $\nu >> \omega$.

Another attempt was that made by Suzuki[8] to explain his experimental results on noise emission from InSb under crossed-field conditions (transverse magnetic field, $\vec{B}_o \perp \vec{E}_o$). He interpreted the noise emission as generated by a wave instability due to the presence of a density gradient (Hall voltage) which is established across the sample by the Lorentz force. Under this assumption he was able to obtain very good agreement with his experimental data. In Suzuki's theory, diffusion (i.e., carrier temperature) plays a major role in the sense that the theoretical frequency at the threshold of instability is directly proportional to the temperature; i.e., it would be zero if temperature effects were neglected. Without diffusion, his theory could not therefore account for high-frequency noise.

Another attempt was made by Robinson and Swartz.[9-11] They observed that coherent microwave emission was generated by InSb at 77° K with an injected electron current transverse to a magnetic field.

---

[8] T. Suzuki, "Microwave Emission and Low Frequency Instabilities in InSb," *Japanese Journal of Applied Physics*, Vol. 4, Sept. 1965, p. 700.

[9] B. B. Robinson and G. A. Swartz, "Two-Stream Instability in Semiconductor Plasmas," *Journal of Applied Physics*, Vol. 38, May 1967, pp. 2461-2465.

[10] G. A. Swartz and B. B. Robinson, "Coherent Microwave Instabilities in a Thin-Layer Solid-State Plasma," *Journal of Applied Physics*, Vol. 40, October 1969, pp. 4598-4611.

[11] G. A. Swartz, "Coherent Emission from Indium Antimonide with Closely Spaced Coplanar Contacts," *Journal of Applied Physics*, Vol. 40, August 1969, pp. 5343-5349.

Grooves cut into the Suhl surface of the rod-shaped InSb imposed the coherence and determined the frequency range of coherent operation. Wavelength measurements of a surface wave using a double stripline system showed that the effective groove width was equal to about a half-wavelength. They proposed a collision-induced instability based on double-stream interaction in a semiconductor plasma. Their theory predicted most of the qualitative and some of the quantitative features of the observed emission.

Another attempt was made by Gandhi and Grow[12] in our laboratory. They explained the microwave emissions from plasmas in InSb at 77° K with and without magnetic fields were due to the instabilities of pseudolongitudinal waves of drifting semiconductor plasma. Their theory well explained qualitatively the instabilities observed in n- and p-type InSb with and without transverse magnetic field and the dependence of the instability frequency on the magnetic field. Meanwhile, in our laboratory, the wave propagations in a cylindrical semiconductor based on double-stream interactions were generally discussed by Christensen, Durney, and Grow.[13] And furthermore,

---

[12] O. P. Gandhi and R. W. Grow, "Microwave Emission from InSb With and Without Magnetic Fields," *IEEE Transactions on ED*, Vol. ED-18, October 1971, pp. 853-865.

[13] D. A. Christensen, C. H. Durney, and R. W. Grow, "An Exact Small-Signal Analysis of the Interaction of Two Electron Streams in a Finite Longitudinal Magnetic Field," *IEEE Transactions on ED*, Vol. ED-16, July 1969, pp. 615-624.

Goodrich and Durney[14] studied the effects of velocity spread on wave propagations and instabilities. Goodrich also observed some microwave emission from InSb samples operated in the high-field region.

Consequently, the report of the observation of microwave radiation set off the proposal of a double-stream interaction mechanism which seems highly possible.† However, in only a limited number of cases has there been an attempt to compare both qualitatively and quantitatively the results of the theory with the experiment. The problem has been that in many cases the experimental conditions have not been sufficiently well defined to allow such comparison. Such parameters as the densities of electrons and holes and their spatial variation†† of the electric field in InSb have not been known to the

---

† The acoustoelectric interaction mechanism[15-17] might appear to be responsible for part of the observed emission for InSb.

†† This is emphasized by Thompson and Kino (see Ref. 15). They found substantial enhancement of electric-field inhomogeneity near the contact in the presence of transverse or longitudinal magnetic field.

[14] L. C. Goodrich and C. H. Durney, "A Small Signal Field Analysis of Double Stream Interactions in Finite Semiconductors," Ph.D. dissertation, University of Utah, 1969.

[15] A. H. Thompson and G. S. Kino, "Noise Emission from InSb," *IBM Journal of Research and Development*, Vol. 13, September 1969, pp. 616-620.

[16] T. Arizumi, T. Aoki, and K. Hayakawa, "Microwave Emission from Acoustoelectrically Oscillating n-InSb," *Journal of the Physical Society of Japan*, Vol. 23, December 1967, pp. 1251-1256.

[17] C. W. Turner, "The Role of Acoustic Wave Amplification in the Emission of Microwave Noise from InSb," *IBM Journal of Research and Development*, Vol. 13, September 1969, pp. 611-615.

experimentalists sufficiently well, in many cases, to allow good tests of the theories. And furthermore, the experimental configuration has not achieved a high-efficiency coupling of the emission to the detecting system; the actual strength of the interaction is still unknown. Furthermore, most theories mentioned above mainly derived the dominant propagation constants only and they cannot be measured directly. Thus there is no good way of correlating theory to experiment.

Consequently, experimental investigation of space-charge wave phenomenon in InSb plasma is badly needed. In this report the ground work for a new impedance concept[18] is presented to investigate the double-stream interaction mechanism in semiconductor plasmas which will overcome the experimental difficulties and provide a great deal of information. This new concept is not only realistic but also feasible. The impedance is defined as $Z = V/J_T A$, where the voltage is given by $V = \int_0^d E_z dz$, J_T is the total current density, and A is the sample cross-sectional area. The electric field E_z is the sum of the longitudinal z-component electric fields of all possible waves existing in the semiconductor plasma. Hence once all the possible waves are found, then the impedance can be calculated theoretically. Vice-versa once the impedance can be measured, then the waves can be

---

[18] P. W. Chen, C. H. Durney, and R. W. Grow, "Theoretical and Experimental Investigation of Solid-State Mechanisms for Generating Coherent Radiation in the Ultraviolet and X-ray Regions," Final Report under Grant NGR 45-003-027, Microwave Device and Physical Electronics Laboratory, University of Utah, Salt Lake City, Utah, July 1969.

properly correlated. This method provides a new way to detect and measure the space-charge wave behavior in a semiconductor plasma.

Therefore, in Chapter II, a general theoretical analysis of electromagnetic waves propagating through drifting semiconductor plasmas based on a one-dimensional model is first described from a macroscopic point of view. The permittivity tensor of drifting semiconductor charges with collision and diffusion effects is derived. Then two special cases with longitudinal and transverse external magnetic field are analyzed.

In Chapter III the impedance concept is introduced to study the electromagnetic waves in a semiconductor plasma, especially the space-charge wave and the pseudolongitudinal wave. The procedures of calculation and the boundary conditions are described. The impedance based on one-carrier and two-carrier stream interactions are calculated. How the propagation constant affects the impedance is analyzed. The comparison with a dielectric diode case is given to provide better understanding of impedance concepts.

InSb has been mentioned as a prominent semiconductor material for studying the double-stream interaction mechanism. Hence InSb will be chosen as a sample for our impedance study. Therefore, in Chapter IV the author describes the general physical properties (e.g., n- or p-type, densities, mobilities, injection, breakdown, pinch, etc.) of InSb from a macroscopic point of view so that InSb can be understood better under any experimental condition.

In Chapter V the experimental techniques are introduced. In

the microwave frequency range, the standing-wave-ratio measurement, using a slotted X-band waveguide, is used. The observations of the impedance change due to the pulsed drifting field and the relaxation phenomenon due to the excess electron-hole recombination are reported. In the radio-frequency range, the sensitive bridge measurement is adopted. The observations and the results are reported. The impedance is plotted in a complex plane with pulsed voltage as parameter. Although strict quantitative correlation between theory and measurements has not yet been obtained, the results do indicate the existence of space-charge waves in InSb plasma.

Finally, in Chapter VI, some important results are summarized, some conclusions from this investigation are drawn, and some suggestions for further work are outlined.

II. ELECTROMAGNETIC WAVE PROPAGATION THROUGH DRIFTING SEMICONDUCTOR PLASMAS

A general theoretical analysis of electromagnetic waves propagating through drifting semiconductor plasmas based on a one-dimensional model is described from a macroscopic point of view. The permittivity tensor of drifting semiconductor charges with collision and diffusion effects is first derived. Next the general dispersion relation of propagation is derived. Then two special cases with longitudinal and transverse external magnetic fields are analyzed.

2.1 Effective Permittivity Tensor

As far as the behavior of large numbers of carriers (electrons and holes) interacting with their self-created or externally imposed electromagnetic field or both are concerned, most experimental observations are determined by the average ensemble. Therefore, the appropriate theoretical description must be a statistical one, and it should be, in general, a quantum-statistical description. However, in the long wavelength limit, the quantum mechanical description goes over to the classical description. In this report the research interest is restricted to the long-wavelength excitation and the classical hydrodynamic model is adopted. Use of the hydrodynamic model means that the streaming carriers (electrons or holes) with a charged fluid are characterized by a few parameters such as mean density ω_{pi}, mean velocity v_{oi}, mean collision frequency ν_{ci}, and

thermal velocity V_{Ti}.

The general orientations of the carrier drifting velocities $\vec{V}_{oi}$'s, propagation vector $\vec{k}$, and the external dc magnetic field $\vec{B}_o$ are assumed. These vectors can be written as:

$$\vec{V}_{oi} = V_{oix}\,\hat{x} + V_{oiy}\,\hat{y} + V_{oiz}\,\hat{z}$$

$$\vec{k} = k_x\,\hat{x} + k_y\,\hat{y} + k_z\,\hat{z}$$

$$\vec{B}_o = B_{ox}\,\hat{x} + B_{oy}\,\hat{y} + B_{oz}\,\hat{z}$$

$\hat{x}$, $\hat{y}$, and $\hat{z}$ are the unit vectors of general coordinates.

Assuming that waves propagate as $e^{j(\omega t - \vec{k}\cdot\vec{r})}$, the effect of streaming carriers (electrons or holes) on the effective permittivity tensor of semiconductor plasma can be obtained by solving simultaneously:

Lorentz's hydrodynamic equation --

$$\frac{d\vec{v}_i}{dt} + \frac{\vec{v}_i}{\tau_i} = \eta_i\left(\vec{E} + \vec{v}_i \times \vec{B}_o + \vec{V}_{oi} \times \vec{B}\right) - \frac{\nabla \cdot \underline{\underline{P}}_i}{n_i m_i} \qquad (1)$$

Maxwell's curl $\vec{E}$ equation --

$$\nabla \times \vec{E} = -j\omega\mu\vec{H} \qquad (2)$$

Maxwell's curl $\vec{H}$ equation --

$$\nabla \times \vec{H} = \vec{J} + j\omega\varepsilon\vec{E}$$

$$= j\omega\underline{\underline{\varepsilon}}\vec{E} \qquad (3)$$

the definition of the current density --

$$\underset{\sim}{\vec{J}}_i = \rho_{oi} \underset{\sim}{\vec{v}}_i + \underset{\sim}{\rho}_i \vec{V}_{oi} \tag{4}$$

and the continuity equation --

$$\nabla \cdot \vec{J}_i = -j\omega \underset{\sim}{\rho}_i \tag{5}$$

where the subscript i denotes the quantities pertaining to various classes of carriers and takes on the symbol e or h for electrons and holes, respectively; the additional subscript o refers to the dc value, and a wiggle underneath the symbol to the ac value of the respective quantities.

$\underset{\sim}{\vec{v}}_i$ = ac velocity of i^{th} carriers

$\vec{V}_{oi}$ = dc velocity

$\tau_i = 1/\nu_{ci}$

ν_{ci} = the collision frequency of i^{th} carriers

ρ_{oi} = dc charge density of i^{th} particle

$\underset{\sim}{\rho}_i$ = ac charge density

$\eta_i = q_i/m_i^*$

q_i = charge of i^{th} carriers

m_i^* = effective mass of i^{th} carriers

$\underline{\underline{P}}_i$ = partial pressure tensor due to i^{th} carriers = $n_i k_B \underline{\underline{T}}_i$

$\underline{\underline{T}}_i$ = temperature tensor

Further assume that the permittivity of the semiconductor material

without the carrier streaming effect is isotropic† and the partial pressure tensor $\underline{\underline{P}}_i$'s are isotropic also. Then

$$\frac{\nabla \cdot \underline{\underline{P}}_i}{n_i m_i^*} = \frac{\nabla \rho_i}{\rho_{oi}} V_{Ti}^2$$

where $V_{Ti} = \left(k_B T_i / m_i^*\right)^{1/2}$.

For simplicity we define

$$j\Omega_i = \frac{d}{dt} + \frac{1}{\tau_i} = j\left(\omega - \vec{k} \cdot \vec{V}_{oi} - j\nu_{ci}\right)$$

$$w_i = \omega - \vec{k} \cdot \vec{V}_{oi}$$

$\omega_{pi} = \left(\eta_i \rho_{oi} / \varepsilon\right)^{1/2}$, the plasma radian frequency of the i^{th} carrier

Since all the ac quantities are varying with exp $j(\omega t - \vec{k} \cdot \vec{r})$ and can be written as

$$\vec{\underset{\sim}{A}}(\vec{r},t) = \vec{\underset{\sim}{A}}(0,0)\ e^{j(\omega t - \vec{k} \cdot \vec{r})} \qquad (6)$$

where $\vec{\underset{\sim}{A}}(0,0)$ is a constant vector, then

$$\nabla \cdot \vec{\underset{\sim}{A}}(r,t) = \nabla \cdot \vec{\underset{\sim}{A}}(0,0)\ e^{-j\vec{k} \cdot \vec{r}}$$

$$= \vec{\underset{\sim}{A}}(0,0) \cdot \nabla\ e^{-j\vec{k} \cdot \vec{r}}$$

$$= -j\vec{k} \cdot \vec{\underset{\sim}{A}}(0,0)\ e^{-j\vec{k} \cdot \vec{r}}$$

---

† which is valid for InSb, InAs, and most III-IV compound semiconductors

$$= -jk\ \hat{k} \cdot \vec{\tilde{A}}(0,0)\ e^{-j\vec{k} \cdot \vec{r}}$$

$$= -jk\ \hat{k} \cdot \vec{\tilde{A}} \tag{7}$$

Similarly,

$$\nabla \times \vec{A}(r,t) = -j\vec{k} \times \vec{A}$$

$$= -jk\ \hat{k} \times \vec{\tilde{A}} \tag{8}$$

where the unit vector $\hat{k}$ is defined by $\hat{k} = \vec{k}/k$. Combining the above equations, we obtain

$$j\Omega_i\left(\Omega_i^2 - \omega_{ci}^2\right)\vec{\tilde{v}}_i = \frac{\eta_i}{\omega}\left\{w_i\left[\Omega_i^2\,\vec{\tilde{E}} + j\Omega_i\vec{\omega}_{ci} \times \vec{\tilde{E}} - \left(\vec{\omega}_{ci} \cdot \vec{\tilde{E}}\right)\vec{\omega}_{ci}\right]\right.$$

$$\left. + \left(\vec{V}_{oi} \cdot \vec{\tilde{E}} + j\,\frac{V_{Ti}^2\omega\rho_i}{\omega_{pi}^2\,\varepsilon}\right)\left[\Omega_i^2\vec{k} + j\Omega_i\vec{\omega}_{ci} \times \vec{k} - \left(\vec{\omega}_{ci} \cdot \vec{k}\right)\vec{\omega}_{ci}\right]\right\}$$

$$= \frac{\eta_i}{\omega}\left\{w_i\vec{x}_i + \left(\vec{V}_{oi} \cdot \vec{\tilde{E}} + j\,\frac{V_{Ti}^2\omega\rho_i}{\omega_{pi}^2\varepsilon}\right)\vec{Y}_i\right\} \tag{9}$$

$$\rho_i = \frac{\rho_{oi}\vec{k} \cdot \vec{v}_i}{w_i}$$

where

$\vec{\omega}_{ci} = \eta_i\vec{B}_o$, the cyclotron radian frequency of i^{th} carrier

$$\vec{x}_i = \Omega_i^2 \underset{\sim}{\vec{E}} + j\Omega_i \vec{\omega}_{ci} \times \underset{\sim}{\vec{E}} - \left(\vec{\omega}_{ci} \cdot \underset{\sim}{\vec{E}}\right)\vec{\omega}_{ci} \tag{10}$$

$$\vec{Y}_i = \Omega_i^2 \vec{k} + j\Omega_i \vec{\omega}_{ci} \times \vec{k} - \left(\vec{\omega}_{ci} \cdot \vec{k}\right)\vec{\omega}_{ci} \tag{11}$$

The permittivity tensor can be derived from Eqs. 3, 4, 5, and 9. After simplification the permittivity tensor can be written as

$$\underline{\underline{\varepsilon}} = \varepsilon \begin{bmatrix} \varepsilon_{11} & \varepsilon_{12} & \varepsilon_{13} \\ \varepsilon_{21} & \varepsilon_{22} & \varepsilon_{23} \\ \varepsilon_{31} & \varepsilon_{32} & \varepsilon_{33} \end{bmatrix} \tag{12}$$

where

$$\varepsilon_{11} = 1 - \sum_i \lambda_i \left\{ w_i\left(\Omega_i^2 - \omega_{cix}^2\right) + V_{oix}\, Y_{ix} + \frac{\Omega_i\left(\Omega_i^2 - \omega_{ci}^2\right)V_{oix} + V_{Ti}^2\, Y_{ix}}{D} \right.$$

$$\cdot \left(w_i\left[k_x\left(\Omega_i^2 - \omega_{cix}^2\right) + k_y\left(j\Omega_i\omega_{ciz} - \omega_{cix}\omega_{ciy}\right) + k_z\left(-j\Omega_i\omega_{ciy} - \omega_{cix}\omega_{ciz}\right)\right] \right.$$

$$\left. \left. + \left[k^2\, V_{oix}\left(\Omega_i^2 - \left(\vec{\omega}_{ci} \cdot \hat{k}\right)^2\right)\right] \right) \right\} \tag{13}$$

$$\varepsilon_{12} = - \sum_i \lambda_i \left\{ w_i\left(-j\Omega_i\omega_{ciz} - \omega_{ciy}\omega_{cix}\right) + V_{oiy}\, Y_{iy} \right.$$

$$+ \frac{\Omega_i\left(\Omega_i^2 - \omega_{ci}^2\right)V_{oix} + V_{Ti}^2\, Y_{ix}}{D}\left(w_i\left[k_x\left(-j\Omega_i\omega_{ciz} - \omega_{ciy}\omega_{cix}\right)\right.\right.$$

$$\left. + k_y\left(\Omega_i^2 - \omega_{ciy}^2\right) + k_z\left(j\Omega_i\omega_{cix} - \omega_{ciy}\omega_{ciz}\right)\right]$$

$$\left.\left. + \left[k^2\, V_{oiy}\left(\Omega_i^2 - \left(\vec{\omega}_{ci} \cdot \hat{k}\right)\right)\right]\right)\right\} \qquad (14)$$

$$\varepsilon_{13} = - \sum_i \lambda_i \left\{ w_i\left(j\Omega_i\omega_{ciy} - \omega_{ciz}\omega_{cix}\right) + V_{oiz}\, Y_{ix}\right.$$

$$+ \frac{\Omega_i\left(\Omega_i^2 - \omega_{ci}^2\right)V_{oix} + V_{Ti}^2\, Y_{ix}}{D}\left(w_i\left[k_x\left(j\Omega_i\omega_{ciy} - \omega_{ciz}\omega_{cix}\right)\right.\right.$$

$$\left. + k_y\left(-j\Omega_i\omega_{cix} - \omega_{ciz}\omega_{ciy}\right) + k_z\left(\Omega_i^2 - \omega_{ciz}^2\right)\right]$$

$$\left.\left. + \left[k^2\, V_{oiz}\left(\Omega_i^2 - \left(\vec{\omega}_{ci} \cdot \hat{k}\right)^2\right)\right]\right)\right\} \qquad (15)$$

$$\varepsilon_{21} = - \sum_i \lambda_i \left\{ w_i\left(j\Omega_i\omega_{ciz} - \omega_{cix}\omega_{ciy}\right) + V_{oix}\, Y_{iy}\right.$$

$$+ \frac{\Omega_i\left(\Omega_i^2 - \omega_{ci}^2\right)V_{oiy} + V_{Ti}^2\, Y_{iy}}{D} \left(w_i\left[k_x\left(\Omega_i^2 - \omega_{cix}^2\right)\right.\right.$$

$$\left. + k_y\left(j\Omega_i\omega_{ciz} - \omega_{cix}\omega_{ciy}\right) + k_z\left(-j\Omega_i\omega_{ciy} - \omega_{cix}\omega_{ciz}\right)\right]$$

$$\left.\left. + \left[k^2\, V_{oix}\left(\Omega_i^2 - \left(\vec{\omega}_{ci} \cdot \hat{k}\right)^2\right)\right]\right)\right\} \qquad (16)$$

$$\varepsilon_{22} = 1 - \sum_i \lambda_i \left\{w_i\left(\Omega_i^2 - \omega_{ciy}^2\right) + V_{oiy}\, Y_{iy} + \frac{\Omega_i\left(\Omega_i^2 - \omega_{ci}^2\right)V_{oiy} + V_{Ti}^2\, Y_{iy}}{D}\right.$$

$$\cdot \left(w_i\left[k_x\left(-j\Omega_i\omega_{ciz} - \omega_{ciy}\omega_{cix}\right) + k_y\left(\Omega_i^2 - \omega_{ciy}^2\right) + k_z\left(-j\Omega_i\omega_{ciy}\omega_{ciz}\right)\right]\right.$$

$$\left.\left. + \left[k^2\, V_{oiy}\left(\Omega_i^2 - \left(\vec{\omega}_{ci} \cdot \hat{k}\right)^2\right)\right]\right)\right\} \qquad (17)$$

$$\varepsilon_{23} = -\sum_i \lambda_i \left\{w_i\left(-j\Omega_i\omega_{cix} - \omega_{ciz}\omega_{ciy}\right) + V_{oiz}\, Y_{iy}\right.$$

$$+ \frac{\Omega_i\left(\Omega_i^2 - \omega_{ci}^2\right)V_{oiy} + V_{Ti}^2\, Y_{iy}}{D} \left(w_i\left[k_x\left(j\Omega_i\omega_{ciy} - \omega_{ciz}\omega_{cix}\right)\right.\right.$$

$$+ k_y\left(-j\Omega_i\omega_{cix} - \omega_{ciz}\omega_{ciy}\right) + k_z\left(\Omega_i^2 - \omega_{ciz}^2\right)$$

$$+ \left[k^2 V_{oiz}\left(\Omega_i^2 - \left(\vec{\omega}_{ci} \cdot \hat{k}\right)^2\right)\right]\Bigg)\Bigg\} \tag{18}$$

$$\varepsilon_{31} = -\sum_i \lambda_i \Bigg\{ w_i\left(-j\Omega_i\omega_{ciy} - \omega_{cix}\omega_{ciz}\right) + V_{oix}\, Y_{iz}$$

$$+ \frac{\Omega_i\left(\Omega_i^2 - \omega_{ci}^2\right)V_{oiz} + V_{Ti}^2\, Y_{iz}}{D}\Bigg(w_i\Big[k_x\left(\Omega_i^2 - \omega_{cix}^2\right)$$

$$+ k_y\left(j\Omega_i\omega_{ciz} - \omega_{cix}\omega_{ciy}\right) + k_z\left(-j\Omega_i\omega_{ciy} - \omega_{cix}\omega_{ciz}\right)\Big]$$

$$+ \left[k^2 V_{oix}\left(\Omega_i^2 - \left(\vec{\omega}_{ci} \cdot \hat{k}\right)^2\right)\right]\Bigg)\Bigg\} \tag{19}$$

$$\varepsilon_{32} = -\sum_i \lambda_i \Bigg\{ w_i\left(j\Omega_i\omega_{cix} - \omega_{ciy}\omega_{ciz}\right) + V_{oiy}\, Y_{iz}$$

$$+ \frac{\Omega_i\left(\Omega_i^2 - \omega_{ci}^2\right) V_{oiz} + Y_{Ti}^2\, Y_{iz}}{D}\Bigg(w_i\Big[k_x\left(-j\Omega_i\omega_{ciz} - \omega_{ciy}\omega_{cix}\right)$$

$$+ k_y\left(\Omega_i^2 - \omega_{ciy}^2\right)\Big] + \left[k_z\left(j\Omega_i\omega_{cix} - \omega_{ciy}\omega_{ciz}\right)\right]\Big)\Bigg\} \tag{20}$$

$$\varepsilon_{33} = 1 - \sum_i \lambda_i \Bigg\{ w_i\left(\Omega_i^2 - \omega_{ciz}^2\right) + V_{oiz}\, Y_{iz} + \frac{\Omega_i\left(\Omega_i^2 - \omega_{ci}^2\right)V_{oiz} + V_{Ti}^2 Y_{iz}}{D}$$

$$\cdot \Bigg(w_i\Big[k_x\left(j\Omega_i\omega_{ciy} - \omega_{ciz}\omega_{cix}\right) + k_y\left(-j\Omega_i\omega_{cix} - \omega_{ciz}\omega_{ciy}\right)$$

$$+ k_z\left(\Omega_i^2 - \omega_{ciz}^2\right)\Big] + \Big[k^2\, V_{oiz}\left(\Omega_i^2 - \left(\vec{\omega}_{ci} \cdot \hat{k}\right)^2\right)\Big]\Bigg)\Bigg\} \tag{21}$$

$$\lambda_i = \omega_{pi}^2 \Big/ \omega^2 \Omega_i\left(\Omega_i^2 - \omega_{ci}^2\right)$$

$$D = w_i\Omega_i\left(\Omega_i^2 - \omega_{ci}^2\right) - k^2\, V_{Ti}^2\left(\Omega_i^2 - \left(\vec{\omega}_{ci} \cdot \hat{k}\right)^2\right)$$

2.2 General Dispersion Relation of Drifting Semiconductor Plasma

The wave equation can be obtained by combining the two curl equations,

$$\nabla \times \underset{\sim}{\vec{H}} = j\omega \underline{\underline{\varepsilon}}\, \underset{\sim}{\vec{E}}$$

$$\nabla \times \underset{\sim}{\vec{E}} = -j\omega\mu\, \underset{\sim}{\vec{H}}$$

in the usual fashion, getting

$$\nabla^2 \vec{\underset{\sim}{E}} - \nabla(\nabla \cdot \vec{\underset{\sim}{E}}) + \omega^2 \mu \underline{\underline{\varepsilon}} \cdot \vec{E} = 0 \qquad (22)$$

For convenience, Eq. 22 can be written in the tensor form:

$$\begin{bmatrix} k^2 - k_x^2 - \omega^2\mu\varepsilon\,\varepsilon_{11} & -k_xk_y - \omega^2\mu\varepsilon\,\varepsilon_{12} & -k_xk_z - \omega^2\mu\varepsilon\,\varepsilon_{13} \\ -k_yk_x - \omega^2\mu\varepsilon\,\varepsilon_{21} & k^2 - k_y^2 - \omega^2\mu\varepsilon\,\varepsilon_{22} & -k_yk_z - \omega^2\mu\varepsilon\,\varepsilon_{23} \\ -k_zk_x - \omega^2\mu\varepsilon\,\varepsilon_{31} & -k_zk_y - \omega^2\mu\varepsilon\,\varepsilon_{32} & k^2 - k_z^2 - \omega^2\mu\varepsilon\,\varepsilon_{33} \end{bmatrix} \cdot \begin{bmatrix} E_x \\ E_y \\ E_z \end{bmatrix} = 0 \qquad (23)$$

or

$$\left[\delta_{mn}\, k^2 - k_m k_n - \omega^2\mu\varepsilon\,\varepsilon_{mn}\right] E_n = 0 \;^{\dagger} \qquad (24)$$

where m, n are chosen as x, y, or z.

Equation 23 is the general wave equation which describes all the possible wave solutions if $\vec{V}_{oi}$, $\vec{B}_o$ and all the material parameters

---

† Einstein's notation.

(e.g., ν_{ci}, ω_{pi}, V_{Ti}, etc.) are given. From the nontrivial solutions of Eq. 23, we can obtain the dispersion relations of the possible modes and their corresponding field. Each wave has different propagation constants which depend on the order of the corresponding dispersion relation. The complete solution for a particular wave should be a linear combination of all possible solutions, and it can be expressed as

$$\vec{x} = A_o \vec{x}_o + \sum_{m=1}^{n} A_m \vec{x}_m e^{-j\vec{k}_m \cdot \vec{r}} = \sum_{m=0}^{n} A_m \vec{x}_m e^{-j\vec{k}_m \cdot \vec{r}} \qquad (25)$$

$\vec{x}$ could be the electric field, carrier current densities, or carrier velocities. $\vec{x}$ can also be represented by a column matrix:

$$\vec{x} = \begin{bmatrix} \vec{v}_i \\ \vec{J}_i \\ \vec{E} \end{bmatrix}$$

where the A_m's are undetermined constants which depend upon the boundary conditions, and the x_m's are eigenvectors corresponding to each of the $\vec{k}_i$ propagation constants.

In the following section, two special and interesting cases will be discussed.

2.3 Special Case I ($\vec{B}_o \| \vec{E}_o \| \hat{z}$)

If $\vec{k} \| \vec{V}_{oi} \| \hat{z}$, $\vec{B}_o \| \hat{z}$, then

$$\vec{\omega}_{ci} \cdot \hat{x} = \omega_{cix} = 0$$

$$\vec{\omega}_{ci} \cdot \hat{y} = \omega_{ciy} = 0$$

$$Y_{ix} = 0$$

$$Y_{iy} = 0$$

$$Y_{iz} = \Omega_i^2 \, k - \omega_{ci}^2 \, k$$

$$D = w_i \Omega_i \left(\Omega_i^2 - \omega_{ci}^2\right) - k^2 \, V_{Ti}^2 \left(\Omega_i^2 - \omega_{ci}^2\right)$$

And the elements of the effective permittivity tensor can be simplified as:

$$\varepsilon_{11} = \varepsilon_{22} = 1 - \sum_{i=e,h} \frac{\omega_{pi}^2 \, w_i \Omega_i}{\omega^2 \left(\Omega_i^2 - \omega_{ci}^2\right)} = \varepsilon_1$$

$$\varepsilon_{12} = -\varepsilon_{21} = \sum \frac{j \, \omega_{pi}^2 \, w_i \, \omega_{ci}}{\omega^2 \left(\Omega_i^2 - \omega_{ci}^2\right)} = j\varepsilon_2$$

$$\varepsilon_{23} = \varepsilon_{32} = 0$$

$$\varepsilon_{33} = 1 - \sum_{i=e,h} \frac{\omega_{pi}^2}{w_i \Omega_i - k^2 \, V_{Ti}^2} = \varepsilon_3$$

The general expression of Eq. 25 can be written as

$$\begin{bmatrix} k^2 - \omega^2\mu\varepsilon\ \varepsilon_{11} & -\omega^2\mu\varepsilon\ \varepsilon_{12} & 0 \\ +\omega^2\mu\varepsilon\ \varepsilon_{12} & k^2 - \omega^2\mu\varepsilon\ \varepsilon_{11} & 0 \\ 0 & 0 & -\omega^2\mu\varepsilon\ \varepsilon_{33} \end{bmatrix} \begin{bmatrix} E_x \\ E_y \\ E_z \end{bmatrix} = 0$$

The dispersion relation is

$$\left[\left(k^2 - \omega^2\mu\varepsilon\ \varepsilon_{11}\right)^2 + \left(\omega^2\mu\varepsilon\ \varepsilon_{12}\right)^2\right] \left[-\omega^2\mu\varepsilon\ \varepsilon_{33}\right] = 0 \qquad (26)$$

If $\left(k^2 - \omega^2\mu\varepsilon\ \varepsilon_{11}\right)^2 + \left(\omega^2\mu\varepsilon\ \varepsilon_{12}\right)^2 = 0$, i.e.,

$$\left(k^2 - \omega^2\mu\varepsilon\ \varepsilon_{11}\right) = \pm j\omega^2\mu\varepsilon\ \varepsilon_{12}$$

$$k^2 = k_o^2\left(\varepsilon_{11} \pm j\varepsilon_{12}\right)$$

$$k^2 = k_o^2\left[1 - \sum \frac{\omega_{pi}^2\ w_i}{\omega^2\left(\Omega_i^2 \pm \omega_{ci}\right)}\right] \qquad (27)$$

This implies

$$\vec{E} = E_x\ \hat{x} + E_y\ \hat{y}$$

$$= \left(E_1\ \hat{x} \pm jE_1\ \hat{y}\right) \perp \vec{B}_o \qquad (28)$$

where $k_o^2 = \omega^2\mu\varepsilon$.

This is a transverse wave, and it is usually called a helicon wave, which may have either counterclockwise (positive) polarization or clockwise (negative) polarization of electric field. Bok and Nozieres' result[19] can be obtained from Eq. 27.

If

$$-\omega^2 \mu\varepsilon \, \varepsilon_{33} = 0 \tag{29}$$

i.e.,

$$1 - \sum_{i=e,h} \frac{\omega_{pi}^2}{w_i \Omega_i - k^2 V_{Ti}^2} = 0 \tag{30}$$

$$1 - \sum_{i=e,h} \frac{\omega_{pi}^2}{\left(\omega - kV_{oi}\right)\left(\omega - kV_{oi} - j\nu_{ci}\right) - k^2 V_{Ti}^2} = 0$$

This implies $\vec{E} = E\hat{z}$, a pure longitudinal wave (or space-charge wave). Equation 30 is the familiar double-stream interaction equation.† The complete solution can be obtained by solving the linear simultaneous equations (1-5) and the result is

---

[19] J. Bok and P. Nozieres, *op. cit.*

† R. W. Grow, "Physical Electronics," multilithed notes handed out in class.

$$\vec{x} = \begin{bmatrix} v_i \\ J_i \\ E \end{bmatrix} = \sum_{m=0}^{4} A_m \begin{bmatrix} \dfrac{\eta_i w_i}{j\left[w_i\Omega_i - k_m^2 V_{Ti}^2\right]} \\ \dfrac{\eta_i \omega \rho_{oi}}{j\left[w_i\Omega_i - k_m^2 V_{Ti}^2\right]} \\ 1 \end{bmatrix} e^{-jk_m z} \tag{31}$$

Since $J_i + j\omega\varepsilon E = J_T = \text{const.}$, then

$$\left[\sum_i \frac{\eta_i \rho_{oi}}{j\ \omega - j\nu_{ci}} + j\omega\varepsilon\right] A_o = J_T \tag{32}$$

and

$$A_o = \frac{J_T}{j\omega\varepsilon + \sum_i \dfrac{\eta_i \rho_{oi}}{j\left(\omega - j\nu_{ci}\right)}} \tag{33}$$

The A_m's ($m = 1, 4$) can be determined by other boundary conditions.

Furthermore, if the $k_m^2 V_{Ti}^2$'s are small (i.e., a small diffusion effect),

$$\vec{x} = \sum_{m=0}^{4} A_m \begin{bmatrix} \dfrac{\eta_i}{j\Omega_i} \\ \dfrac{\eta_i \omega \rho_{oi}}{j w_i \Omega_i} \\ 1 \end{bmatrix} e^{-jk_m z} \tag{34}$$

2.4 Special Case II $\left(\vec{B}_o \perp (\vec{E}_o \parallel \hat{z})\right)$

If $\vec{k} \parallel \vec{E}_o \parallel \hat{z}$ and $\vec{B}_o \parallel \hat{y}$, then

$$\omega_{ci} \cdot \hat{x} = \omega_{cix} = 0$$

$$\omega_{ci} \cdot \hat{z} = \omega_{ciz} = 0$$

$$Y_{ix} = j\Omega_i \, \omega_{ci} \, k$$

$$Y_{iy} = 0$$

$$Y_{iz} = \Omega_i^2 \, k$$

$$D = w_i \Omega_i \left(\Omega_i^2 - \omega_{ci}^2\right) - k^2 \, V_{Ti}^2 \, \Omega_i^2$$

The elements of the effective tensor can be simplified as

$$\varepsilon_{11} = 1 - \sum \frac{\omega_{pi}^2 \, w_i \left[w_i \Omega_i - k^2 \, V_{Ti}^2\right]}{\omega^2 \left[w_i \left(\Omega_i^2 - \omega_{ci}^2\right) - k^2 \, V_{Ti}^2 \, \Omega_i\right]}$$

$$\varepsilon_{12} = \varepsilon_{21} = 0$$

$$\varepsilon_{13} = -\varepsilon_{31} = \sum \frac{j \, \omega_{ci} \, w_i \, \omega_{pi}^2}{\omega \left[w_i \left(\Omega_i^2 - \omega_{ci}^2\right) - k^2 \, V_{Ti}^2 \, \Omega_i\right]}$$

$$\varepsilon_{22} = 1 - \sum \frac{\omega_{pi}^2 \, w_i}{\omega^2 \Omega_i}$$

$$\varepsilon_{33} = 1 - \sum \frac{\omega_{pi}^2 \, \Omega_i}{w_i\left(\Omega_i^2 - \omega_{ci}^2\right) - k^2 \, V_{Ti}^2 \, \Omega_i}$$

The wave equation (Eq. 23) can be written as

$$\begin{bmatrix} k^2 - k_o^2\varepsilon_{11} & 0 & k_o^2\varepsilon_{13} \\ 0 & k^2 - k_o^2\varepsilon_{22} & 0 \\ -k_o^2\varepsilon_{13} & 0 & -k_o^2\varepsilon_{33} \end{bmatrix} \begin{bmatrix} E_x \\ E_y \\ E_z \end{bmatrix} = 0 \qquad (35)$$

So the dispersion relation is

$$\left(k^2 - k_o^2\varepsilon_{22}\right)\left[\left(k^2 - k_o^2\varepsilon_{11}\right)\left(-k_o^2\varepsilon_{33}\right) + k_o^2\varepsilon_{13}^2\right] = 0 \qquad (36)$$

Either factor will lead to possible propagation. If

$$k^2 - k_o^2\varepsilon_{22} = 0 \qquad (37)$$

i.e., $k = \pm k_o \sqrt{\varepsilon_{22}}$, then

$$k^2 = k_o^2 \left[1 - \sum \frac{\omega_{pi}^2\left(\omega - kV_{oi}\right)}{\omega^2\left(\omega - kV_{oi} - j\nu_{ci}\right)}\right] \qquad (38)$$

This implies that $E_x = E_z = 0$ and

$$\vec{E} = E_1 \hat{y} \parallel \vec{B}_o \tag{39}$$

This is usually called an ordinary transverse wave.

If $\left(k^2 - k_o^2 \varepsilon_{11}\right)\left(-k_o^2 \varepsilon_{33}\right) + k_o^4 \varepsilon_{13}^2 = 0$, then

$$k^2 = k_o^2 \frac{\varepsilon_{11}\varepsilon_{33} + \varepsilon_{13}^2}{\varepsilon_{33}} \tag{40}$$

This implies

$$E_x = - \frac{\varepsilon_{33}}{\varepsilon_{13}} E_z$$

$$E_y = 0$$

$$\vec{E} = \left(- \frac{\varepsilon_{33}}{\varepsilon_{13}} E_1 \hat{x} + E_1 \hat{z} \right) \perp \vec{B}_o \tag{41}$$

This is a hybrid wave.

With the slow wave approximation, $k >> k_o$, the dispersion relation of Eq. 40 can be simplified to

$$\varepsilon_{33} \simeq 0 \tag{42}$$

i.e.,

$$1 - \sum_{i=e,h} \frac{\omega_{pi}^2 \, \Omega_i}{w_i\left(\Omega_i^2 - \omega_{ci}^2\right) - k^2 V_{Ti}^2 \, \Omega_i} = 0 \tag{43}$$

and $E_x \simeq 0$, $\vec{E} \simeq E_1 \hat{z} \parallel \vec{k}$.

So this is usually called a pseudolongitudinal or quasi-longitudinal wave, which has almost the same properties as space charge waves. The complete form of Eq. 43 is:

$$1 - \sum_{i=e,h} \frac{\omega_{pi}^2\left(\omega - kV_{oi} - j\nu_{ci}\right)}{\left(\omega - kV_{oi}\right)\left[\left(\omega - kV_{oi} - j\nu_{ci}\right)^2 - \omega_{ci}^2\right] - k^2V_{Ti}^2\left(\omega - kV_{oi} - j\nu_{ci}\right)} = 0 \tag{44}$$

This is a sixth order equation. There will be six possible propagation constants in this case. Hence the complete solution will be the linear combination of six components corresponding to these six propagation constants, which can be written in a matrix form as

$$\begin{bmatrix} v_{ix} \\ v_{iz} \\ J_{ix} \\ J_{iz} \\ E \end{bmatrix} = \sum_{m=0}^{6} A_m \begin{bmatrix} \dfrac{\eta_i w_i \omega_{ci}}{\omega\left(\Omega_i^2 - \omega_{ci}^2\right)} \\ \dfrac{\eta_i w_i \Omega_i}{jw_i\left(\Omega_i^2 - \omega_{ci}^2\right) - jk^2V_{Ti}^2\Omega_i} \\ \dfrac{\eta_i \omega_{ci} \rho_{oi}}{\left(\Omega_i^2 - \omega_{ci}^2\right)} \\ \dfrac{\eta_i \rho_{oi} \Omega_i \omega}{jw_i\left(\Omega_i^2 - \omega_{ci}^2\right) - jk^2V_{Ti}^2\Omega_i} \\ 1 \end{bmatrix} e^{-jk_m z} \tag{45}$$

where $k_m = 0$ when $m = 0$. The first term of $m = 0$ corresponds to the steady-state solution and the k_m's ($m = 1$ to 6) are the possible propagation constants. The A_m's ($m = 1$ to 6) are the undetermined constants which depend upon the boundary conditions. While A_o can be determined by $J_T = J + j\omega\varepsilon E$ = a constant independent of z; i.e.,

$$J_T = \left(j\omega\varepsilon + \sum_{i=e,h} \frac{\eta_i \rho_{oi} \left(\omega - j\nu_{ci}\right)}{\left[\left(\omega - j\nu_{ci}\right)^2 - \omega_{ci}^2\right]} \right) A_o$$

so

$$A_o = \frac{J_T}{\sum_{i=e,h} \frac{\eta_i \rho_{oi} \left(\omega - j\nu_{ci}\right)}{j\left[\left(\omega - j\nu_{ci}\right)^2 - \omega_{ci}^2\right]} + j\omega\varepsilon} \qquad (46)$$

2.5 Summary

The behavior of waves propagating through the semiconductor plasma has been generally discussed. The possible existing waves and their corresponding fields and ac velocity variations are derived under two special cases, one is $\vec{B}_o \parallel \vec{E}_o \parallel \hat{z}$ and the other is $\vec{B}_o \perp \vec{E}_o \parallel \hat{z}$.

III. IMPEDANCE ANALYSIS

3.1 Introduction

From the previous chapter, it is known that different waves exist in a semiconductor plasma if a drifting field and an external magnetic field are applied. These waves may be longitudinal waves, pseudolongitudinal waves, transverse waves, or hybrid waves which mainly depend upon the orientation of the magnetic field.

From conventional circuit theory, the voltage is defined as $V = \int_a^b \vec{E} \cdot d\vec{z}$, and the impedance is defined as $Z = V/I_T$ where I_T is total current flow. Now let us consider the voltage between two different specific planes AA' and BB' in a semiconductor plasma, as shown in Fig. 3.1, which are parallel to the xy plane. The voltage

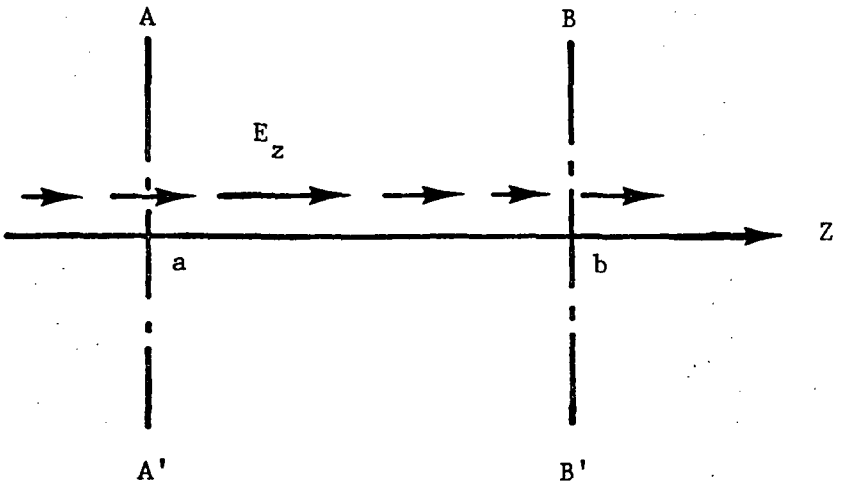

Fig. 3.1. The voltage difference between AA' and BB'.

between AA' and BB' is determined mainly by the electric field which is the sums of the existence of waves in the plasma. If a longitudinal

wave exists, a voltage difference between AA' and BB' will be found, since $V = \int_a^b E_z \, dz \neq 0$. If a transverse wave exists, a voltage difference will not be found due to $V = \int_a^b \vec{E} \cdot d\vec{z} = 0$. If a hybrid wave exists, a voltage will be found as $V = \int_a^b (\vec{E} \cdot \hat{z}) dz$. In other words, the voltage difference is caused by the $\hat{z}$ component of electric field of the existing wave, and the total voltage difference is the sum of each voltage difference due to each specific wave since there may be several waves in a plasma. In the one-dimensional case, the total current density, which is the sum of convection current and displacement current, is a constant (independent of z). So the voltage difference can be converted very easily to the impedance change due to the existence of waves. By measuring the impedance, it may be possible to detect the existence of waves, especially longitudinal or pseudolongitudinal waves. This could be an excellent tool for investigating the wave behavior inside a plasma. Of course, this impedance idea will not contribute anything to the transverse wave case.

This impedance concept has been adopted by Llewellyn and Peterson[20] to study the electronic tube, and furthermore to study

---

[20] F. B. Llewellyn and L. C. Peterson, "Vacuum-Tube Network," *Proceedings of the IRE*, Vol. 32, March 1944, pp. 144-166.

plasma diodes,[21] avalanche Read[22,23] diodes, and Gunn diodes[24] quite successfully. It is our belief that this concept will provide some information about the space-charge wave behavior in a semiconductor plasma, which has been puzzling for a long time.

In this chapter we will first define the impedance more clearly. Then a procedure to calculate the interaction impedance will be described. Next we will discuss the boundary condition and analyze the impedance of one-carrier stream interaction, two-carrier stream interactions with and without the external magnetic field. In the meantime the effects of thermal diffusion and the hole velocity on the wave-propagations and the interaction impedances will be clearly discussed. Finally, a summary of impedance concepts will be given.

3.2 Definition of Impedance

Impedance concepts at microwave frequencies are complicated

---

[21] F. R. Holmstrom, "Stability and RF Behavior of Plasma Diode," Technical Report No. 0833-2, Stanford Electronics Laboratory, Stanford University, Stanford, California, August 1964.

[22] M. Gilden and M. E. Hines, "Electronic Tuning Effects in the Read Microwave Avalanche Diode," *IEEE Transactions on ED*, Vol. ED-13, January 1966, pp. 169-175.

[23] T. Misawa, "Negative Resistance in p-n Junctions under Avalanche Breakdown Conditions, Part I," *IEEE Transactions on ED*, Vol. ED-13, January 1966, pp. 137-143.

[24] R. W. H. Engelmann and C. F. Quate, "Linear or Small Signal Theory for Gunn Effect," *IEEE Transactions on ED*, Vol. ED-13, January 1966, pp. 44-52.

because unique voltage and currents cannot always be defined. There are, however, special situations in which meaningful voltages and currents can be defined, and sometimes an impedance can be defined in terms of voltage and power, or current and voltage.

Let us discuss a cylindrical semiconductor plasma with perfectly conducting planes at both ends as shown in Fig. 3.2. It is

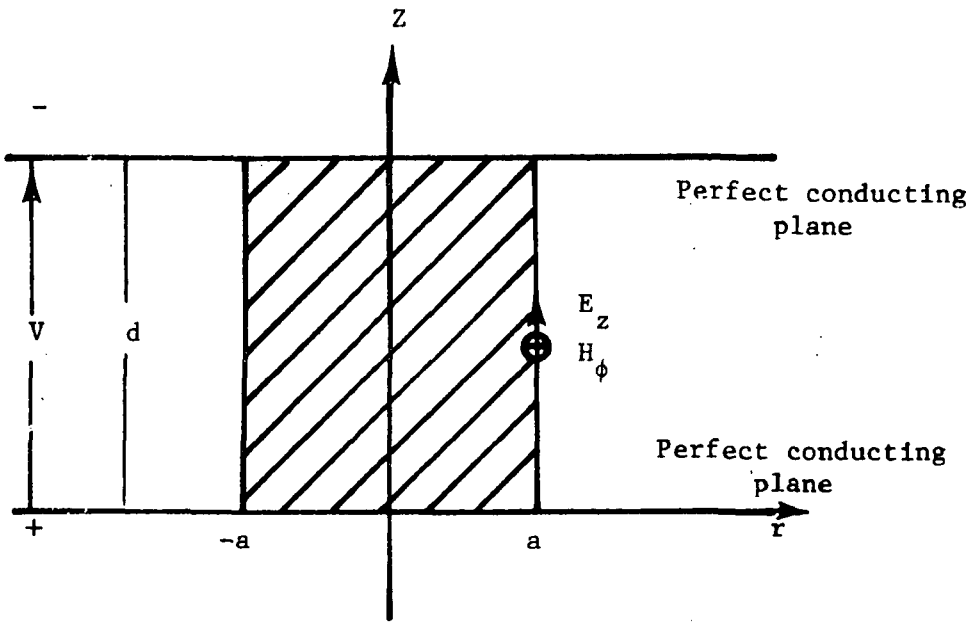

Fig. 3.2. A cylindrical semiconductor plasma with perfectly conducting planes at both ends.

assumed that $\partial/\partial r = \partial/\partial\phi = 0$, and d is extremely small compared to a wavelength. Then the semiconductor can be regarded as a point source to an external circuit. Therefore a meaningful voltage can be defined as

$$V = \int_0^d E(z)\, dz \tag{47}$$

A meaningful current can be defined as

$$I_T = \oint \vec{H} \cdot d\vec{\ell} = \int_0^{2\pi} H_\phi\, a\, d\phi = 2\pi\, a\, H_\phi \tag{48}$$

Since

$$\nabla \times \vec{H} = \vec{J} + j\omega\epsilon\vec{E} = \vec{J}_T = \text{constant} \tag{49}$$

$$I_T = J_T \cdot \pi a^2 \tag{50}$$

Thus

$$H_\phi = \frac{J_T a}{2} \tag{51}$$

The impedance is often simply defined as $Z = V/I_T$, which fits with the idea of low-frequency circuit analysis. However, from the microwave point of view, which is more appropriate here, there can be no ac currents in the perfect conductors, and hence no power can be transmitted through the conductors. The only alternative is that the microwave power be transmitted radially through the r = a boundary to the external circuit. This does not fit well with circuit theory concepts, and makes the definition of impedance as $Z = V/I_T$ questionable.

In addition, in a three-dimensional analysis, I_T will in general be a function of z, which further complicates the definition of impedance, because an impedance which is a function of z would not be useful in this case. A meaningful impedance can be defined, however, in terms of voltage and power. To get the impedance in the normal sense (i.e., a resistance corresponds to a power loss), the power is taken to be the power in the -r direction; that is, the power passing into the diode through the r = a boundary. Then the impedance is defined as

$$Z = V^2/P \tag{52}$$

Happily, it can be shown that this impedance is exactly the same as V/I_T for the one-dimensional case, in which case I_T is not a function of z. The power is given by

$$P = \int_S \vec{E} \times \vec{H} \cdot d\vec{S}$$

In the one-dimensional case, this reduces to

$$P = \int_0^d \int_0^{2\pi} E_z H_\phi \, a d\phi \, dz = 2\pi a \int_0^d E_z H_\phi \, dz$$

Using Eqs. 51, 50, and 47,

$$P = \frac{2\pi a^2 J_T}{2} \int_0^d E_z \, dz = I_T V$$

Hence

$$Z = V^2/I_T V = V/I_T \qquad (53)$$

Thus the definition of impedance given in Eq. 53 is a general definition which is valid for short samples and which satisfies the microwave field concepts in the general case and reduces to the ordinary circuit-theory kind of impedance for the one-dimensional case. We will use Eq. 53 in all our subsequent work.

The concept of impedance given by our definition is very important, because it provides a method of getting a good approximate solution to the very complicated problem of the coupling of the semiconductor sample to an external microwave circuit. The principal alternative to the impedance kind of analysis is writing infinite-series field solutions inside and outside of the semiconductor and matching the boundary conditions. This seems to be hopelessly complicated and not likely to provide insight into the solution of the problem.

3.3 Calculation Procedures

The procedures for calculating the impedance are summarized below.

1. Write down the equations of motion for carriers (electrons or holes): The Lorentz force equations, the continuity equation, the current definition, and Maxwell's equations.
2. From the above equations, get the dispersion equation from which the propagation constants can be calculated. Also,

the wave quantities corresponding to each propagating wave can be calculated.

3. Obtain the amplitude ratios of each propagating wave by matching boundary conditions at the ends.
4. Calculate the voltage between the two metal plates by integrating the electric field from injecting plate to collecting plate.
5. Calculate the impedance defined by Eq. 53.

3.4 Boundary Conditions

The boundary conditions usually can be obtained by proper integration of Maxwell's equations. In the one-dimensional case shown in Fig. 3.3, the dc electric field is applied in the negative x-direction;

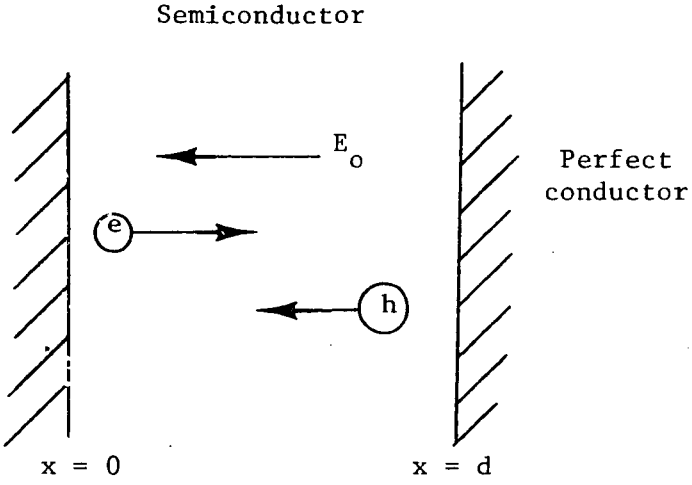

Fig. 3.3. Boundary conditions between a semiconductor and perfect metal contacts.

the boundary conditions are $D = \rho_s$, $J + j\omega\epsilon E = J_T$ = constant, since only a longitudinal electric field is present in the one-dimensional case.

Unfortunately, these boundary conditions cannot provide enough information to solve the problem. Some other boundary conditions must be found or postulated. Van der Ziel[25] used as boundary conditions that the ac electric field $\underset{\sim}{E} = 0$ and the ac potential $\phi = 0$ at the initial plate $x = 0$, and the ac potential $\phi = \phi_a$ at the second plate, $x = d$, in the space-charge-limited solid-state diode case. Kawamura[26] used the boundary conditions that the ac normal electric field $\underset{\sim}{E}$ must be zero at both ends, $x = 0$ and $x = d$.

Van der Ziel's boundary conditions do not fit the present problem because it is not the space-charge-limited case. Kawamura's boundary conditions appear to be unreasonable. Normal $\underset{\sim}{E} = 0$ at both ends implies that no surface charge exists on the perfect conducting surface. The author thinks that there needs to be a better physical explanation.

As shown in Fig. 3.3, electrons move against the dc electric field, i.e., they move from $x = 0$ to $x = d$, while holes move along the dc electric field, i.e., move from $x = d$ to $x = 0$. In this case, the ac velocity of electrons should be zero at the initial plate,

---

[25] A. van der Ziel, S. T. Hsu, "High-Frequency Admittance of Space-Charge-Limited Solid-State Diodes," *Proceedings of the IEEE*, Vol. 54, September 1966, p. 1194.

[26] M. Kawamura, S. Morishita, "A New Negative Resistance of Semiconductor Bulk," *Proceedings of the IEEE*, Vol. 56, July 1968, pp. 1213-1215.

i.e., $v_e = 0$ at $x = 0$, as the first priority boundary condition for reasons which follow. In the perfect conductor the ac field, current and charge density are all zero; the electrons which leave the perfect conductor and enter the semiconductor will be accelerated by the ac electric field in the semiconductor. But since it takes a finite time for these electrons to acquire ac velocity, their ac velocities at the initial plane must be zero. For the same reason the ac velocity of holes should be zero at the end plate, i.e., $v_h = 0$ at $x = d$ if necessary; otherwise this boundary condition can be removed.

If further boundary conditions are required, $J_e = 0$ at $x = 0$ will be used as a second priority boundary condition by adopting the same kind of physical arguments. The boundary condition of $\rho_e = 0$ at $x = 0$ can naturally replace $J_e = 0$ at $x = 0$. Since $J_e = \rho_e V_{oe} + \rho_{oe} v_e$, $v_e = 0$ and $J_e = 0$ at $x = 0$ implies $v_e = 0$ and $\rho_e = 0$ at $x = 0$, too.

These boundary conditions mentioned above have been used successfully in the electron beam cases and some semiconductor cases. They give quite satisfactory results which appear to explain some important physical results.

3.5 Impedance Analysis of Double-Stream Interaction in Solid-State Plasma without Magnetic Field or with Longitudinal Magnetic Field

From the previous chapter, the dispersion relation for space-charge waves under a longitudinal or no magnetic field is

$$1 - \sum \frac{\omega_{pi}^2}{\left(\omega - kV_{oi}\right)\left(\omega - kV_{oi} - j\nu_{ci}\right) - k^2 V_{Ti}^2} = 0 \qquad (30)$$

If no approximations are made, Eq. 30 is a fourth-order equation. It will have four propagation constants in this situation. The complete solutions are given in Eq. 31 in Chapter II. It is impossible to solve Eq. 30 analytically without the aid of a computer. However, in the InSb case, some of the factors (e.g., the hole drifting velocity V_{oh}, the diffusion velocities V_{Ti}'s, and $|\omega - kV_{oi}| \ll \nu_{ci}$ collision dominant case) are so small that they can be neglected or simplified compared to some dominant terms. Such approximations and simplfications can result in reducing the order of Eq. 30 and still give a good expression for the wave properties in a semiconductor.

In the following sections, the dispersion relation of Eq. 30 will be investigated under some simple and proper assumptions so that the wave properties can be analyzed algebraically, and then the impedances will be calculated based on such assumptions.

A. Assume no hole drift velocity ($V_{oh} = 0$), no diffusion effect (i.e., a zero temperature model $V_{Ti} = 0$), and the collision dominant case $\left(\omega - kV_{oi} - j\nu_{ci} \simeq -j\nu_{ci}\right)$; then Eq. 30 can be rewritten as

$$1 - \frac{\omega_{pe}^2}{\left(-j\nu_{ce}\right)\left(\omega - kV_{oe}\right)} - \frac{\omega_{ph}^2}{\left(-j\omega\nu_{ch}\right)} = 0 \qquad (54)$$

Then

$$kV_{oe} = \omega - \frac{j\,\omega_{pe}^2}{\nu_{ce}\left(1 - j\,\dfrac{\omega_{ph}^2}{\omega\nu_{ch}}\right)} \qquad (55)$$

Defining $\sigma_i = \varepsilon\omega_{pi}^2/\nu_{ci}$, we have

$$kV_{oe} = \omega - j\,\frac{\sigma_e}{\varepsilon\left(1 + \frac{\sigma_h}{j\omega\varepsilon}\right)} \tag{56}$$

If $\sigma_h = 0$ (no holes exist), then

$$kV_{oe} = \omega - j\,\frac{\sigma_e}{\varepsilon} \tag{57}$$

This is a one-stream carrier wave which is heavily damped. If $\sigma_h <$ $j\omega\varepsilon$, then

$$kV_{oe} = \omega - j\,\frac{\sigma_e}{\varepsilon}\left[1 + j\,\frac{\sigma_h}{\omega\varepsilon} - \frac{\sigma_h^2}{\omega^2\varepsilon^2} + \ldots\right] \tag{58}$$

So the existence of hole plasma can reduce the magnitude of the damping.

The main difference between Eq. 56 and Eq. 57 is the background medium. In Eq. 56 the electron carrier wave is propagating through a stationary hole plasma background, while in Eq. 57 it is propagating through an ordinary dielectric background. Furthermore, Eq. 56 can be written as

$$kV_{oe} = \omega - j\,\frac{\sigma_e\left(1 + j\,\frac{\sigma_h}{\omega\varepsilon}\right)}{\varepsilon\left(1 + \frac{\sigma_h^2}{\omega^2\varepsilon^2}\right)}$$

$$= \omega + \frac{\sigma_e\left(\frac{\sigma_h}{\omega\varepsilon}\right)}{\varepsilon\left(1 + \frac{\sigma_h^2}{\omega^2\varepsilon^2}\right)} - j\,\frac{\sigma_e}{\varepsilon\left(1 + \frac{\sigma_h^2}{\omega^2\varepsilon^2}\right)} \qquad (59)$$

We can see that the damping factor of the electron carrier wave decreases radically due to the existence of the hole plasma, so the hole plasma makes the electron carrier wave much more significant. If $\sigma_h >> \omega\varepsilon$, Eq. 59 can be further expressed as

$$kV_{oe} = \left(\omega + \frac{\sigma_\varepsilon \omega}{\sigma_h}\right) - j\,\frac{\sigma_e \omega^2 \varepsilon}{\sigma_h^2}$$

$$= \omega\left(1 + \frac{n_e\mu_e}{n_h\mu_h}\right) - j\omega\,\frac{n_e\mu_e}{n_h\mu_h}\,\frac{\omega\nu_{ch}}{\omega_{ph}^2}$$

i.e.,

$$k = \frac{\omega}{V_{oe}}\left(1 + \frac{n_e\mu_e}{n_h\mu_h}\right) - j\,\frac{\omega}{V_{oe}}\,\frac{n_e\mu_e}{n_h\mu_h}\,\frac{\omega\nu_{ch}}{\omega_{ph}^2} \qquad (60)$$

Since $\omega << \nu_{ch}$, ω_{ph} in InSb, the damping term can be considered very small.

The complete solution for electron velocity, current density, and electric field is

$$\begin{bmatrix} v_e \\ J_e \\ E \end{bmatrix} = \sum_{m=0}^{1} A_m \begin{bmatrix} \frac{\eta_e}{\nu_{ce}} \\ \frac{\eta_e \omega \rho_{oe}}{\nu_{ce}\left(\omega - kV_{oe}\right)} \\ 1 \end{bmatrix} e^{-jk_m z} \tag{61}$$

where

$$A_o = \frac{J_T}{\left(j\omega\varepsilon + \sum_i \mu_i \rho_{oi}\right)} \tag{62}$$

Using $v_e = 0$ at $z = 0$ as a boundary condition, which is equivalent to $E = 0$ at $z = 0$ in this case, we have

$$A_1 = -A_o \tag{63}$$

so

$$E = A_o\left[1 - e^{-jkz}\right] \tag{64}$$

As shown before, the impedance of the carrier wave can be derived as

$$Z = \frac{1}{J_T A} \int_0^d E \, dz$$

$$= \frac{A_o d}{J_T A}\left[1 - \frac{e^{-jkd} - 1}{-jkd}\right]$$

$$= \frac{d}{A\left[j\omega\varepsilon + \sum_i \mu_i \rho_{oi}\right]} \left[1 - \frac{e^{-jkd} - 1}{-jkd}\right] \qquad (65)$$

If the presence of the holes is neglected so that the interaction becomes a one-carrier stream interaction,

$$k = \frac{\omega}{V_{oe}} - j \frac{\sigma_e}{\varepsilon V_{oe}} \qquad (57)$$

Then $e^{-jkd} << 1$ and $|1/kd| << 1$. Hence

$$Z \simeq \frac{d}{A\left[j\omega\varepsilon + \sigma_e\right]} \qquad (66)$$

which is the impedance of a leaky capacitor, as expected.

For the two-carrier stream interaction,

$$k = \frac{\omega}{V_{oe}} \left(1 + \frac{n_e \mu_e}{n_h \mu_h}\right) - j \frac{\omega}{V_{oe}} \frac{n_e \mu_e}{n_h \mu_h} \frac{\omega \nu_{ch}}{\omega_{ph}^2} \qquad (60)$$

If the damping term is neglected, then

$$Z \simeq \frac{d}{A\left[j\omega\varepsilon + \sigma_e + \sigma_h\right]} \left[1 - \frac{e^{-j\theta} - 1}{-j\theta}\right]$$

$$= \frac{d}{A\left[j\omega\varepsilon + \sigma_e + \sigma_h\right]} \left[\frac{\theta - \sin\theta}{\theta} + j \frac{(1 - \cos\theta)}{\theta}\right] \qquad (67)$$

where

$$\theta = \frac{\omega}{V_{oe}} \left(1 + \frac{n_e \mu_e}{n_h \mu_h}\right) d$$

and

$$\sigma_i = \mu_i \rho_{oi}$$

The impedance is a spiral curve and is a function of θ in which ω, V_{oe}, n_e, n_h, μ_e, μ_h, and d are involved.

If it is a high resistivity dielectric diode (e.g., a silicon diode), $\omega_{pe} \simeq 0$. Then

$$Z = \frac{d}{j\omega\epsilon A} \left(\frac{1 - j\theta - e^{-j\theta}}{-j\theta}\right) \qquad (68)$$

which is quite similar to the impedance of the space-charge-limited diode derived originally by Shao and Wright.[27] The derivation will be given in Appendix 1.

If the frequency is not so low that the inductive effect plays a significant role in the hole plasma, i.e., the $-j\nu_{ch}$ term in the above equation should be replaced by $(\omega - j\nu_{ch})$, then the propagation constant of the carrier wave should be modified as

---

[27] J. Shao and G. T. Wright, "Characteristics of the Space-Charge-Limited Dielectric Diode at Very High Frequency," *Solid State Electronics*, Vol. 3, November 1961, pp. 291-303.

$$k = \frac{\omega}{V_{oe}}\left[1 + \frac{n_e\mu_e}{n_h\mu_h}\cdot\left(1 + j\frac{\omega}{\nu_{ch}}\right)\right]$$

$$- j\frac{\omega}{V_{oe}}\frac{n_e\mu_e}{n_h\mu_h}\cdot\left(1 + j\frac{\omega}{\nu_{ch}}\right)\cdot\frac{\omega\nu_{ch}}{\omega_p^2}\left(1 + j\frac{\omega}{\nu_{ch}}\right)$$

$$\simeq \frac{\omega}{V_{oe}}\left(1 + \frac{n_e\mu_e}{n_h\mu_h}\right) - j\frac{\omega}{V_{oe}}\frac{n_e\mu_e}{n_h\mu_h}\cdot\left[\frac{\omega}{\nu_{ch}}\frac{\nu_{ch}^2}{\omega_{ph}^2}\left(1 - \frac{\omega^2}{\nu_{ch}^2}\right) - 1\right] \quad (69)$$

Obviously the carrier wave will be a growing wave if

$$\left[\frac{\nu_{ch}^2}{\omega_{ph}^2}\left(1 - \frac{\omega^2}{\nu_{ch}^2}\right) - 1\right] < 0 \quad (70)$$

This implies

$$\omega_{ph}^2 > \nu_{ch}^2 \quad (71)$$

From the impedance point of view, the wave will not change its magnitude drastically since the growing rate is still small compared with phase velocity. How the propagation constant affects the impedance will be studied in the following section.

B. Assuming no diffusion effect ($V_{Ti} = 0$), the collision-dominant case $\left[(\omega - kV_{oi} - j\nu_{ci}) \simeq -j\nu_{ci}\right]$, and small hole drifting velocity, we have

$$1 - \frac{j\omega_{pe}^2}{\nu_{ce}\left(\omega - kV_{oe}\right)} - \frac{j\omega_{ph}^2}{\nu_{ch}\left(\omega - kV_{oh}\right)} = 0 \qquad (72)$$

i.e.,

$$k^2 - k\left[\frac{\omega}{V_{oe}} + \frac{\omega}{V_{oh}} - j\,\frac{\omega_{pe}^2}{\nu_{ce}V_{oe}} - j\,\frac{\omega_{ph}^2}{\nu_{ch}V_{oh}}\right]$$

$$+ \left[\frac{\omega^2}{V_{oe}V_{oh}} - j\,\frac{\omega_{pe}^2\,\omega}{\nu_{ce}V_{oe}V_{oh}} - j\,\frac{\omega_{ph}^2\,\omega}{\nu_{ch}V_{oh}V_{oe}}\right] = 0 \qquad (73)$$

Solutions of Eq. 73 are:

$$k = \frac{1}{2}\left\{\left(\frac{\omega}{V_{oe}} + \frac{\omega}{V_{oh}}\right) - j\left(\frac{\omega_{pe}^2}{\nu_{ce}V_{oe}} + \frac{\omega_{ph}^2}{\nu_{ch}V_{oh}}\right) \pm \left[\left(\frac{\omega}{V_{oe}} - \frac{\omega}{V_{oh}}\right)^2\right.\right.$$

$$\left.\left. - \left(\frac{\omega_{pe}^2}{\nu_{ce}V_{oe}} + \frac{\omega_{ph}^2}{\nu_{ch}V_{oh}}\right)^2 - 2j\left(\frac{\omega}{V_{oe}} - \frac{\omega}{V_{oh}}\right)\left(\frac{\omega_{pe}^2}{\nu_{ce}V_{oe}} - \frac{\omega_{ph}^2}{\nu_{ch}V_{oh}}\right)\right]^{1/2}\right\} \qquad (74)$$

We shall be interested in the situation where ω/V_{oe}, ω/V_{oh} are much smaller than $\omega_{pe}^2/\nu_{ce}V_{oe}$, $\omega_{ph}^2/\nu_{ch}V_{oh}$. Then

$$k_{1_2} = \frac{1}{2}\left\{\left(\frac{\omega}{V_{oe}} + \frac{\omega}{V_{oh}}\right) - j\left(\frac{\omega_{pe}^2}{\nu_{ce}V_{oe}} + \frac{\omega_{ph}^2}{\nu_{ch}V_{oh}}\right)\right.$$

$$\pm (-j)\left(\frac{\omega_{pe}^2}{\nu_{ce}V_{oe}} + \frac{\omega_{ph}^2}{\nu_{ch}V_{oh}}\right)\left[1 + j\,\frac{\left(\frac{\omega}{V_{oe}} - \frac{\omega}{V_{oh}}\right)\left(\frac{\omega_{pe}^2}{\nu_{ce}V_{oe}} - \frac{\omega_{ph}^2}{\nu_{ch}V_{oh}}\right)}{\left(\frac{\omega_{pe}^2}{\nu_{ce}V_{oe}} + \frac{\omega_{ph}^2}{\nu_{ch}V_{oh}}\right)}\right.$$

$$\left.\left. - 2\left(\frac{\frac{\omega}{V_{oe}} - \frac{\omega}{V_{oh}}}{\frac{\omega_{pe}^2}{\nu_{ce}V_{oe}} + \frac{\omega_{ph}^2}{\nu_{ch}V_{ch}}}\right)^2\left(\frac{\frac{\omega_{pe}^2}{\nu_{ce}V_{oe}}\,\frac{\omega_{ph}^2}{\nu_{ch}V_{oh}}}{\left(\frac{\omega_{pe}^2}{\nu_{ce}V_{oe}} + \frac{\omega_{ph}^2}{\nu_{ch}V_{oh}}\right)^2}\right)\right]\right\} \qquad (75)$$

Taking the upper sign, we have

$$k_1 = \frac{1}{2}\left\{\left(\frac{\omega}{V_{oe}} + \frac{\omega}{V_{oh}}\right) + \left(\frac{\omega}{V_{oe}} - \frac{\omega}{V_{oh}}\right)\frac{\frac{\omega_{pe}^2}{\nu_{ce}V_{oe}} - \frac{\omega_{ph}^2}{\nu_{ch}V_{oh}}}{\frac{\omega_{pe}^2}{\nu_{ce}V_{oe}} + \frac{\omega_{ph}^2}{\nu_{ch}V_{oh}}}\right.$$

$$\left. - j2\left(\frac{\omega_{pe}^2}{\nu_{ce}V_{oe}} + \frac{\omega_{ph}^2}{\nu_{ch}V_{oh}}\right)\right\}$$

Assuming $V_{oh} << V_{oe}$ and $V_{oh}/V_{oe} << n_e\mu_e/n_h\mu_h$,

$$k_1 = \frac{1}{2}\left\{\frac{\omega}{V_{oh}}\left(1 + \frac{V_{oh}}{V_{oe}}\right) + \frac{\omega}{V_{oh}}\left(1 - \frac{V_{oh}}{V_{oe}}\right)\left(1 - 2\,\frac{n_e\mu_e}{n_h\mu_h}\,\frac{V_{oh}}{V_{oe}}\right)\right.$$

$$\left. - j2\,\frac{\omega_{ph}^2}{\nu_{ce}V_{oh}}\left(1 + \frac{n_e\mu_e}{n_h\mu_h}\,\frac{V_{oh}}{V_{oe}}\right)\right\}$$

$$= \frac{\omega}{V_{oh}}\left[1 - \frac{n_e\mu_e}{n_h\mu_h}\,\frac{V_{oh}}{V_{oe}}\right] - j\,\frac{\sigma_h}{\varepsilon V_{oh}}\left(1 + \frac{n_e\mu_e}{n_h\mu_h}\,\frac{V_{oh}}{V_{oe}}\right)$$

$$\simeq \frac{\omega}{V_{oh}} - j\,\frac{\sigma_h}{\varepsilon V_{oh}} \qquad (76)$$

Thus, k_1 is the hole carrier wave which is heavily damped since $\sigma_h > \omega\varepsilon$.

Taking the lower sign, we have

$$k_2 = \frac{1}{2}\left\{\left(\frac{\omega}{V_{oe}} + \frac{\omega}{V_{oh}}\right) - \frac{\left(\frac{\omega}{V_{oe}} - \frac{\omega}{V_{oh}}\right)\left(\frac{\omega_{pe}^2}{\nu_{ce}V_{oe}} - \frac{\omega_{ph}^2}{\nu_{ch}V_{oh}}\right)}{\left(\frac{\omega_{pe}^2}{\nu_{ce}V_{oe}} + \frac{\omega_{ph}^2}{\nu_{ch}V_{oh}}\right)}\right.$$

$$- 2j \left(\frac{\frac{\omega}{V_{oe}} - \frac{\omega}{V_{oh}}}{\frac{\omega_{pe}^2}{\nu_{ce} V_{oe}} + \frac{\omega_{ph}^2}{\nu_{ch} V_{oh}}} \right)^2 \left(\frac{\frac{\omega_{pe}^2}{\nu_{ce} V_{oe}} - \frac{\omega_{ph}^2}{\nu_{ch} V_{oh}}}{\frac{\omega_{pe}^2}{\nu_{ce} V_{oe}} + \frac{\omega_{ph}^2}{\nu_{ch} V_{oh}}} \right) \Bigg\}$$

$$= \frac{\omega}{V_{oe}} \left[1 + \frac{n_e \mu_e}{n_h \mu_h} \left(1 + \frac{V_{oh}}{V_{oe}} \right) \right] - j \frac{\omega}{V_{oe}} \frac{n_e \mu_e}{n_h \mu_h} \cdot \frac{\omega \nu_{ch}}{\omega_{ph}^2}$$

$$\cdot \left(1 - 2 \frac{V_{oh}}{V_{oe}} - 3 \frac{n_e \mu_e}{n_h \mu_h} \frac{V_{oh}}{V_{oe}} \right) \tag{77}$$

Thus k_2 is the electron carrier wave, which is less damped.

If V_{oh} approaches zero, then

$$k_1 \to -\infty + j\infty \tag{78}$$

$$k_2 \to \frac{\omega}{V_{oe}} \left(1 + \frac{n_e \mu_e}{n_h \mu_h} \right) - j \frac{\omega}{V_{oe}} \frac{n_e \mu_e}{n_h \mu_h} \frac{\omega \nu_{ch}}{\omega_{ph}^2} \tag{79}$$

which is the same as the first case. From Eq. 77, we can see that the effect of hole drift velocity on the electron carrier wave is to increase its damping since the ratio of V_{oh} to V_{oe} is negative.

The complete solution for electric field is

$$E_z = A_o + A_1 e^{-jk_1 z} + A_2 e^{-jk_2 z} \tag{80}$$

Using $v_e = 0$ at $z = 0$ and $v_h = 0$ at $z = d$ (which is equivalent to $E = 0$ at $z = 0$ and $z = d$), we obtain

$$A_o + A_1 + A_2 = 0 \tag{81}$$

$$A_1 + A_1 e^{-jk_1 d} + A_2 e^{-jk_2 d} = 0 \tag{82}$$

Then

$$A_1 = \frac{1 - e^{-jk_2 d}}{e^{-jk_2 d} - e^{-jk_1 d}} A_o \simeq 0 \tag{83}$$

$$A_2 = \frac{e^{-jk_1 d} - 1}{e^{-jk_2 d} - e^{-jk_1 d}} A_o \simeq -A_o \tag{84}$$

and

$$V = \int_0^d E dz = A_o d + A_1 \frac{e^{-jk_1 d} - 1}{-jk_1} + A_2 \frac{e^{-jk_2 d} - 1}{-jk_2} \tag{85}$$

Substituting Eqs. 83 and 84 into Eq. 85,

$$V = A_o d + \frac{A_o\left(e^{-jk_1 d} - 1\right)\left(e^{-jk_2 d} - 1\right)}{\left(e^{-jk_2 d} - e^{-jk_1 d}\right)}\left(\frac{1}{-jk_2} - \frac{1}{-jk_1}\right)$$

$$Z = \frac{V}{J_T A} = \frac{A_o d}{J_T A}\left[1 + \frac{\left(e^{-jk_1 d} - 1\right)\left(e^{-jk_2 d} - 1\right)}{\left(e^{-jk_2 d} - e^{-jk_1 d}\right)}\left(\frac{1}{-jk_2 d} - \frac{1}{-jk_1 d}\right)\right] \quad (86)$$

If we assume $V_{oh} \to 0$, then $k_1 \to \infty - j\infty$ and $e^{-jk_1 d} \to \infty$.

Equation 86 becomes

$$Z = \frac{A_o d}{J_T A}\left[1 - \frac{e^{-jk_2 d} - 1}{-jk_2 d}\right]$$

which is exactly identical to Eq. 67.

C. Assuming collision dominant $\left[\left(\omega - kV_{oe} - j\nu_{ci}\right) \simeq -j\nu_{ci}\right]$ and small diffusion effect $\left(4\ V_{Te}^2/V_{oe}^2 \cdot \omega/\nu_{ce} << 1,\ V_{Th} = 0\right)$, we have

$$1 - \frac{\omega_{pe}^2}{\left(\omega - kV_{oe}\right)\left(-j\nu_{ce}\right) - k^2 V_{Te}^2} - \frac{\omega_{ph}^2}{\omega\left(-j\nu_{ch}\right)} = 0 \quad (87)$$

i.e.,

$$k^2 V_{Te}^2 + j\nu_{ce}\left(\omega - kV_{oe}\right) + \frac{\omega_{pe}^2}{1 - j\dfrac{\omega_{ph}^2}{\omega\nu_{ch}}} = 0$$

then,

$$k_{\substack{1\\2}} = \frac{1}{2V_{Te}^2}\left\{ j\nu_{ce} V_{oe} \pm \left[-\nu_{ce}^2 V_{oe}^2 - 4V_{Te}^2 \left(j\omega\nu_{ce} + \frac{\omega_{pe}^2}{1 - j\dfrac{\omega_{ph}^2}{\omega\nu_{ch}}} \right) \right]^{1/2} \right\}$$

We have

$$k_1 = -\frac{\omega}{V_{oe}}\left(1 + \frac{n_e\mu_e}{n_h\mu_h}\right) + j\,\frac{\nu_{ce}V_{oe}}{V_{Te}^2} \tag{88}$$

$$k_2 = \frac{\omega}{V_{oe}}\left(1 + \frac{n_e\mu_e}{n_h\mu_h}\right) - j\,\frac{\omega}{V_{oe}}\,\frac{n_e\mu_e}{n_h\mu_h}\,\frac{\omega\nu_{ch}}{\omega_{ph}^2} - j\,\frac{V_{Te}^2}{V_{oe}^2}\,\frac{\omega}{\nu_{ce}}\left[1 + \frac{n_e\mu_e}{n_h\mu_h}\right]^2 \cdot \frac{\omega}{V_{oe}} \tag{89}$$

Thus there are two waves existing in this case; one wave k_1 is the reflected wave with quite a large damping factor, and the other wave k_2 is the usual electron carrier wave traveling in the direction of electron drift. The effect of the diffusion on the electron carrier wave is to increase its damping factor, which is physically reasonable.

The complete solution for electric field is

$$E = A_o + A_1 e^{-jk_1 z} + A_2 e^{-jk_2 z}$$

Using $v_e = 0$ at $z = 0$ and $v_h = 0$ at $z = d$ as our boundary conditions, we have once again

$$A_1 = \frac{1 - e^{-jk_2 d}}{e^{-jk_2 d} - e^{-jk_1 d}} A_o$$

$$A_2 = \frac{1 - e^{-jk_1 d}}{e^{-jk_1 d} - e^{-jk_2 d}} A_o$$

Then the impedance is given by

$$Z = \frac{E_o d}{J_T A}\left[1 + \frac{\left(e^{-jk_1 d} - 1\right)\left(e^{-jk_2 d} - 1\right)}{\left(e^{-jk_2 d} - e^{-jk_1 d}\right)}\left(\frac{1}{-jk_2 d} - \frac{1}{-jk_1 d}\right)\right]$$

If V_{Te} approaches zero, then

$$k_1 \to -\frac{\omega}{V_{oe}}\left(1 + \frac{n_e \mu_e}{n_h \mu_h}\right) + j\infty \qquad (90)$$

$$k_2 \to \frac{\omega}{V_{oe}}\left(1 + \frac{n_e \mu_e}{n_h \mu_h}\right) - j\,\frac{\omega}{V_{oe}}\,\frac{n_e \mu_e}{n_h \mu_h}\,\frac{\nu_{ch}\omega}{\omega_{ph}^2} \qquad (91)$$

$$A_1 \to 0$$

$$A_2 \to A_o$$

$$e^{-jk_1 d} \to \infty$$

and the impedance is given by

$$Z \to \frac{A_o d}{J_T A}\left[1 - \frac{e^{-jk_2 d} - 1}{-jk_2 d}\right]$$

which is the same as the former case.

D. Summary: Under a longitudinal or no magnetic field and low-temperature condition, the impedance of a semiconductor plasma based on carrier stream interaction is approximately equal to

$$Z = \frac{d}{A\left[j\omega\varepsilon + \sigma_e + \sigma_h\right]}\left[\frac{\theta - \sin\theta}{\theta} + j\,\frac{1 - \cos\theta}{\theta}\right] \qquad (67)$$

where A is the cross-sectional area of the sample, d is the length of the sample, and $\theta = \omega/V_{oe}\left(1 + n_e\mu_e/n_h\mu_h\right)$.

Obviously, the impedance Z is a function of A. By choosing A, the impedance can be calculated theoretically. Of course, this impedance is a realistic one† and able to be measured experimentally if proper operating conditions†† are given.

3.6 Impedance Analysis of Double-Stream Interaction in Solid-State Plasma with a Transverse Magnetic Field

From Section 2.4, the dispersion relation for a pseudolongitudinal wave is

---

† The impedance of the space-charge-limited dielectric diode has been measured by Shao and Wright.

†† This will be discussed in the next chapter.

$$1 - \sum_{i=e,h} \frac{\omega_{pi}^2 \, \Omega_i}{w_i\left(\Omega_i^2 - \omega_{ci}^2\right) - k^2 V_{Ti}^2 \, \Omega_i} = 0 \qquad (44)$$

If no assumptions are made, this is a sixth order equation. However, Eq. 44 will only be studied under some simple and proper assumptions so that it can be analyzed algebraically. Furthermore the calculation of the impedance will be based on such assumptions.

A. Assuming no hole drift velocity, no diffusion effect (absolute zero temperature, $V_{Ti} = 0$), low-frequency and the collision-dominant case, $\omega - kV_{oi} - j\nu_{ci} \simeq -j\nu_{ci}$, we can rewrite Eq. 44 as

$$1 - \frac{j\omega_{pe}^2 \nu_{ce}}{\left(\omega - kV_{oe}\right)\left(\nu_{ce}^2 + \omega_{ce}^2\right)} - \frac{j\omega_{ph}^2}{\omega\left(\nu_{ch}^2 + \omega_{ch}^2\right)} = 0 \qquad (92)$$

The propagation constant can be solved for from

$$\frac{\left(\omega - kV_{oe}\right)\left(\nu_{ce}^2 + \omega_{ce}^2\right)}{j\,\omega_{pe}^2\,\nu_{ce}} = \frac{1}{1 - \dfrac{j\,\omega_{ph}^2\,\nu_{ch}}{\omega\left(\nu_{ch}^2 + \omega_{ch}^2\right)}} \qquad (93)$$

Since

$$\frac{\omega_{ph}^2 \, \nu_{ch}}{\omega\left(\nu_{ch}^2 + \omega_{ch}^2\right)} >> 1$$

then

$$\frac{1}{1 - \dfrac{j\,\omega_{ph}^2\,\nu_{ch}}{\omega\left(\nu_{ch}^2 + \omega_{ch}^2\right)}} \simeq \frac{j\omega\left(\nu_{ch}^2 + \omega_{ch}^2\right)}{\omega_{ph}^2\,\nu_{ch}} \left[1 - j\,\frac{\omega\left(\nu_{ch}^2 + \omega_{ch}^2\right)}{\omega_{ph}^2\,\nu_{ch}}\right] \quad (94)$$

Substituting Eq. 94 into Eq. 93, we have

$$\left(\omega - kV_{oe}\right) = -\omega\,\frac{\omega_{pe}^2\nu_{ce}\left(\nu_{ch}^2 + \omega_{ch}^2\right)}{\omega_{ph}^2\nu_{ch}\left(\nu_{ce}^2 + \omega_{ce}^2\right)} \left[1 - j\,\frac{\omega\left(\nu_{ch}^2 + \omega_{ch}^2\right)}{\omega_{ph}^2\,\nu_{ch}}\right]$$

$$= -\omega\,\frac{n_e\mu_e}{n_h\mu_h} \cdot \frac{\left(1 + \mu_h^2 B_o^2\right)}{\left(1 + \mu_e^2 B_o^2\right)} \left[1 - j\,\frac{\omega\left(\nu_{ch}^2 + \omega_{ch}^2\right)}{\omega_{ph}^2\,\nu_{ch}}\right] \quad (95)$$

and

$$k = \frac{\omega}{V_{oe}} \left[1 + \frac{\omega_{pe}^2\nu_{ce}\left(\nu_{ch}^2 + \omega_{ch}^2\right)}{\omega_{ph}^2\nu_{ch}\left(\nu_{ce}^2 + \omega_{ce}^2\right)}\right] - j\,\frac{\omega^2}{V_{oe}}\,\frac{\omega_{pe}^2\nu_{ce}\left(\nu_{ch}^2 + \omega_{ch}^2\right)^2}{\omega_{ph}^4\,\nu_{ch}^2} \quad (96)$$

The phase velocity is

$$v_p = \frac{\omega}{k_{real}} = \frac{V_{oe}}{1 + \dfrac{\omega_{pe}^2\nu_{ce}\left(\nu_{ch}^2 + \omega_{ch}^2\right)}{\omega_{ph}^2\nu_{ch}\left(\nu_{ce}^2 + \omega_{ce}^2\right)}}$$

$$= \frac{V_{oe}}{1 + \dfrac{n_e\mu_e}{n_h\mu_h} \cdot \dfrac{1 + \mu_h^2 B_o^2}{1 + \mu_e^2 B_o^2}} \quad (97)$$

and since $\omega << \nu_{ch}$, it is found that Im[k] << Re[k].

When B_o approaches zero, v_p approaches $V_o/\left(1 + n_e\mu_e/n_h\mu_h\right)$, which is identical (as expected) to the formal case without B_o. The presence of the external magnetic field causes an increase in v_p since $\left(1 + \mu_h^2 B_o^2\right)/\left(1 + \mu_e^2 B_o^2\right)$ is always less than 1.

From Eq. 45 the complete solution for the electric field E and an electron velocity v_{ez} can be written as

$$\begin{bmatrix} v_{ez} \\ \\ E \end{bmatrix} = A_o \begin{bmatrix} \dfrac{+j\eta_e\left(-j\nu_{ce}\right)}{\nu_{ce}^2 + \omega_{ce}^2} \\ \\ 1 \end{bmatrix} + A_1 \begin{bmatrix} \dfrac{+j\eta_e\left(-j\nu_{ce}\right)}{\nu_{ce}^2 + \omega_{ce}^2} \\ \\ 1 \end{bmatrix} e^{-jkz} \qquad (98)$$

where

$$A_o = J_T \Big/ \left[\sum \frac{+j\eta_i \rho_{oi}\left(-j\nu_{ci}\right)}{\nu_{ci}^2 + \omega_{ci}^2} + j\omega\varepsilon \right] \qquad (99)$$

Matching the boundary condition $v_{ez} = 0$ at $z = 0$, we have $A_1 = -A_o$. So

$$E = A_o - A_o\, e^{-jkz} \qquad (100)$$

The impedance is

$$Z = \frac{\int_0^d E\, dz}{J_T A} = \frac{A_o}{J_T A}\left[d - \frac{e^{-jkd} - 1}{-jk}\right]$$

$$= \frac{1}{A\left[\sum_{i=e,h} \frac{\eta_i \rho_{oi} \nu_{ci}}{\nu_{ci}^2 + \omega_{ci}^2} + j\omega\varepsilon\right]} \cdot \left[d - \frac{e^{-jkd} - 1}{-jk}\right] \qquad (101)$$

where A is the cross-sectional area of the sample. The imaginary part of the propagation constant k is far less than the real part of k. In other words, this carrier wave is very slightly damped. If the decaying term is neglected, the impedance will not change very much.

Furthermore, if the second order terms of $(\omega - kV_{oi})$ are considered, then k will be modified and will be obtained more accurately. Under this assumption,

$$\frac{\omega_{pi}^2 (\omega - kV_{oi} - j\nu_{ci})}{(\omega - kV_{oi})\left[(\omega - kV_{oi} - j\nu_{ci})^2 - \omega_{ci}^2\right]}$$

$$\simeq \frac{\omega_{pi}^2\, j\nu_{ci} \left(1 + j\,\frac{\omega - kV_{oi}}{\nu_{ce}}\right)}{(\omega - kV_{oi})(\nu_{ci}^2 + \omega_{ci}^2)\left(1 + j\,\frac{(\omega - kV_{oi})\nu_{ci}}{(\nu_{ci}^2 + \omega_{ci}^2)}\right)}$$

$$\approx \frac{j\,\omega_{pi}^2\,\nu_{ci}}{\left(\omega - kV_{oi}\right)\left(\nu_{ci}^2 + \omega_{ci}^2\right)} \cdot \left[1 + j\,\frac{\left(\omega - kV_{oi}\right)\left(-\nu_{ci}^2 + \omega_{ci}^2\right)}{\nu_{ce}\left(\nu_{ce}^2 + \omega_{ce}^2\right)}\right] \quad (102)$$

So the dispersion relation, Eq. 44, can be rewritten as

$$1 - \frac{j\,\omega_{pe}^2\,\nu_{ce}}{\left(\omega - kV_{oe}\right)\left(\nu_{ce}^2 + \omega_{ce}^2\right)}\left[1 + j\,\frac{\left(\omega - kV_{oe}\right)\left(-\nu_{ce}^2 + \omega_{ce}^2\right)}{\nu_{ce}\left(\nu_{ce}^2 + \omega_{ce}^2\right)}\right]$$

$$- \frac{j\,\omega_{ph}^2\,\nu_{ch}}{\omega\left(\nu_{ch}^2 + \omega_{ch}^2\right)} \cdot \left[1 + j\,\frac{\omega\left(-\nu_{ch}^2 + \omega_{ch}^2\right)}{\nu_{ch}\left(\nu_{ch}^2 + \omega_{ch}^2\right)}\right] = 0 \quad (103)$$

After some mathematical operations, we obtain

$$\left(\omega - kV_{oe}\right) = -\frac{\omega\omega_{pe}^2\nu_{ce}\left(\nu_{ch}^2 + \omega_{ch}^2\right)}{\omega_{ph}^2\nu_{ch}\left(\nu_{ce}^2 + \omega_{ce}^2\right)}\left[1 - j\,\frac{\omega\left(-\nu_{ch}^2 + \omega_{ch}^2\right)}{\nu_{ch}\left(\nu_{ch}^2 + \omega_{ch}^2\right)}\right.$$

$$\left. - j\,\frac{\omega\left(\nu_{ch}^2 + \omega_{ch}^2\right)}{\nu_{ch}\omega_{ph}^2} - j\,\frac{\omega\omega_{pe}^2\left(\nu_{ch}^2 + \omega_{ch}^2\right)\left(-\nu_{ch}^2 + \omega_{ce}^2\right)}{\omega_{ph}^2\nu_{ch}\left(\nu_{ce}^2 + \omega_{ce}^2\right)^2}\right] \quad (104)$$

The instability condition is

$$k_{Im} > 0 \quad (105)$$

i.e.,

$$-\frac{\omega\left(+\nu_{ch}^2+\omega_{ch}^2\right)}{\nu_{ch}\omega_{ph}^2}\;1+\frac{\omega_{pe}^2\left(-\nu_{ce}^2+\omega_{ce}^2\right)}{\left(\nu_{ce}^2+\omega_{ce}^2\right)^2}+\frac{\omega_{ph}^2\left(-\nu_{ch}^2+\omega_{ch}^2\right)}{\left(\nu_{ch}^2+\omega_{ch}^2\right)^2}>0$$

$$1+\frac{\omega_{pe}^2\left(-\nu_{ce}^2+\omega_{ce}^2\right)}{\left(\nu_{ce}^2+\omega_{ce}^2\right)^2}+\frac{\omega_{ph}^2\left(-\nu_{ch}^2+\omega_{ch}^2\right)}{\left(\nu_{ch}^2+\omega_{ch}^2\right)}<0$$

$$1+\frac{\omega_{pe}^2\left(\mu_e^2B_o^2-1\right)}{\nu_{ce}^2\left(\mu_e^2B_o^2+1\right)^2}-\frac{\omega_{ph}^2\left(1-\mu_h^2B_o^2\right)}{\nu_{ch}^2\left(1+\mu_h^2B_o^2\right)}<0 \qquad (106)$$

This threshold condition is equivalent to Gandhi's and Grow's[28] result. However, from an impedance point of view, it still does not influence the impedance value very much if the growing factor is omitted (assuming the sample length is not too long).

B. Assuming no diffusion effect, $V_{Ti}=0$, the collision-dominant case, and small hole drift velocity, we have

$$1-\frac{j\,\omega_{pe}^2\,\nu_{ce}}{\left(\omega-kV_{oe}\right)\left(\nu_{ce}^2+\omega_{ce}^2\right)}-\frac{j\,\omega_{ph}^2\,\nu_{ch}}{\left(\omega-kV_{oh}\right)\left(\nu_{ch}^2+\omega_{ch}^2\right)}=0 \qquad (107)$$

---

[28] O. P. Gandhi and R. W. Grow, *op. cit.*

Expanding Eq. 107 we obtain

$$k^2 - k\left[\left(\frac{\omega}{V_{oe}} + \frac{\omega}{V_{oh}}\right) - j\left(\frac{A}{V_{oe}} + \frac{B}{V_{oh}}\right)\right]$$

$$+ \left[\frac{\omega^2}{V_{oe}V_{oh}} - j\frac{A\omega}{V_{oe}V_{oh}} - j\frac{B\omega}{V_{oe}V_{oh}}\right] = 0 \qquad (108)$$

where

$$A = \frac{\omega_{pe}^2 \nu_{ce}}{\left(\nu_{ce}^2 + \omega_{ce}^2\right)}$$

$$B = \frac{\omega_{ph}^2 \nu_{ch}}{\left(\nu_{ch}^2 + \omega_{ch}^2\right)}$$

Equation 108 is a second order equation; it has roots of

$$k_{\frac{1}{2}} = \frac{1}{2}\left\{\left(\frac{\omega}{V_{oe}} + \frac{\omega}{V_{oh}}\right) - j\left(\frac{A}{V_{oe}} + \frac{B}{V_{oh}}\right) \pm \left[\left(\frac{\omega}{V_{oe}} + \frac{\omega}{V_{oh}} - j\frac{A}{V_{oe}} - j\frac{B}{V_{oh}}\right)^2\right.\right.$$

$$\left.\left. - 4\frac{\omega^2 - jA\omega - jB\omega}{V_{oe}V_{oh}}\right]^{1/2}\right\}$$

$$= \frac{1}{2}\left\{\left(\frac{\omega}{V_{oe}} + \frac{\omega}{V_{oh}}\right) - j\left(\frac{A}{V_{oe}} + \frac{B}{V_{oh}}\right) \pm \left[\left(\frac{\omega}{V_{oe}} - \frac{\omega}{V_{oh}}\right)^2 - 2j\left(\frac{\omega}{V_{oe}} - \frac{\omega}{V_{oh}}\right)\right.\right.$$

$$\cdot \left(\frac{A}{V_{oe}} - \frac{B}{V_{oh}}\right)\Bigg]^{1/2}\Bigg\} \qquad (109)$$

Since $\left(\omega/V_{oe} \pm \omega/V_{oh}\right) < \left(A/V_{oe} \pm B/V_{oh}\right)$, then

$$k_{\substack{1\\2}} = \frac{1}{2}\left\{\left(\frac{\omega}{V_{oe}} + \frac{\omega}{V_{oh}}\right) - j\left(\frac{A}{V_{oe}} + \frac{B}{V_{oh}}\right) \pm j\left(\frac{A}{V_{oe}} + \frac{B}{V_{oh}}\right)\right.$$

$$\left.\cdot\left[1 - \frac{\left(\frac{\omega}{V_{oe}} - \frac{\omega}{V_{oh}}\right)^2}{\left(\frac{A}{V_{oe}} + \frac{B}{V_{oh}}\right)^2} + \frac{2j\left(\frac{\omega}{V_{oe}} - \frac{\omega}{V_{oh}}\right)\left(\frac{A}{V_{oe}} - \frac{B}{V_{oh}}\right)}{\left(\frac{A}{V_{oe}} + \frac{B}{V_{oh}}\right)^2}\right]^{1/2}\right\}$$

$$= \frac{1}{2}\left\{\left(\frac{\omega}{V_{oe}} + \frac{\omega}{V_{oh}}\right) - j\left(\frac{A}{V_{oe}} - \frac{B}{V_{oh}}\right) \pm j\left(\frac{A}{V_{oe}} + \frac{B}{V_{oh}}\right)\cdot\left[1 - \frac{1}{2}\frac{\left(\frac{\omega}{V_{oe}} - \frac{\omega}{V_{oh}}\right)^2}{\left(\frac{A}{V_{oe}} + \frac{B}{V_{oh}}\right)^2}\right.\right.$$

$$\left.\left. + j\frac{\left(\frac{\omega}{V_{oe}} - \frac{\omega}{V_{oh}}\right)\left(\frac{A}{V_{oe}} - \frac{B}{V_{oh}}\right)}{\left(\frac{A}{V_{oe}} + \frac{B}{V_{oh}}\right)^2} + \frac{1}{2}\frac{\left(\frac{\omega}{V_{oe}} - \frac{\omega}{V_{oh}}\right)^2\left(\frac{A}{V_{oe}} - \frac{B}{V_{oh}}\right)^2}{\left(\frac{A}{V_{oe}} + \frac{B}{V_{oh}}\right)^2}\right]\right\}$$

$$= \frac{1}{2} \left\{ \left(\frac{\omega}{V_{oe}} + \frac{\omega}{V_{oh}} \right) - j \left(\frac{A}{V_{oe}} + \frac{B}{V_{oh}} \right) \pm j \left(\frac{A}{V_{oe}} + \frac{B}{V_{oh}} \right) \right.$$

$$\left. \mp \frac{\left(\frac{\omega}{V_{oe}} - \frac{\omega}{V_{oh}} \right)\left(\frac{A}{V_{oe}} - \frac{B}{V_{oh}} \right)}{\left(\frac{A}{V_{oe}} + \frac{B}{V_{oh}} \right)} \mp j2 \frac{\left(\frac{\omega}{V_{oe}} - \frac{\omega}{V_{oh}} \right)^2 \frac{AB}{V_{oe}V_{oh}}}{\left(\frac{A}{V_{oe}} - \frac{B}{V_{oh}} \right)^3} \right\} \qquad (110)$$

Taking the upper sign we have

$$k_1 = \frac{\omega}{V_{oe}} + \frac{\omega}{V_{oe}} \frac{A}{B} - j \frac{\omega^2}{V_{oe}} \frac{A}{B^2} \left(1 - 2 \frac{V_{oh}}{V_{oe}} - 3 \frac{AV_{oh}}{BV_{oe}} \right)$$

$$= \frac{\omega}{V_{oe}} \left[1 + \frac{\omega_{pe}^2 \nu_{ce} \left(\nu_{ch}^2 + \omega_{ch}^2 \right)}{\omega_{ph}^2 \nu_{ch} \left(\nu_{ce}^2 + \omega_{ce}^2 \right)} \right] - j \frac{\omega^2}{V_{oe}} \frac{\omega_{pe}^2 \nu_{ce} \left(\nu_{ch}^2 + \omega_{ch}^2 \right)^2}{\omega_{ph}^4 \nu_{ch}^2 \left(\nu_{ce}^2 + \omega_{ce}^2 \right)}$$

$$\cdot \left[1 - 2 \frac{V_{oh}}{V_{oe}} - 3 \frac{\omega_{pe}^2 \nu_{ce} \left(\nu_{ch}^2 + \omega_{ch}^2 \right)}{\omega_{ph}^2 \nu_{ch} \left(\nu_{ce}^2 + \omega_{ce}^2 \right)} \frac{V_{oh}}{V_{oe}} \right] \qquad (111)$$

Taking the lower sign we have

$$k_2 = \frac{\omega}{V_{oh}} - j \left(\frac{A}{V_{oe}} + \frac{B}{V_{oh}} \right)$$

$$= \frac{\omega}{V_{oh}} - j \frac{B}{V_{oh}} \left[1 + \frac{AV_{oh}}{BV_{oe}} \right]$$

$$= \frac{\omega}{V_{oh}} - j \frac{\omega\omega_{ph}^2 \nu_{ch}}{V_{oh}\left(\nu_{ch}^2 + \omega_{ch}^2\right)} \left[1 + \frac{\omega_{pe}^2 \nu_{ce}\left(\nu_{ch}^2 + \omega_{ch}^2\right)}{\omega_{ph}^2 \nu_{ch}\left(\nu_{ce}^2 + \omega_{ce}^2\right)} \frac{V_{oh}}{V_{oe}} \right] \tag{112}$$

Obviously the wave constant k_1 is associated with electron drift, while k_2 is associated with hole drift.

If $V_{oh} \to 0$, then

$$k_1 = \frac{\omega}{V_{oe}} 1 + \frac{\omega_{pe}^2 \nu_{ce}\left(\nu_{ch}^2 + \omega_{ch}^2\right)}{\omega_{ph}^2 \nu_{ch}\left(\nu_{ce}^2 + \omega_{ce}^2\right)} - j \frac{\omega^2}{V_{oe}} \frac{\omega_{pe}^2 \nu_{ce}\left(\nu_{ch}^2 + \omega_{ch}^2\right)^2}{\omega_{ph}^4 \nu_{ch}^2 \left(\nu_{ce}^2 + \omega_{ce}^2\right)}$$

which is the same as Eq. 96, and $k_2 \to -\infty + j\infty$, which means the wave is heavily damped.

The complete solution under these assumptions can be written as:

$$\begin{bmatrix} v_{ez} \\ v_{hz} \\ E \end{bmatrix} = \sum_{m=0}^{2} A_m \begin{bmatrix} \dfrac{\eta_e \nu_{ce}}{\left(\nu_{ce}^2 + \omega_{ce}^2\right)} \\ \dfrac{\eta_h \nu_{ch}}{\left(\nu_{ch}^2 + \omega_{ch}^2\right)} \\ 1 \end{bmatrix} e^{-jk_m z} \tag{113}$$

The boundary conditions $v_{ez} = 0$ at $z = 0$ and $v_{hz} = 0$ at $z = d$ imply

$$A_o + A_1 + A_2 = 0 \tag{114}$$

and

$$A_o + A_1 e^{-jk_1 d} + A_2 e^{-jk_2 d} = 0 \tag{115}$$

Then

$$A_1 = \frac{1 - e^{-jk_2 d}}{e^{-jk_2 d} - e^{-jk_1 d}} A_o \tag{116}$$

$$A_2 = \frac{e^{-jk_1 d} - 1}{e^{-jk_2 d} - e^{-jk_1 d}} A_o \tag{117}$$

where

$$A_o = J_T \Big/ \left[\sum_{i=e,h} \frac{\eta_i \rho_{oi} \nu_{ci}}{\nu_{ci}^2 + \omega_{ci}^2} + j\omega\epsilon \right] \tag{118}$$

Then the impedance is

$$Z = \frac{1}{J_T A} \int_o^d E \, dz$$

$$= \frac{1}{J_T A}\left[A_o d + A_1 \frac{e^{-jk_1 d} - 1}{-jk_1} + A_2 \frac{e^{-jk_2 d} - 1}{-jk_2}\right] \qquad (119)$$

Substituting Eqs. 116 and 117 into Eq. 119, we obtain

$$Z = \frac{A_o d}{J_T A}\left[1 + \frac{\left(e^{-jk_1 d} - 1\right)\left(e^{-jk_2 d} - 1\right)}{e^{-jk_2 d} - e^{-jk_1 d}}\left(\frac{1}{-jk_2 d} - \frac{1}{-jk_1 d}\right)\right] \qquad (120)$$

If we assume that $V_{oh} \to 0$, then $k_2 \to -\infty + j\infty$ and $e^{-jk_2 d} \to \infty$.

Then, from Eq. 120,

$$Z \to \frac{A_o d}{J_T A}\left[1 - \frac{e^{-jk_1 d} - 1}{-jk_1 d}\right]$$

which is exactly identical to Eq. 101. So the effect of the hole drift velocity on the impedance can be seen as shown in Eq. 120.

C. Assuming no hole drift velocity $V_{oh} = 0$, the collision-dominant case, and small diffusion effects $\left(V_{Te}/V_{oe} < 1,\ V_{Th} = 0\right)$, we have

$$1 - \frac{j\,\omega_{pe}^2\,\nu_{ce}}{\left(\omega - kV_{oe}\right)\left(\nu_{ce}^2 + \omega_{ce}^2\right) - jk^2\,V_{Te}^2\,\nu_{ce}} - \frac{j\,\omega_{ph}^2\,\nu_{ch}}{\omega\left(\nu_{ch}^2 + \omega_{ch}^2\right)} = 0 \qquad (121)$$

Expanding Eq. 121 we have

$$\left(\omega - kV_{oe}\right)\left(\nu_{ce}^2 + \omega_{ce}^2\right) - jk^2 V_{Te}^2 \nu_{ce} = \frac{j \omega_{pe}^2 \nu_{ce}}{1 - \frac{j \omega_{ph}^2 \nu_{ch}}{\omega\left(\nu_{ch}^2 + \omega_{ch}^2\right)}}$$

i.e.,

$$k^2 V_{oe}^2 \left(\frac{V_{Te}^2}{V_{oe}^2}\right) j\nu_{ce} + kV_{oe}\left(\nu_{ce}^2 + \omega_{ce}^2\right) - \frac{\omega_{pe}^2 \nu_{ce} \omega\left(\nu_{ch}^2 + \omega_{ch}^2\right)}{\omega_{ph}^2 \nu_{ch}}$$

$$\cdot \left[1 - j \frac{\omega\left(\nu_{ch}^2 + \omega_{ch}^2\right)}{\omega_{ph}^2 \nu_{ch}}\right] - \omega\left(\nu_{ch}^2 + \omega_{ch}^2\right) = 0 \qquad (122)$$

Then

$$kV_{oe} = \frac{1}{2j\left(\frac{V_{Te}^2}{V_{oe}^2}\right)\nu_{ce}} \left\{-\left(\nu_{ce}^2 + \omega_{ce}^2\right) \pm \left[\left(\nu_{ce}^2 + \omega_{ce}^2\right)^2 - 4\left(\frac{V_{Te}^2}{V_{oe}^2}\right) j\nu_{ce} X\right]^{1/2}\right\}$$

where

$$X = - \frac{\omega_{pe}^2 \nu_{ce} \omega\left(\nu_{ch}^2 + \omega_{ch}^2\right)}{\omega_{ph}^2 \nu_{ch}} \left[1 - \frac{j\omega\left(\nu_{ch}^2 + \omega_{ch}^2\right)}{\omega_{ph}^2 \nu_{ch}}\right] - \omega\left(\nu_{ch}^2 + \omega_{ch}^2\right)$$

$$kV_{oe} = \frac{1}{2\left(\frac{V_{Te}^2}{V_{oe}^2}\right) j\nu_{ce}} \left\{ -\left(\nu_{ce}^2 + \omega_{ce}^2\right) \pm \left(\nu_{ce}^2 + \omega_{ce}^2\right) \left[1 - \frac{2\left(\frac{V_{Te}^2}{V_{oe}^2}\right) j\nu_{ce}}{\left(\nu_{ce}^2 + \omega_{ce}^2\right)^2} (X) \right] \right\}$$

Then

$$k_1 V_{oe} = \omega \left[1 + \frac{\omega_{pe}^2 \nu_{ce}\left(\nu_{ch}^2 + \omega_{ch}^2\right)}{\omega_{ph}^2 \nu_{ch}\left(\nu_{ce}^2 + \omega_{ce}^2\right)} \right] - j \frac{\omega^2 \omega_{pe}^2 \nu_{ce}\left(\nu_{ch}^2 + \omega_{ch}^2\right)^2}{\omega_{ph}^4 \nu_{ch}^2\left(\nu_{ce}^2 + \omega_{ce}^2\right)}$$

$$- j \frac{\omega^2 \left(\frac{V_{Te}^2}{V_{oe}^2}\right) \nu_{ce}}{\left(\nu_{ce}^2 + \omega_{ce}^2\right)} \left[1 + \frac{\omega_{pe}^2 \nu_{ce}\left(\nu_{ch}^2 + \omega_{ch}^2\right)}{\omega_{ph}^2 \nu_{ch}\left(\nu_{ce}^2 + \omega_{ce}^2\right)} \right]^2 \qquad (123)$$

$$k_2 V_{oe} = -\omega \left[1 + \frac{\omega_{pe}^2 \nu_{ce}\left(\nu_{ch}^2 + \omega_{ch}^2\right)}{\omega_{ph}^2 \nu_{ch}\left(\nu_{ce}^2 + \omega_{ce}^2\right)} \right] + j \frac{\left(\nu_{ce}^2 + \omega_{ce}^2\right)}{\left(\frac{V_{Te}^2}{V_{oe}^2}\right) \nu_{ce}} \qquad (124)$$

The complete solution for the electric field and ac velocity is

$$\begin{bmatrix} v_{ez} \\ v_{eh} \\ E \end{bmatrix} = \sum_{A_m=0}^{2} A_m \begin{bmatrix} \frac{\eta_e \nu_{ce}}{\left(\nu_{ce}^2 + \omega_{ce}^2\right)} \\ \frac{\eta_h \nu_{ch}}{\left(\nu_{ch}^2 + \omega_{ch}^2\right)} \\ 1 \end{bmatrix} e^{-jk_m z}$$

Matching the boundary condition $v_{ez} = 0$ at $z = 0$ and $v_{eh} = 0$ at $z = d$, once again we obtain

$$A_1 = \frac{1 - e^{-jk_2 d}}{e^{-jk_2 d} - e^{-jk_1 d}} A_0 \simeq -A_o$$

$$A_2 = \frac{1 - e^{-jk_1 d}}{e^{-jk_1 d} - e^{-jk_2 d}} A_o \simeq 0$$

The impedance is given by

$$Z = \frac{A_o d}{J_T A}\left[1 + \frac{\left(e^{-jk_1 d} - 1\right)\left(e^{-jk_2 d} - 1\right)}{\left(e^{-jk_2 d} - e^{-jk_1 d}\right)}\left(\frac{1}{-jk_2 d} - \frac{1}{-jk_1 d}\right)\right]$$

If $V_{Te} \to 0$, then the impedance Z once again approaches the value given in Eq. 101.

D. Summary: The impedance of a pseudolongitudinal wave has been calculated in the previous sections under different assumptions. In each case it is approximately equal to

$$Z = \frac{d}{A\left[j\omega\varepsilon + \sum_{i=e,h} \frac{\eta_i \rho_{oi} \nu_{ci}}{\nu_{ci}^2 + \omega_{ci}^2}\right]}\left[1 - \frac{e^{-j\theta} - 1}{-j\theta}\right] \qquad (101)$$

where

$$\theta = \frac{\omega}{V_{oe}} \left(1 + \frac{\eta_e \mu_e}{\eta_h \mu_h} \cdot \frac{1 + \mu_h^2 B_o^2}{1 + \mu_e^2 B_o^2} \right) d$$

It is quite similar to the space charge wave (longitudinal wave) case. However, in the pseudolongitudinal wave case, A is not the cross-sectional area of the sample. The reason is that the transverse magnetic field redistributes the plasma carriers to form a Suhl layer. Hence the quantities of A and ρ_{oi}'s have to be redefined and they are very difficult to evaluate. This complicates the quantitative comparison between theoretical and experimental impedance. However, a qualitative result can always be obtained.

3.7 The Effect of the Propagation Constant on the Interaction Impedance

As shown in previous sections, the complete solution for the electric field $\underset{\sim}{E}$ in the semiconductor can be generally written as

$$E = \sum_{i=0}^{n} A_i e^{-jk_i z} = A_o + \sum_{i=1}^{n} A_i e^{-jk_i z} \qquad (125)$$

where i = 0, $k_o = 0$ implies the steady-state solution. The k_i's (i = 1 to n) are the permitted propagation constants. The impedance is given by

$$Z = \frac{V}{J_T A} = \frac{1}{J_T A} \int_o^d E dz$$

$$= \frac{1}{J_T A} \int_o^d \sum_{i=0}^{n} A_i \, e^{-jk_i z} \, dz$$

$$= \frac{1}{J_T A} \left[A_o d + \sum_{i=1}^{n} \frac{e^{-jk_i d} - 1}{-jk_1 d} \left(A_i d \right) \right] \qquad (126)$$

The first term is the conventional impedance of a lossy capacitance. The remaining terms

$$\frac{1}{J_T A} \sum_{i=1}^{n} \frac{e^{-jk_i d} - 1}{-jk_i d} A_i d$$

are the incremental impedances due to the space-charge-wave effects or the propagating wave effects. In general the number of n's depends upon the mathematical model of the interaction system. And the A_i's (i = 1 to n) are the undetermined constants which depend upon the boundary conditions.

Usually there exists a significant propagating wave in the double-stream interaction system, excluding the steady-state solution. The remaining waves are less dominant and are heavily damped. As shown in previous sections, after matching the boundary conditions at the ends of the sample, only the dominant wave contributes large amounts of change in impedance while the remaining damped waves contribute very little. So the total impedance of Eq. 126 can be written approximately as

$$Z = \frac{1}{J_T A}\left[A_o d + A_i d\,\frac{e^{-jk_i d} - 1}{-jk_1 d}\right] \tag{127}$$

and

$$A_i \simeq - A_o$$

so

$$Z = \frac{A_o d}{J_T A}\left[1 - \frac{e^{-jk_i d} - 1}{-jk_1 d}\right] = \frac{d}{A\left[j\omega\varepsilon + \sum\limits_{i=e,h} \frac{\eta_i \rho_{oi}}{j\left(\omega - j\nu_{ci}\right)}\right]}\left[1 - \frac{e^{-jk_i d} - 1}{-jk_1 d}\right] \tag{128}$$

where

$$A_o = \frac{J_T}{j\omega\varepsilon + \sum\limits_{i=e,h} \frac{\eta_i \rho_{oi}}{j\left(\omega - j\nu_{ci}\right)}}$$

The dominant propagation constants k_i can be written as

$$k_i = k_{i1} + jk_{i2} \tag{129}$$

If k_{i2} is positive, the wave is a growing wave. If k_{i2} is negative, the wave is a decaying wave. Thus,

$$1 - \frac{e^{-jk_i d} - 1}{-jk_1 d} = 1 - \frac{e^{-j\left(k_{i1} + jk_{i2}\right)d} - 1}{-j\left(k_{i1} + jk_{i2}\right)d}$$

$$= 1 - \frac{1}{\left(k_{i1}^2 + k_{i2}^2\right)d}\left[k_{i2}\left(e^{k_{i2}d}\cos k_{i1}d - 1\right) + k_{i1}\, e^{k_{i2}d}\sin k_{i1}d\right]$$

$$- \frac{1}{\left(k_{i1}^2 + k_{i2}^2\right)d}\left[k_{i1}\left(e^{k_{i2}d}\cos k_{i1}d - 1\right) - k_{i2}\, e^{k_{i2}d}\sin k_{i1}d\right] \qquad (130)$$

This can be plotted in the complex plane for different values of k_{i1} and k_{i2} as shown in Fig. 3.4. This is a clockwise-spiral-like curve

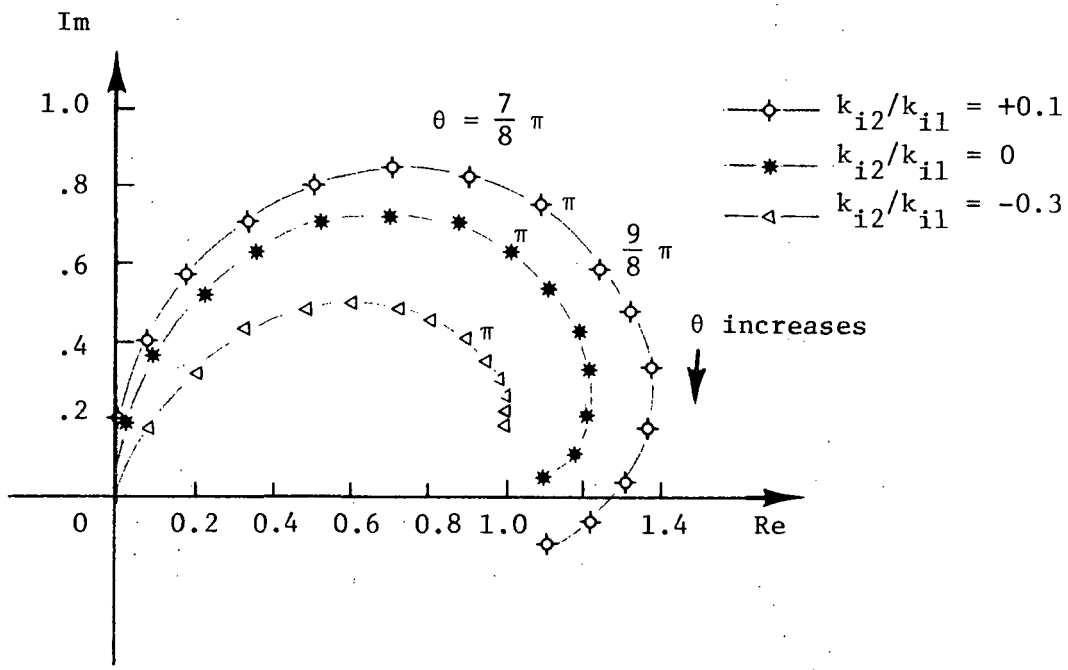

Fig. 3.4. The plot of $\left[1 - \frac{e^{-jk_i d} - 1}{-jk_i d}\right]$.

as $k_{i1}d$ increases for a fixed value of damping term k_{i2}. The larger the values of k_{i2}, the less the amplitudes of the spiral curves converge as $k_{i1}d$ increases. Since k_i is a function of frequency, drift velocities, and number densities of the carriers, changing these factors will change k_i and thus unveil the spiral-like impedance. This provides a relationship between the propagation constant and the measurable impedance. By comparing the measurable impedance and its theoretical value, we can predict the wave behavior in the semiconductor.

The value of $d/A\left[j\omega\varepsilon + \Sigma \frac{\eta_i \rho_{oi}}{j(\omega - j\nu_{ci})}\right]$ is almost a real number in the InSb case since $\omega << \nu_{ci}$. Then the total impedance is linearly proportional to the value of $\left[1 - \left(e^{-jk_i d} - 1\right)/(-jk_i d)\right]$. Presumably, the capacitance effect of the sample is sometimes large due to the inhomogeneous electric field distribution and the accumulation of charge at the contact, especially in the presence of the magnetic field. Then the value of $d/A\left[j\omega\varepsilon + \Sigma \frac{\eta_i \rho_{oi}}{j(\omega - j\nu_{ci})}\right]$ will be modified as a complex value $(a - jb)$, in which case the impedance becomes

$$Z = (a - jb)\left[1 - \frac{e^{-jk_i d} - 1}{-jk_i d}\right]$$

$$= c\, e^{-j\phi}\left[1 - \frac{e^{-jk_i d} - 1}{-jk_i d}\right] \qquad (131)$$

where

$$c = \sqrt{a^2 + b^2}$$

$$\phi = \tan^{-1} \frac{b}{a}$$

Under this situation, Z and $\left[1 - \left(e^{-jk_i d} - 1\right)/\left(-jk_i d\right)\right]$ are no longer in phase, which is physically reasonable for the space-charge-limited dielectric diode case.

3.8 Summary

The impedance concept can be applied to the longitudinal and pseudolongitudinal wave case, not to the transverse wave case. The theoretical impedances of a semiconductor plasma due to one-carrier and two-carrier stream interactions have been calculated. The results are summarized as follows:

A. The impedances due to one-carrier stream interactions are small and cannot be detected since the wave behaviors in this case are not prominent. The diode looks like a passive leaky capacitor.

B. The impedances due to two-carrier stream interactions are comparably large and detectable. The wave behaviors are quite prominent according to the two-carrier stream interaction model.

C. The impedance and the propagation constants are related to each other. An impedance measurement is feasible and a comparison of these will provide information about the wave behavior in the semiconductor. Impedance measurements provide a direct proof of the existence of space-charge waves.

D. The carrier diffusion velocities V_{Ti}'s and the hole drift velocity V_{oh} affect the propagation constants, which directly influence the impedance value.

E. The transverse magnetic field produces the Suhl layer, which complicates the impedance calculation. However, the qualitative result of the impedance for pseudolongitudinal waves can be predicted and is quite similar to the space-charge wave case.

IV. THE PHYSICAL PROPERTIES OF InSb

4.1 Introduction

The wave propagation characteristics and the impedance analysis based on a one-dimensional mathematical model have been discussed in the previous chapter. The dispersion relation mainly depends upon the physical parameters such as the number densities, diffusion constants, and mobilities of carriers, the external applied electric and magnetic fields, and the signal frequency. Once these factors are determined, the wave propagation constants can be predicted.

Since the carriers of InSb material have low effective masses ($m_e^* = 0.013\ m_o$, $m_h^* = 0.16\ m_o$, m_o is the free electron mass) and high mobilities ($\mu_e \simeq 50$ m/vs, $\mu_h = 1$ m/vs), InSb material has been considered to be the most prominent material for studying the semiconductor plasma effect. It is the objective of this chapter to determine these physical parameters which are critically important to the wave constants, and discuss some important effects which will affect the determination of these physical parameters in InSb material.

The material properties of InSb have been studied extensively since the early 1960's. It is impossible and not necessary to outline all the detail in this report. Only the important conclusions which are useful for the later work will be discussed. The description will not be in great detail, but brief and from a macroscopic point of view.

In this chapter, first the number densities of carriers (electron

and hole) will be discussed. Next the pinch effect and the mobilities and velocities of carriers will be studied. Finally miscellaneous effects such as contact effects and diffusion effects will be described.

4.2 The Determination of the Number Densities of Electrons and Holes in InSb

The number densities of electrons and holes in a semiconductor in thermal equilibrium is derived in most semiconductor textbooks.[29] The number density of electrons in the conduction band of a semiconductor crystal is given by

$$n_{eo} = 2\left(2\pi\ m_e^*\ kT/h^2\right)^{3/2}\ e^{\left(\mu\ -\ E_g\right)/kT} \qquad (132)$$

and the number density of holes in the valence band is given by

$$n_{ho} = 2\left(2\pi\ m_h^*\ kT/h^2\right)^{3/2}\ e^{-\mu/kT} \qquad (133)$$

where μ is the Fermi level and E_g is the energy gap, and the subscript o means under thermal equilibrium conditions.

Multiplying Eqs. 132 and 133 together, we obtain the interesting and important result that

$$n_{eo}\ n_{ho} = 4\left(2\pi\ kT/h^2\right)^3\ \left(m_e^*\ m_h^*\right)^{3/2}\ e^{-E_g/kT} \qquad (134)$$

---

[29] C. Kittel, *Introduction to Solid State Physics*, Third Edition, John Wiley and Sons, Inc., New York, 1968, pp. 300-331.

Thus we find that the product of the electron density and the hole density is a constant which depends on temperature, but not on the position of Fermi level. If an impurity semiconductor is doped with donor atoms, n_{eo} is large and n_{ho} is small. If it is doped with acceptor atoms, n_{ho} is large and n_{eo} is small. However, the total charge density within the semiconductor must remain zero.

When an external electric field is applied to an InSb sample through ohmic contacts, the injection effect occurs. It has been observed[30] in p-type InSb that the electrons are injected from a contact into p-type material due to the high mobility. They are driven by the applied field E_o to drift into the sample at their natural drift velocity $\mu_e E_o$. However, if only electrons were injected with n'_e comparable to the equilibrium density of holes n_{ho}, large fields would be produced inside the crystal because of space charge. Therefore a roughly equal number of compensating holes must be associated with the injected electrons in order to conserve space-charge neutrality. These holes may receive energy from the same contact as the electrons or from the region of the crystal surrounding the contact, in which case they are ultimately replaced from the opposite contact. There results a neutral electron-hole plasma moving down the crystal.

The total current I_T is the sum of the ohmic current I_Ω and the injected plasma current I'.

---

[30] B. Ancker-Johnson, R. W. Cohen, and M. Glicksman, "Properties of Injected Plasmas in Indium Antimonide," *Physical Review*, Vol. 124, December 1961, pp. 1745-1753.

Assuming that

$$n_e = n_{eo} + n_e' \simeq n_e' \tag{135}$$

$$n_h = n_{ho} + n_h' \tag{136}$$

$$n_e' = n_h' = n' \tag{137}$$

$$b = \mu_e/\mu_h \tag{138}$$

Then we have

$$I_\Omega = e\left(n_{eo}\ \mu_e\ E_o + n_{ho}\ \mu_h\ E_o\right)A$$

$$\simeq en_{ho}\ \mu_h\ E_o\ A \tag{139}$$

$$I' = e\left(n_e'\ \mu_e\ E_o + n_h'\ \mu_h\ E_o\right)A$$

$$= en'\ \mu_h\ E_o\ (1 + b)\ A \tag{140}$$

$$I_T = I_\Omega + I'$$

$$= en_{ho}\ \mu_h\ E_o\ A\left[1 + (b + 1)\ n'/n_{ho}\right] \tag{141}$$

where n_e', n_h' are the injected densities of electrons and holes, and A is the cross-sectional area of the p-type material. Thus the injection ratio n'/n_{ho} can be determined by

$$\frac{n'}{n_{ho}} = \left[\frac{I_T}{en_{ho}\,\mu_h\,E_o\,A} - 1\right] \cdot \frac{1}{b+1}$$

$$= \left[\frac{I_T - I_\Omega}{I_\Omega}\right] \cdot \frac{1}{b+1} \qquad (142)$$

Once the injection ratio is obtained, the number densities of the sample are determined.

In order to obtain reasonably uniform plasma distribution throughout a crystal, it is vitally important that the lifetime of the plasma exceed the time required for the plasma front to traverse the sample. The traversal time for a 1 mm long p-InSb sample is about 15 nsec at the maximum velocity and twice that time with 100 V/cm applied electric field. The measured lifetime of the injected plasma is 1 μsec through a plasma density range of 1×10^{12} to 2.5×10^{13} cm^{-3}. If the lifetimes were as short at the higher density as at the lower, plasma experiments would be very difficult to perform.

If the external electric field reaches the breakdown region at about 400 V/cm, the injected carriers become energetic enough to excite additional electron-hole pairs by impact ionization. In this case the current rises very steeply. The electron and hole densities still can be determined by Eqs. 135-142. This density, however, cannot be controlled as can the injected plasma density. Also, impact-ionization plasma usually undergoes pinching† promptly after production

† The pinch effect will be discussed later in this chapter.

so that their density distributions are unknown and essentially uncontrollable.

Furthermore injection in n-type material is also possible, but it is not as strongly affected as was the case in p-type material[31] since the injected carriers are holes. It is reported[32] that it is not possible to produce an injected plasma of significant density in samples with the donors or acceptors much larger than 2×10^{16} cm^{-3}.

If an external magnetic field is present across the sample (longitudinally or transversely), the conductivity characteristics of the injected plasma are drastically modified. Either field, if large enough, flattens the humps in the I-V curves that are caused by injection. Unless the electric field is high enough to produce avalanche breakdown, the transverse field sweeps the injected carriers to the surface where they recombine. Thus a fraction of the injected carriers are lost by recombination. The longitudinal field also sweeps the injected carriers to the surface because of an increased radial diffusion of the injected carriers.

4.3 Pinch Effect

In 1934 Bennett[33] introduced the concept of current pinching

---

[31] M. Glicksman and W. A. Hicinbotham, "Hot Electrons in Indium Antimonide," *Physical Review*, Vol. 129, February 1963, pp. 1572-1577.

[32] B. Ancker-Johnson, R. W. Cohen, and M. Glicksman, *op. cit.*

[33] W. H. Bennett, "Magnetically Self-Focusing Streams," *Physical Review*, Vol. 45, June 1934, p. 890.

in electron-ion plasmas. With the assumption of an isotropic plasma possessing charge neutrality with more massive positive than negative carriers, a simple theory was developed[34] to predict the critical or minimum current I_c required for the onset of pinching. The critical current is given by

$$I_c = \frac{2c^2k(T_e + T_h)}{eV_{ez}} \simeq 2 \times 10^9 \frac{T_e + T_h}{V_{ez}} \text{ ampere} \qquad (143)$$

where T_e and T_h are the mean kinetic temperatures of the electrons and holes expressed in eV, and V_{ez} is the constant drift velocity of the electrons expressed in cm/sec.

The occurrence of pinching in a solid was first deduced by Glicksman and Steele[35] from conductivity measurements on a plasma produced by impact ionization in n-InSb at 77° K, and was verified by Chynoweth and Murray.[36] The pinch effect was also extensively studied in plasmas produced by injection into p-InSb. Both sets of experimental results represent good agreement between observations and theory. In the presence of a pinch, current would no longer be proportional to current density, and the I-V curve would rise less

---

[34] L. Spitzer, Jr., *Physics of Fully Ionized Gases*, Interscience Publishers, New York, 1956, p. 41.

[35] M. Glicksman and M. C. Steele, "Plasma Pinch Effects in Indium Antimonide," *Physical Review Letters*, Vol. 2, June 1959, pp. 461-462.

[36] A. G. Chynoweth and A. A. Murray, "Pinch Effect in Indium Antimonide," *Physical Review*, Vol. 123, July 1961, pp. 515-516.

steeply than a curve of current density versus voltage. This slowness is enhanced by increased electron-hole scattering due to the high carrier density characteristics. However, the theory does not yield the pinch radius. Thus the actual plasma density and its distribution after the production of pinching is very difficult to predict and essentially uncontrollable.

The presence of both longitudinal and transverse magnetic fields would destroy or inhibit the pinch effect and change the plasma density. And, furthermore, the longitudinal magnetic field would produce the helical instability observed by Glicksman[37] which makes the plasma density random and unestimatable.

4.4 Mobilities and Velocities

The mobilities of InSb are sensitive to the total carrier concentration. For lower doping levels, the mobility is determined principally by scattering by the lattice vibrations. At higher doping levels, however, scattering by ionized impurity atoms becomes increasingly important. The mobilities versus the total carrier concentrations at 77° K for n- and p-type materials are plotted in Figs. 4.1 and 4.2 which were constructed by workers at the Battelle Memorial Institute.[38]

In the presence of an applied electric field, the charge

---

[37] B. Ancker-Johnson, R. W. Cohen and M. Glicksman, *op. cit.*

[38] R. K. Willardson and H. L. Goering, *Compound Semiconductors*, Vol. I, Reinhold Publishing Corporation, New York, 1962, p. 227.

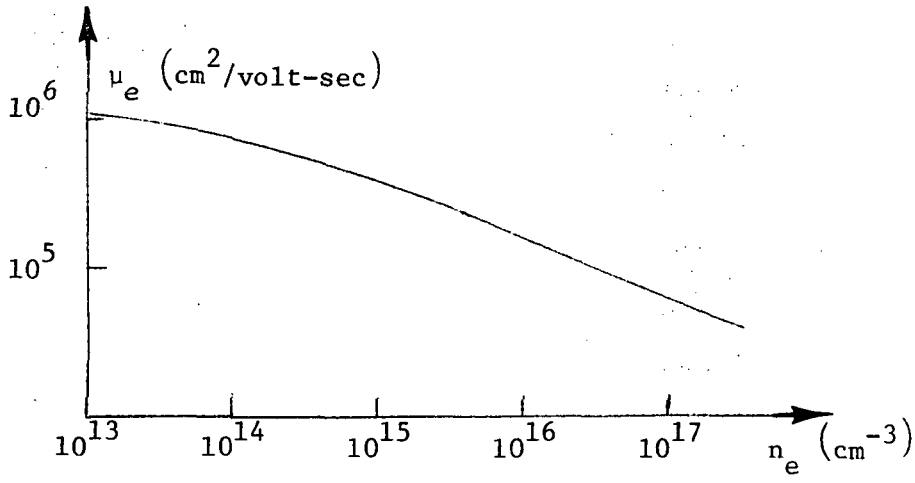

Fig. 4.1. The curve of μ_e versus n_e.
(After Battelle Memorial Institute)

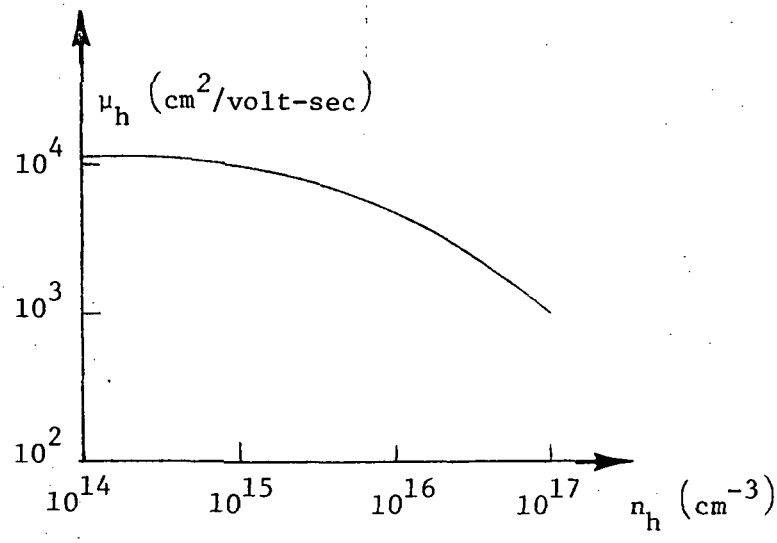

Fig. 4.2. The curve of μ_h versus n_h.
(After Battelle Memorial Institute)

carriers (electrons or holes) acquire a drift velocity. At lower applied electric fields, the drift velocities V_{oi} are linearly proportional to the electric field E_o, the charge carriers are principally scattered by acoustical modes of vibration. At higher values of electric field, the drift velocities increase much less rapidly with increase in the applied field and the drift velocities

are said to become saturated. These saturations are caused by excitation of optical modes of vibration by charge carriers. Pulsed measurements of the Hall voltage in InSb at 77° K allow calculation of the electron drift velocity as a function of the applied electric field. Such experiments were first performed by Glicksman and Hicinbotham.[39] These have been repeated in our laboratory.[40]

Their results of the drift velocities as a function of electric field at different magnetic fields agree qualitatively with each other and are plotted in Fig. 4.3. The saturation value of drift velocity as a function of magnetic field is shown in Fig. 4.4.

The drift velocity with no transverse magnetic field or with a purely longitudinal magnetic field condition is impossible to measure by using Hall effect measurements. Its velocity behavior can only be properly assumed. At lower values of electric field, the carrier velocity is still believed to be linearly proportional to the electric field. While at higher values of electric field, its value is quite difficult to estimate.

4.5 Contact Effects and Diffusion Effects

The contacts of the samples have a strong influence on the nature of the plasma. This was first noted by Eidson and Kino.[41] The

---

[39] M. Glicksman and W. A. Hicinbotham, "Hall Drift Velocity at High Electric Fields in InSb," *Proceedings of the Symposium on Plasma Effects in Solids*, Paris, France, 1964; published by Dunod, Paris, 1965, pp. 137-146.

[40] K. B. Verma and O. P. Gandhi, private communication.

[41] J. C. Eidson and G. S. Kino, "A New Type of Oscillation in InSb," *Applied Physics Letters*, April 1966, pp. 183-185.

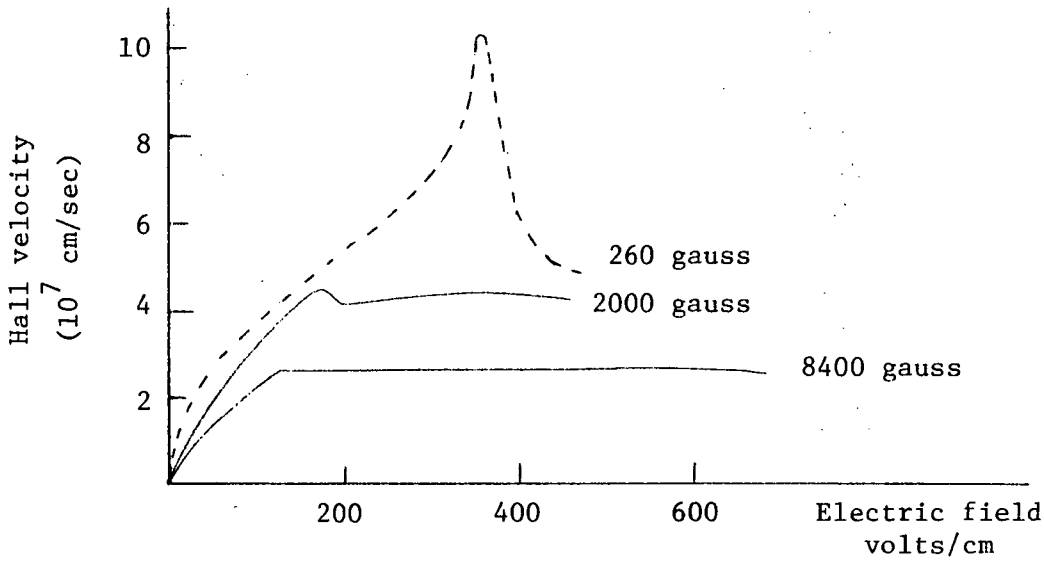

Fig. 4.3. Drift velocity as a function of electric field.
(After M. Glicksman and W. A. Hicinbotham)

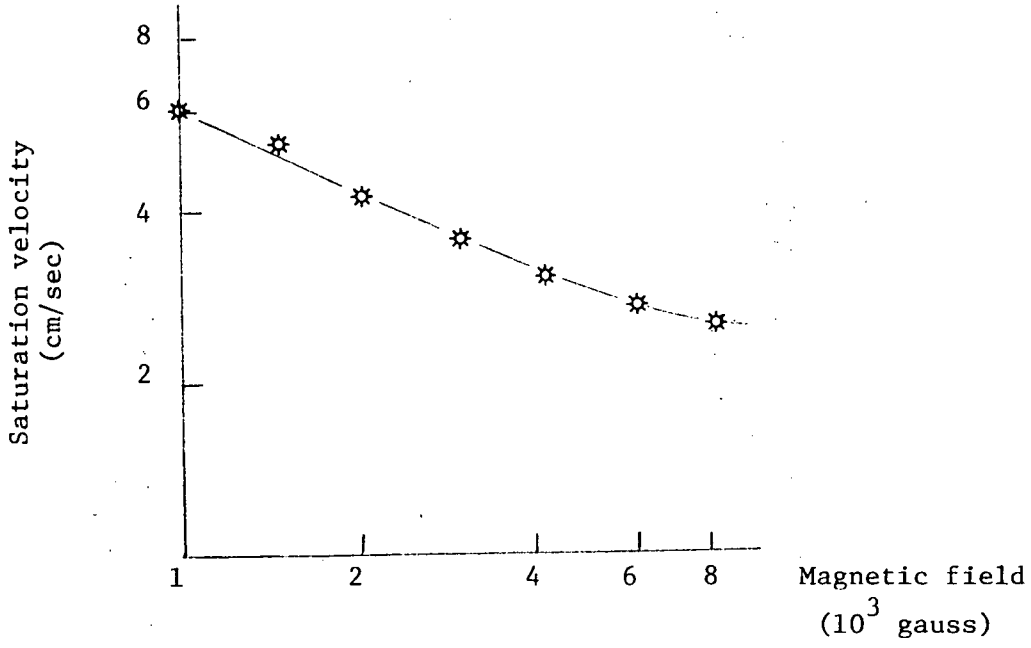

Fig. 4.4. Saturation velocity.
(After Glicksman and Hicinbotham)

samples with different contacts (indium contact on tin contact) have different I-V characteristic curves and different threshold conditions for microwave emission. To investigate the role of the contacts, Kino used a probe to measure the voltage drop along the sample. He showed that an electric-field inhomogenity appeared near the contact, especially in the presence of a transverse or longitudinal magnetic field. However, the samples with low-resistance indium contacts will presumably reduce the inhomogenity of the electric field.

Glicksman and Hicinbotham[42] reported that the ratio of drift to thermal velocity could be as high as 1.5. This suggests the use of the hydrodynamic force equation, which treats the thermal diffusion effect as a perturbation term. The use of the hydrodynamic force equation of a plasma is a rather convenient method to solve the wave propagation problem; however, it does not predict several important properties, such as Landau damping. A better approach which resolves these problems is to use the Boltzman velocity distribution function. This is the most difficult method of attacking the problem, and it will be left for future research.

4.6 Summary

For a uniform and controllable plasma, the pinch effect must be avoided, the helical instability must be excluded, the low-resistance contact must be used. Under such conditions, the number densities,

---

[42] M. Glicksman and W. A. Hicinbotham, *op. cit.*

mobilities, and velocites of carriers can be properly estimated. Consequently the wave behavior in the semiconductor plasma is possible to predict and then the theoretical impedance can be calculated.

V. EXPERIMENTAL WORK

The purpose of the experimental work described in this chapter is to measure the interaction impedance of InSb semiconductor plasmas in the presence of electric field and a magnetic field. The theory predicts that the impedance change due to a two-stream interaction is detectable, so the experimental results can be related to the theory more or less.

5.1 Preparation of the Samples

The InSb samples used in the experimental work were cut from two different doped single crystals supplied by Asarco Intermetallics Corporation. Their physical parameters are:

A. N-type InSb single crystal Is59 with an electron concentration n_e of about 1.1×10^{13} cm^{-3}, a mobility μ_e of 3.28×10^5 cm^2/volt-sec, and a resistivity $1/\sigma$ of 2 ohm-cm.

B. P-type InSb single crystal with $n_h = 3.35 \times 10^{14}$ cm^{-3}, $\mu_h = 9{,}647$ cm^2/volt-sec and $1/\sigma = 0.22$ ohm-cm.

The samples were cut by the wire saw with a cross section of about 0.3 mm x 0.3 mm and with a length of 0.3 mm to 1 mm. Then each sample was dipped in CP4 solution at room temperature for one second to provide a better surface condition. CP4 etchant is composed of one part by volume HF (48 percent), two parts by volume HNO_3 (70 percent), and one part by volume CH_3COOH (glacial). Then the samples were soldered by indium solder (solder No. 2) and indium flux (flux No. 5), obtained from Indium Corporation of America, on 50 mil copper posts.

A 1.5 mil gold wire was soldered on the other end of each sample using same kind of indium solder and flux. All the processes were done in an air atmosphere. Since the melting point of InSb is about 523° C, there was a wide range of allowable temperatures for melting the solder without damaging the crystal. The samples could not be made much shorter than about 4 mils in length because the solder diffused completely through the crystal.

5.2 Impedance Measurement at Microwave Frequency Range

5.2.1 Setup

The sample which was prepared as described in Section 5.1 was inserted as an inductive post in the center of a long armed X-band waveguide as shown in Fig. 5.1. The waveguide was ended by a short or a termination. The copper post served as one lead for the applied voltage as well as a heat sink. The other applied voltage lead is the 1.5 mil gold wire which passes through the waveguide hole and is isolated from the waveguide so that it does not contact the waveguide wall. Then the whole waveguide is lowered in a liquid nitrogen dewar which is located in a Varian two-inch electromagnet gap. The magnet is capable of producing a magnetic field of 15 k gauss at an exciting current of 165 amperes. We also pressurized the waveguide to prevent liquid N_2 vaporation inside the waveguide. A 2 μs width and 5 pps or 10 pps high-current pulser is used to prevent sample heating. So the experiments were operated quite stably in liquid nitrogen (77° K) temperature as shown in Fig. 5.2.

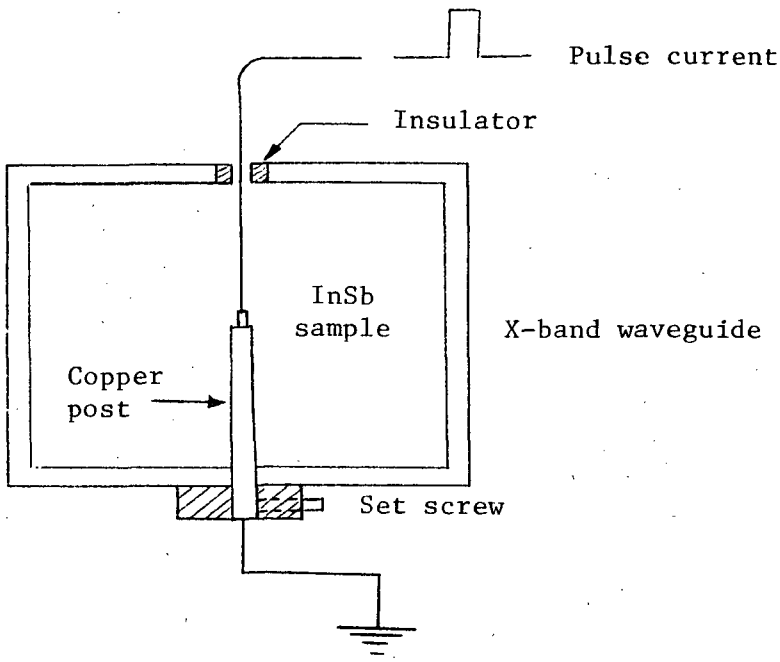

Fig. 5.1. The mounting of InSb sample in the waveguide.

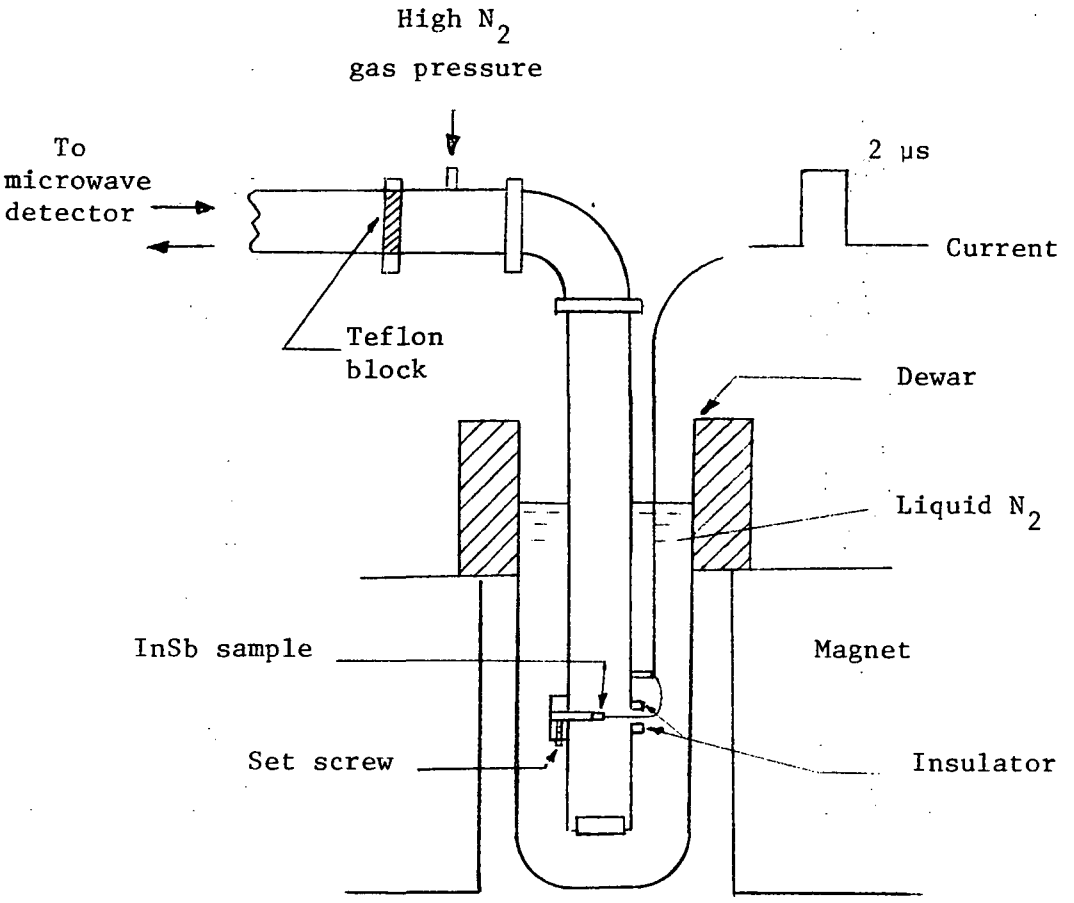

Fig. 5.2. Experimental setup.

The microwave impedance was measured by the standing-wave-ratio and the position of a voltage minimum. The whole experimental arrangement is shown in Fig. 5.3. Two x-band attenuators were used. One which could change the microwave input power was inserted between the klystron and the slotted waveguide. The other one was inserted between the sample waveguide and the detector, and was used to verify that the InSb was producing microwave effects on the detector.

A dummy sample with the resistance approximately equal to the

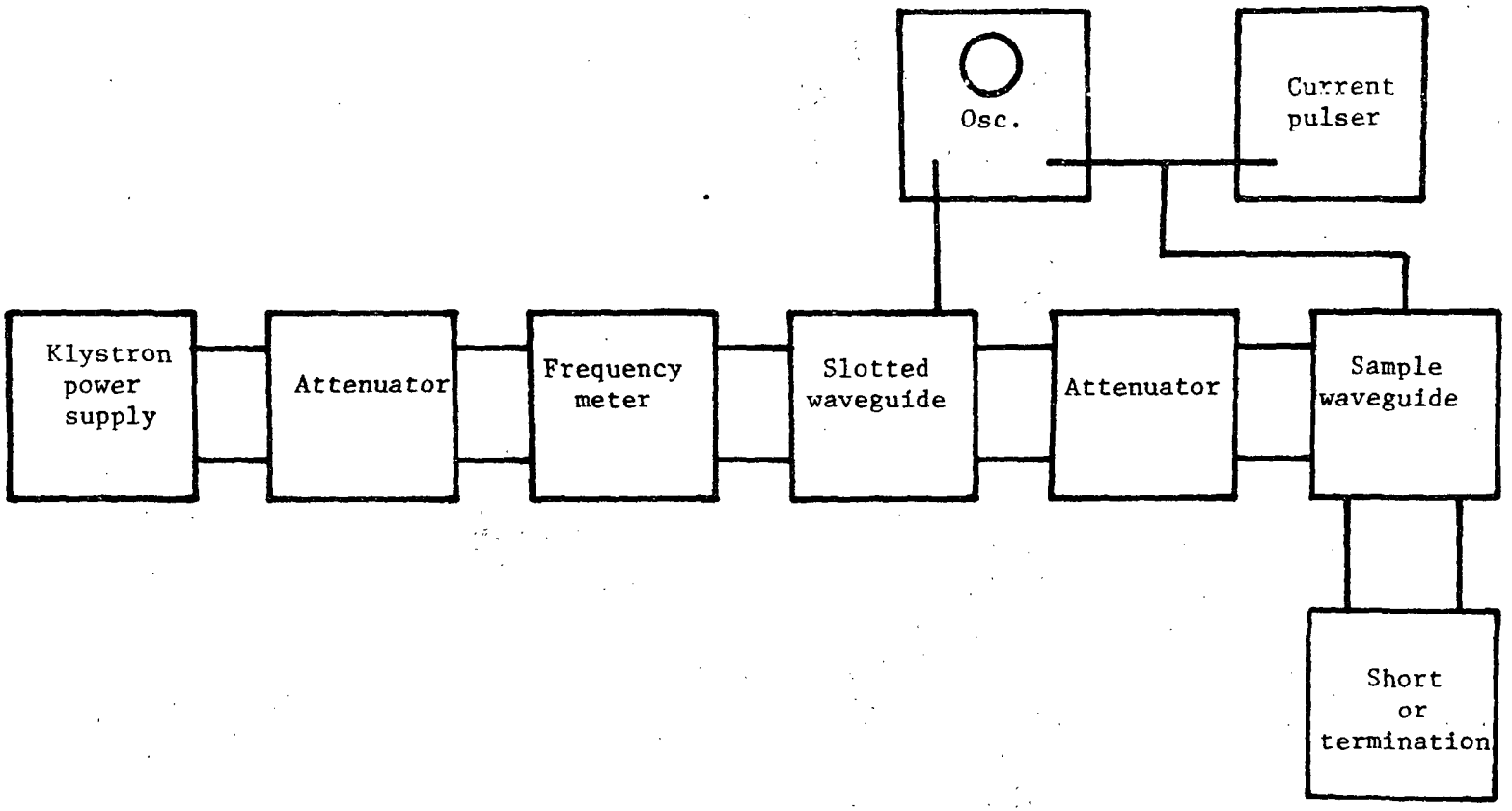

Fig. 5.3. The experimental setup for impedance measurement.

sample was prepared also. By replacing the InSb sample, the dummy sample could be used to test the circuit and make sure any observed effects were produced by the InSb and not by some sort of pickup.

The klystron oscillator generated a CW signal with frequencies in x band, and the detector probe was connected to an oscilloscope. By moving the position of the probe in the slotted waveguide, we were able to measure the SWR and the position of the voltage minimum, and then we could calculate the impedance.

5.2.2 Measurement and Observation

In order to have a better understanding of the InSb samples, the I-V characteristics were first measured. The results are plotted in Figs. 5.4 and 5.5.

In both figures the I-V characteristic curves show how the injected plasma and the pinching affect the linearity of I-V curves. The threshold field for avalanche breakdown is about 300-400 V/cm. The parallel magnetic field eliminates the pinching effect and the injection effect quite prominently as the previous chapter predicts. These data are quite good compared with some authors' results.[43] From the previous chapter it is very easy to estimate the number densities or injection ratio.

In addition, the low-frequency current (or voltage) oscillation was observed in p-type InSb (Is56) in the presence of a longitudinal magnetic field of 4.6 kG as shown in Fig. 5.6. The threshold voltage

---

[43] B. Ancker-Johnson, R. W. Cohen, M. Glicksman, *op. cit.*

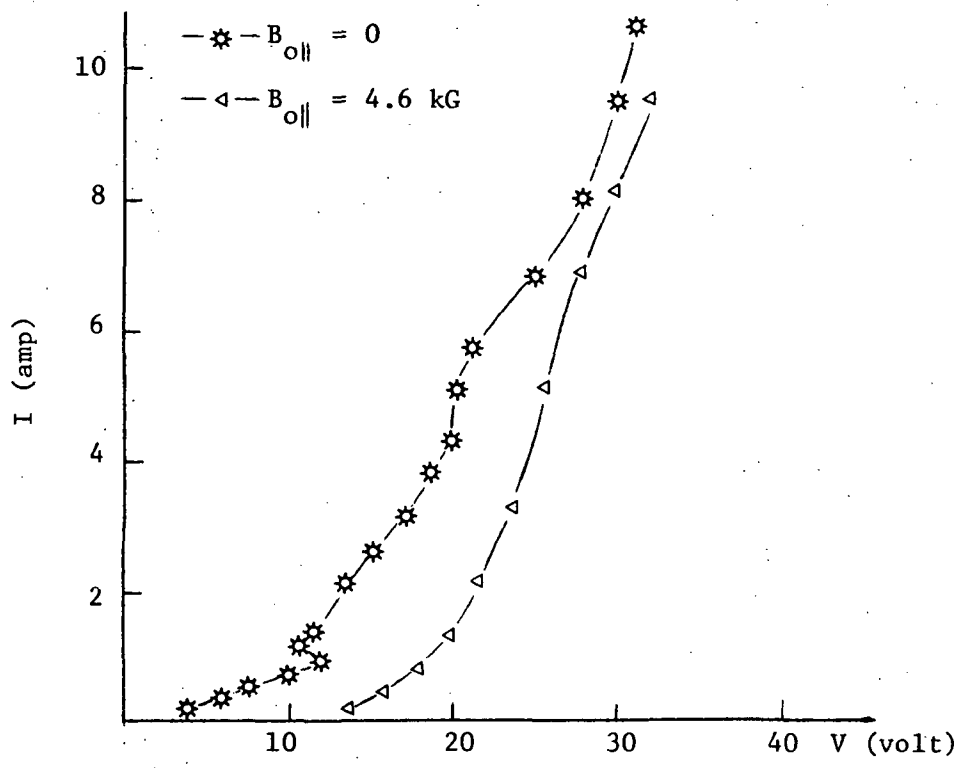

Fig. 5.4. V-I curves of n-InSb Is59 with dimensions of 0.5 x 0.4 x 0.4 mm^3.

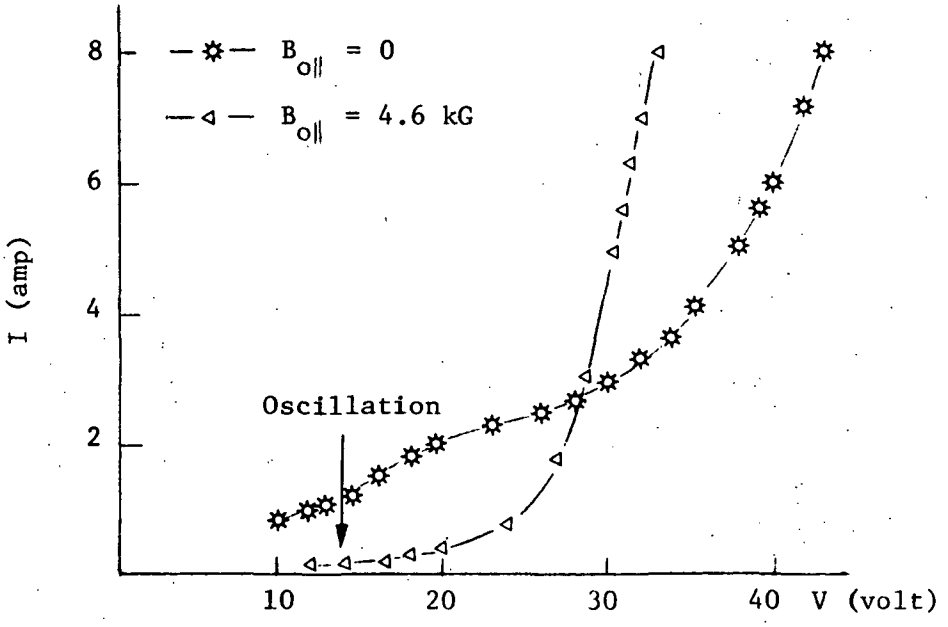

Fig. 5.5. V-I curves of p-type InSb Is56 with dimensions (36 x 10 x 12 mil^3) (0.9 mm x 0.25 mm x .3 mm).

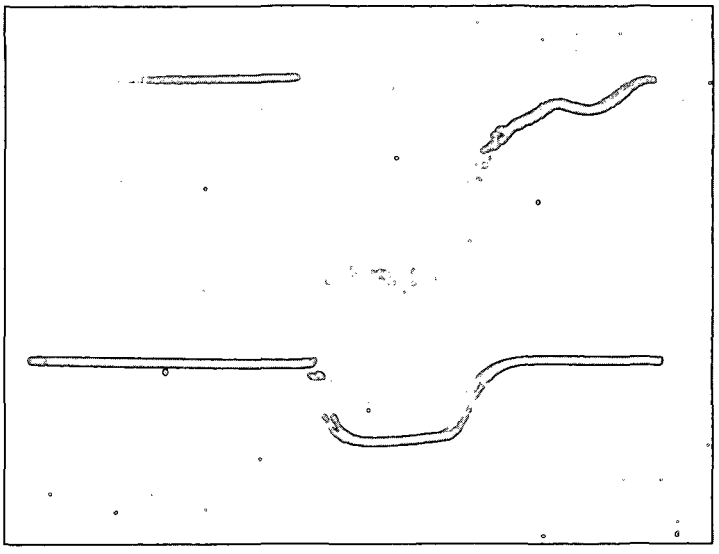

Fig. 5.6. The oscillation of Is56, B_o = 4.6 k gauss. The upper trace is voltage 10 V/cm; the lower trace is current 4 amp/cm.

varied with magnetic field strength. The threshold condition of the low-frequency instability is plotted in Fig. 5.7. The frequency of the oscillation is about 10-40 MHz. This low-frequency instability of the p-type (Is56) InSb sample is interpreted as the instability of the drifted helical waves and was first observed in p-type InSb by Ancker-Johnson and Glicksman in 1961 and was called a standing hydromagnetic wave at that time. The application of a moderate longitudinal magnetic field B_o ($B_o > B_{threshold}$) enhances the amplitude of the oscillations as expected if a helical hydromagnetic wave grows. Further increasing the longitudinal magnetic field B_o produced an oscillation that was no longer coherent. Several superimposed modes with different

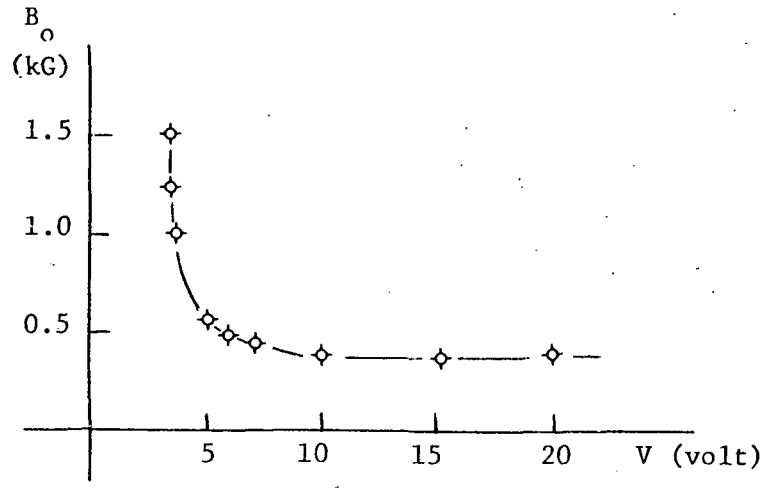

Fig. 5.7. Dependence of threshold magnetic fields on voltage across sample for the helical instability.

frequencies were observed. Furthermore the orientation of the magnetic field also affects this low-frequency oscillation. As shown in Fig. 5.8, the oscillation amplitude is a function of magnetic field orientation. Since this helical instability causes oscillation in the sample, and it will seriously influence the impedance measurement (especially at RF range), the impedance measurement must be carefully treated.†

Observation of Impedance Change Due to the Drifting Pulsed Current

The theoretical impedance of a semiconductor plasma under a drifting field has been calculated in the previous chapter. It is a function of the dc field, signal frequency, etc. When a pulsed

† In the RF range, the existence of the helical instability will rule out the possibility of measurement on impedance.

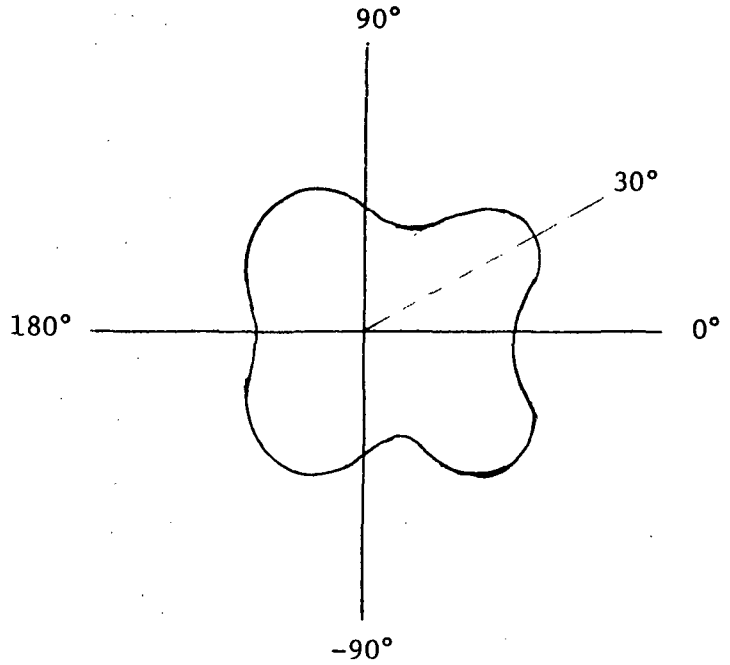

Fig. 5.8. Polar plot of oscillation amplitude versus B_o at a fixed value of current.

current is applied to the sample, the impedance change due to the pulsed current should be observed from the detecting probe in the slotted waveguide. The actual experimental observation from the oscilloscope is shown in Fig. 5.9 as predicted. The magnitude of the dip or the peak in the detector voltage changes sinusoidally as the probe position moves or the signal frequency changes. Also increasing the pulsed voltage (current) changed the magnitude from upward to downward if the detector was fixed, as shown in Fig. 5.10. Increasing the attenuation with either attenuator in the system caused the dip or peak shown on the oscilloscope to die out. This establishes that the dip or peak is actually a microwave effect.

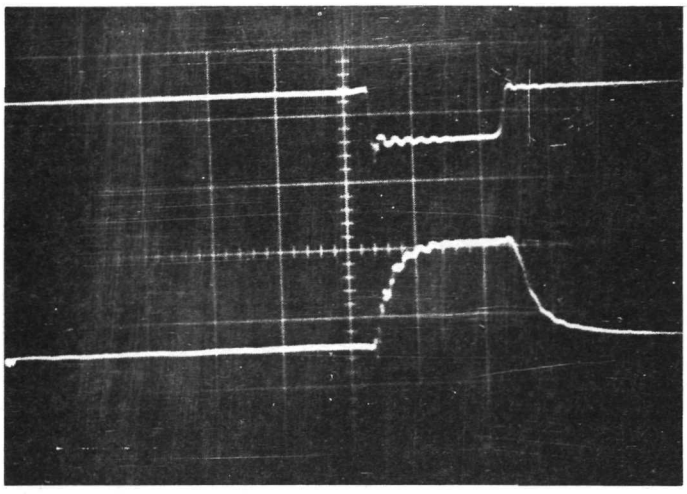

Fig. 5.9. The upper trace is current, 1 amp/cm; the lower trace is detector voltage, 10 mV/cm; time is 1 μs/scale, $B_o = 0$.

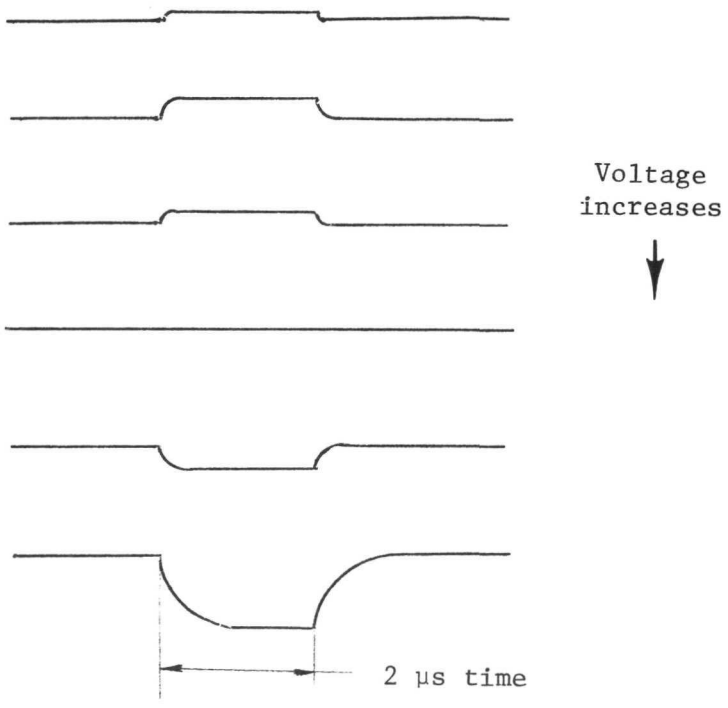

Fig. 5.10. Detector voltage.

The transformed impedance can be measured at the slotted waveguide by measuring the SWR during the 2 μsec period and recording the minimum voltage position. The actual impedance of the sample must be found by some kind of transformation according to transmission-line theory. The actual equivalent circuit for the experimental setup can be drawn as shown in Fig. 5.11.

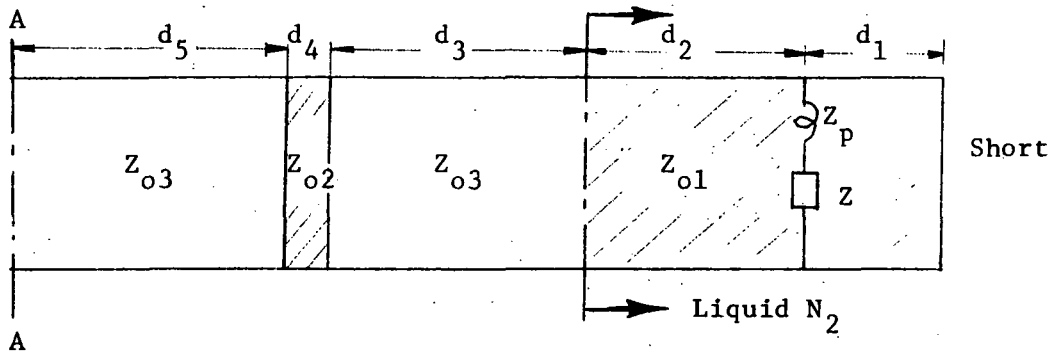

Fig. 5.11. The equivalent circuit of the experimental setup where:

d_1 = the distance from the short to the sample post

d_2 = the distance from the sample post to the liquid nitrogen surface

d_3 = the distance from the liquid nitrogen surface to the teflon block

d_4 = the thickness of the teflon block

d_5 = the distance from teflon to the slotted waveguide

Z_{o3} = the characteristic impedance of waveguide in free air space

Z_{o2} = the characteristic impedance of waveguide in teflon medium

Z_{o1} = the characteristic impedance of waveguide in liquid nitrogen medium

Obtaining the actual impedance of the sample requires several

cumbersome transformations. As a matter of fact, the distances are quite hard to measure precisely and furthermore the liquid nitrogen is vaporizing during the experimental process. These factors affect the precision of the impedance calculation.† Even the measured impedance at the slotted waveguide is quite inconsistent. Experience indicates that a small change in distance causes a large phase shift in the calculation, and that is inevitable. Due to these difficulties, consistent data are hard to obtain.

Observation of a Relaxation Effect in p-InSb Material by a Microwave Technique

In the process of the impedance measurement, a delay relaxation phenomenon was observed when the pulsed current exceeds a certain value of current. This threshold current is above the impact ionization current. This relaxation effect is magnetic field sensitive; the application of a very small longitudinal magnetic field (about 200 gauss) significantly reduces the effect. The typical waveforms are given in Fig. 5.12. The relaxation time is a function of pulsed current. The higher the current, the longer the delay time. The relation can be plotted in Fig. 5.13.

Several samples with different cross sections were tested to study their threshold conditions. The results can be illustrated by Table 5.1.

---

† The effect of vaporization on the phase shift can be eliminated by immersing the detecting probe in the liquid nitrogen if the detecting probe can stand such low temperatures with correct calibration.

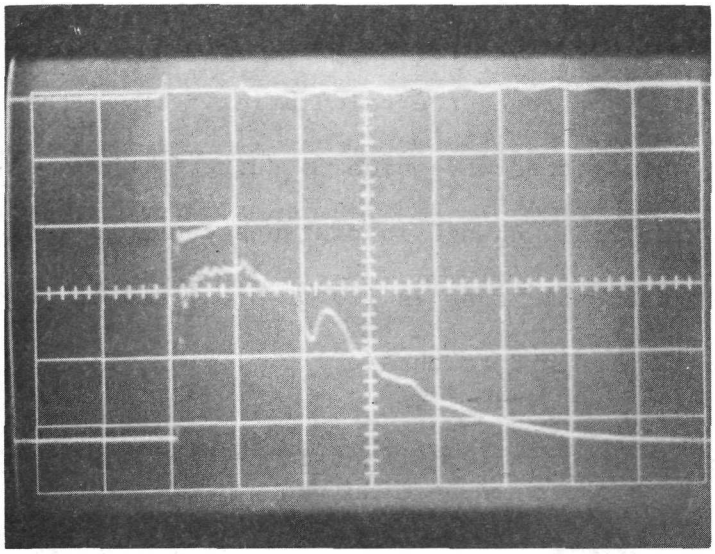

No B_o

Current
4 A/div

Detector
voltage
10 mV/div

Time 2 μs/cm

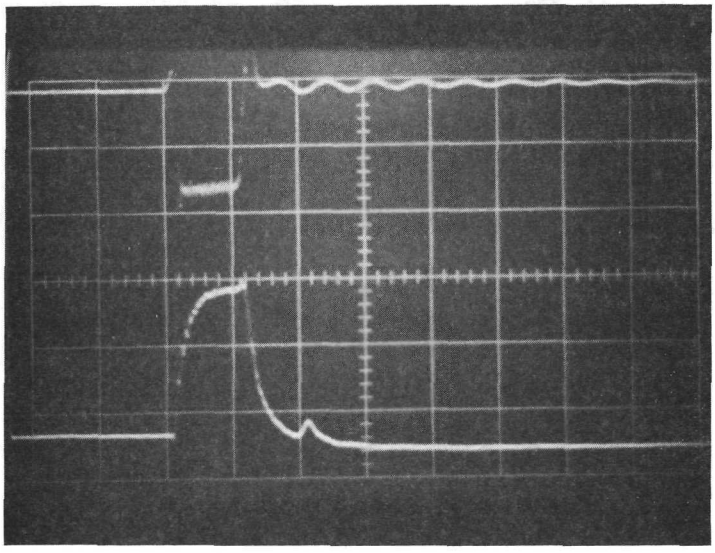

Strong
B_o

Current
4 A/div

Detector
voltage
10 mV/div

Time 2 μs/cm

Fig. 5.12. Microwave relaxation effect.

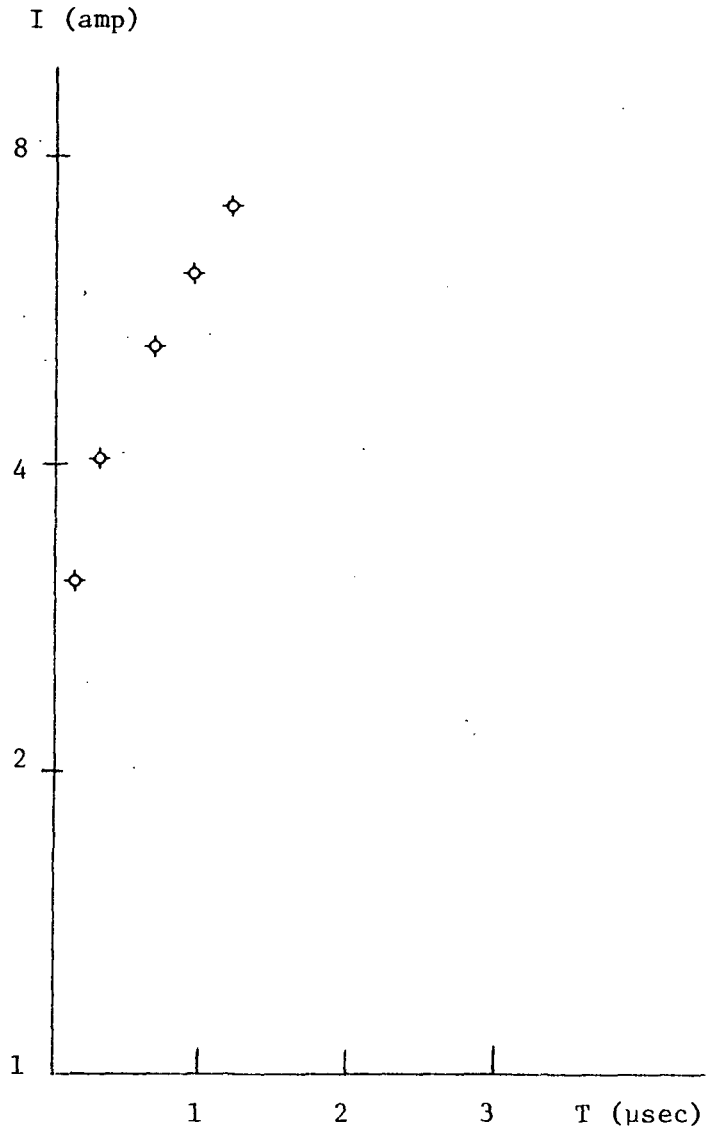

Fig. 5.13. The experimental relation between the recombination time and the initial current where T is delay time observed in the microwave detecting probe after the pulsed current is applied.

Table 5.1. Threshold condition.

Cross section	I_{th} Threshold current	$J_{th} = I_{th}/A$
10.0×11.6 mil^2	2.3 amp	1.98×10^{-2} A/mil^2
13.6×13.5 mil^2	3.5 amp	1.92×10^{-2} A/mil^2
14.0×18.4 mil^2	4.6 amp	1.80×10^{-2} A/mil^2

It seems that the cross sections have nothing to do with the relaxation effect, but it is current density that is important. This effect might be explained by the recombination process of the excess carriers. If the voltage across the sample is above the avalanche breakdown voltage, impact ionization occurs. The voltage (or the electric field) creates electron-hole pairs which then drift, according to the applied field, to produce a large impact ionization current. This current is proportional to the number of electron-hole pairs according to the equation

$$J_o = \left(n|e|\mu_e + p|e|\mu_h\right) E$$

where n and p are the number densities of electrons and holes, and usually $n \simeq p$ in the impact ionization region.

After the voltage pulse is gone, these excess carriers stop drifting and start recombining to produce the equilibrium state. The recombination is characterized by a life time τ. We have

$$\frac{dn}{dt} = -\frac{1}{\tau_n}\Delta n \tag{144}$$

$$\frac{dp}{dt} = -\frac{1}{\tau_p}\Delta p \tag{145}$$

In the impact ionization region, $\tau_n = \tau_p$. Since $\Delta n = n(t) - n_o$, Eq. 144 can be written as

$$\frac{dn(t)}{dt} = -\frac{1}{\tau}\left[n(t) - n_o\right] \tag{146}$$

Solving Eq. 146, we obtain

$$n(t) = \left[n(o) - n_o\right] e^{-t/\tau} + n_o \tag{147}$$

where n_o is the steady-state number density, n(t) is the unequilibrium-state number density, and n(o) is the initial number density. Obviously more time is needed for more excess carriers to return to the equilibrium state.

In our experimental work, the delay time we measured is the recombination time required for these excess carriers. If we plot current versus recombination time in the semilogarithm coordinate, as shown in Fig. 5.13, we find that it has a linear slope of about 0.24; i.e., $\Delta \log I = 0.24 \times 10^6\ \Delta t$. Comparing with Eq. 147[†] $\Delta \log n = \Delta t/\tau \log e$ and $\Delta \log I = \Delta \log n$. So,

---

[†] We assume that $n_o << n(t)$ and $n(o)$.

$$\tau = \frac{\log e \times 10^{-6}}{0.24} = 1.8 \times 10^{-6} \text{ sec}$$

Thus this kind of calculation consequently gives a recombination life time of 1.8×10^{-6} sec which quite agrees with Ancker-Johnson's observation.[44]

So far, the recombination mechanisms are still obscure. This technique appears to provide a direct observation of these effects and contributes qualitative and quantitative data. However, this will not be pursued in this report.

5.2.3 Summary

From previous work we obtained that the propagation constant in a drifting semiconductor plasma was approximately equal to

$$k = \frac{\omega}{u_o}\left[1 + \frac{n_e \mu_e}{n_h \mu_h}\right] \tag{148}$$

and the guide wavelength was

$$\lambda = \frac{2\pi}{k} = \frac{u_o}{f\left[1 + \frac{n_e \mu_e}{n_h \mu_h}\right]} \tag{149}$$

Suppose n_e, n_h, μ_e, μ_h, and u_o are unchanged, then wavelength λ is

---

[44] B. Ancker-Johnson and W. P. Robbins, "Dynamic and Steady-State Injection of Electron-Hole Plasma in p-type InSb," *Journal of Applied Physics*, Vol. 12, February 1971, pp. 762-773.

inversely proportional to the frequency f. In other words, the higher the applied frequency, the shorter the guide wavelength in semiconductor plasma.

If we assume $u_o = 5 \times 10^7$ cm/sec, $f = 10^{10}$ cps, $n_e = n_h$ (at breakdown region), and $\mu_e/\mu_h = 50$ in InSb, then, from Eq. 149, $\lambda \simeq 10^{-4}$ cm $\simeq$ 1 micron.

The shortest sample which can be made at our laboratory is about 7 mils (180 microns). Thus it is still approximately on the order of one hundred plasma wavelengths long at microwave frequency range. From the impedance point of view, this microwave measurement would not make any significant indication of the wave propagation behavior in a plasma. In other words, this measurement of impedance is very hard to correlate with the propagation constant k.

Furthermore the skin effect plays an important role (the first-order effect) at this microwave frequency range. The skin depth is

$$\delta = \frac{1}{\sqrt{\pi f \mu \sigma}} \tag{150}$$

where

$$\mu \text{ (permeability)} = 4\pi \times 10^{-7} \text{ henries/m}$$

$$\sigma \text{ (conductivity)} = n_e e \mu_e + n_h e \mu_h$$

If we assume $f = 10^{10}$ cps, $n_e = 10^{21}$ m^{-3}, $\mu_e = 50$ m/vs, we have

$$\sigma \simeq 8000 \ (\Omega - m)^{-1}$$

$$\delta \simeq 57 \text{ microns}$$

The diameter of our InSb samples is comparable to the skin depth. This makes our one-dimensional model assumption improper since the one-dimensional assumption is good only if the skin depth is wider than the sample width.[45] We, therefore, can no longer adopt a one-dimensional expression at this microwave frequency range. The transverse boundary of the sample cannot be neglected either. Under these conditions, the impedance calculation is impossible. Only if we assume that the propagation effect can be neglected, k = 0 (i.e., no longitudinal variation), then microwave impedance of the semiconductor post can easily be calculated (equivalent to the calculation of the impedance of a round wire at high frequency). Such an attempt had been made by Larrabee.[46]

Due to these two major problems, our experimental observations, described in the previous reports, are very hard to correlate with any space-charge-wave (or carrier wave) propagation. However, this measurement will provide a good technique to study the life times of the carriers and the densities of the carriers (if propagation effect

---

[45] S. Ramo, J. R. Whinnery, and T. V. Duzer, *Fields and Waves in Communication Electronics*, John Wiley and Sons, New York, 1965, p. 296.

[46] R. Larrabee, "Microwave Impedance of Semiconductor Posts in Waveguides, Part I," *Journal of Applied Physics*, Vol. 36, May 1965, p. 1597.

can be negligible[†]).

The two problems mentioned above can be eliminated nicely by reducing the applied frequency. The decrease in frequency will increase the plasma wavelength and increase the skin depth, respectively, and it will make theoretical one-dimensional impedance much more prominent. The radio frequencies from 10 MHz to 50 MHz, which have plasma wavelength from 1 mm to 5 mm, will provide an excellent range for the impedance studies.

5.3 Impedance Measurements in the Radio-Frequency Range

5.3.1 Experimental Setup

The impedance measurement at radio-frequency range can adopt the conventional circuit theory. We use the most sensitive method, an RF bridge measurement, to measure the interaction impedance. The RF bridge used at our laboratory is a Type 1606-A designed by the General Radio Company. Usually an RF bridge is used to measure the impedance of a passive circuit element. When we applied a pulsed current to a sample element in order to measure its impedance, we had to separate the radio-frequency signal and the pulsed voltage.[††] The separation idea can be illustrated by Fig. 5.14.

The functions of the LP (low pass) filter and the HP (high pass)

[†] When $\omega_{ph} << \nu_{ch}$, the carrier waves are heavily damped. The propagation effect can be negligible.

[††] Note that the fundamental frequency of the pulsed signal (2 μs width, 10 pps) is far less than the RF signal frequency.

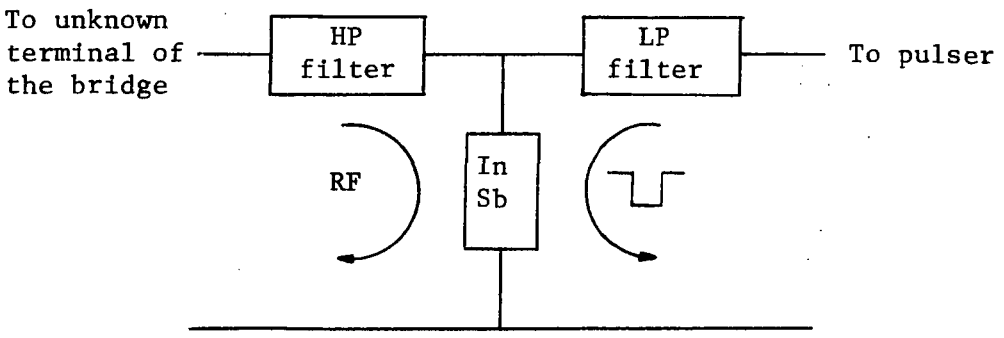

Fig. 5.14. The separation circuit.

filter are designed to separate dc pulsed voltage and the RF signal. The HP filter is to limit the dc pulsed current passing through the bridge circuit to a minimum amount, so most of the pulsed current can only flow through the LP filter and our sample element. The LP filter is to prevent the RF signal leaking through the pulser, so most of the RF signal can only flow through the HP filter and our sample element. If HP and LP filters are properly chosen, the impedance difference due to the pulsed current can be measured in a very simple and accurate way. Our HP filter is a 100 pF condenser which contributes very high impedance to dc pulsed voltage and a rise time of about 10 ns.† Our LP filter is a high frequency choke which is made of a 1-1/2" diameter by 1-3/4" long plastic cylinder with 40 turns of No. 32 copper wire. The impedance characteristics of the choke, as shown in Fig. 5.15, are measured by an HP 4805 RF vector impedance meter designed by the Hewlett-Packard Company. It has a quite high impedance (over 2 k ohms)

† Rise time = RC; C = 100 pF; R ≃ 100 Ω.

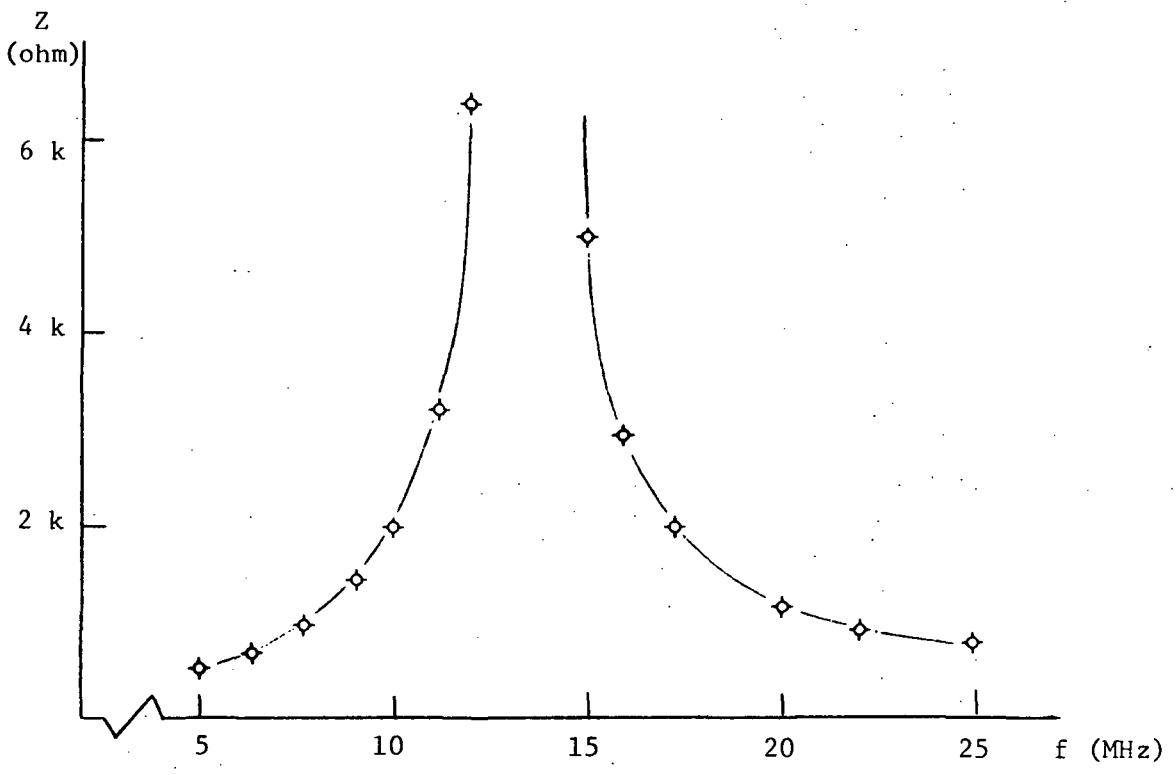

Fig. 5.15. The impedance characteristics of the RF choke.

in the frequency range from 10 MHz to 18 MHz.† Therefore, our applied signal frequency will be restricted in this range unless we design different coils.

The InSb sample is mounted in a cylindrical brass cavity. The arrangement is shown in Fig. 5.16. The cylindrical brass cavity is then lowered longitudinally into a liquid nitrogen dewar which is

† Note the 2 k ohm impedance is much larger than our InSb sample impedance which is about 100 ohms.

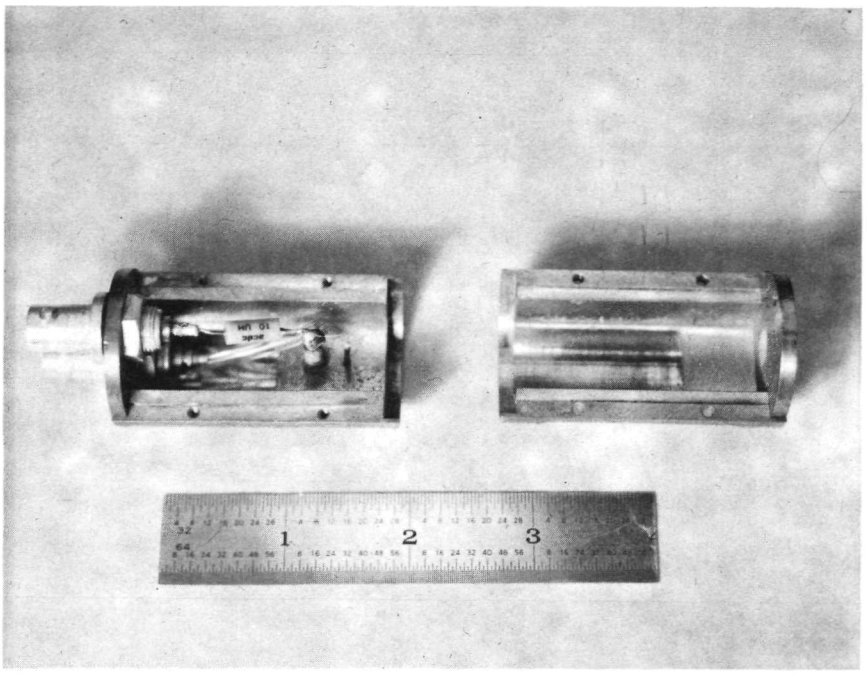

Fig. 5.16. Interior view of brass cavity.

located in a Varian two-inch electromagnet. The connections from cavity to the pulser and the bridge are RG 58A coaxial cable.

The complete experimental setup can be illustrated by Fig. 5.17, and the RF equivalent circuits are shown in Fig. 5.18.

The relation between Z_b and Z_a can be obtained by

$$Z_b = Z_o \frac{Z_a + j\, Z_o \tan \beta\ell}{Z_o + j\, Z_a \tan \beta\ell}$$

where Z_o:characteristic impedance of coaxial transmission line (53 ohms).

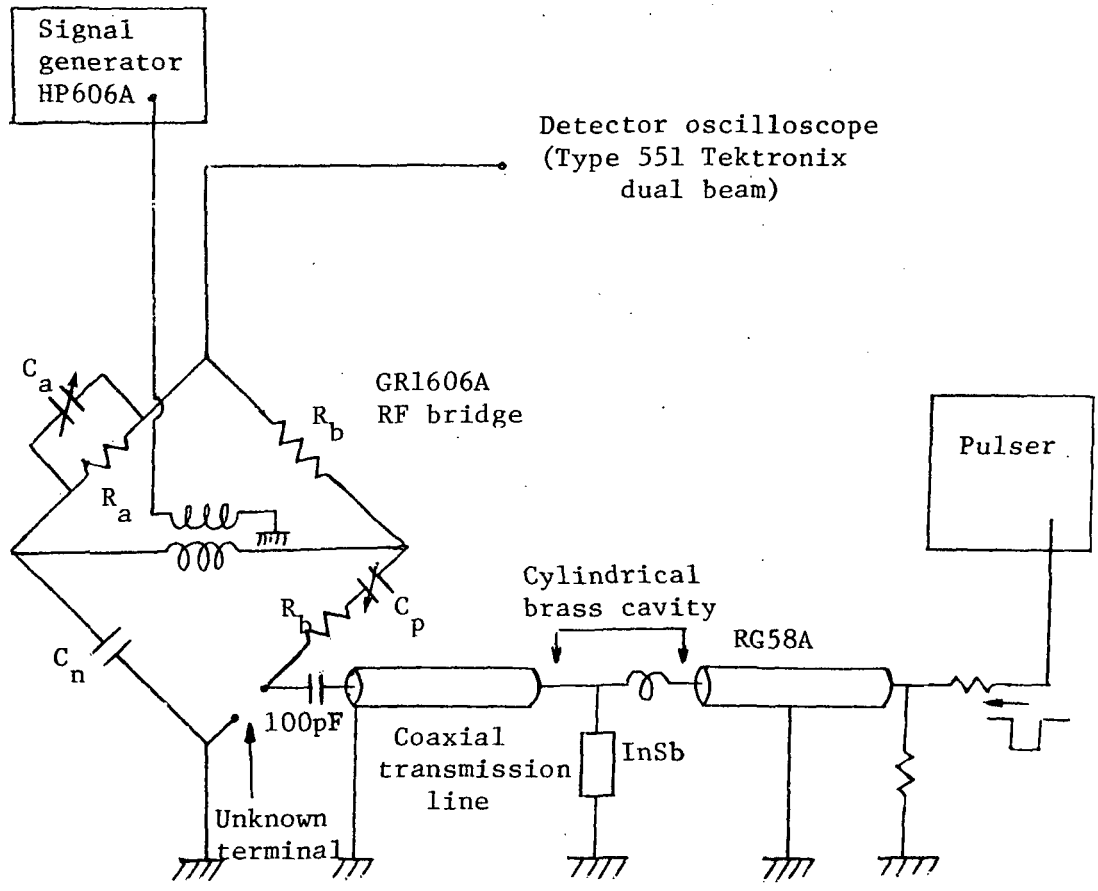

Fig. 5.17. Schematic diagram of RF bridge impedance measurement.

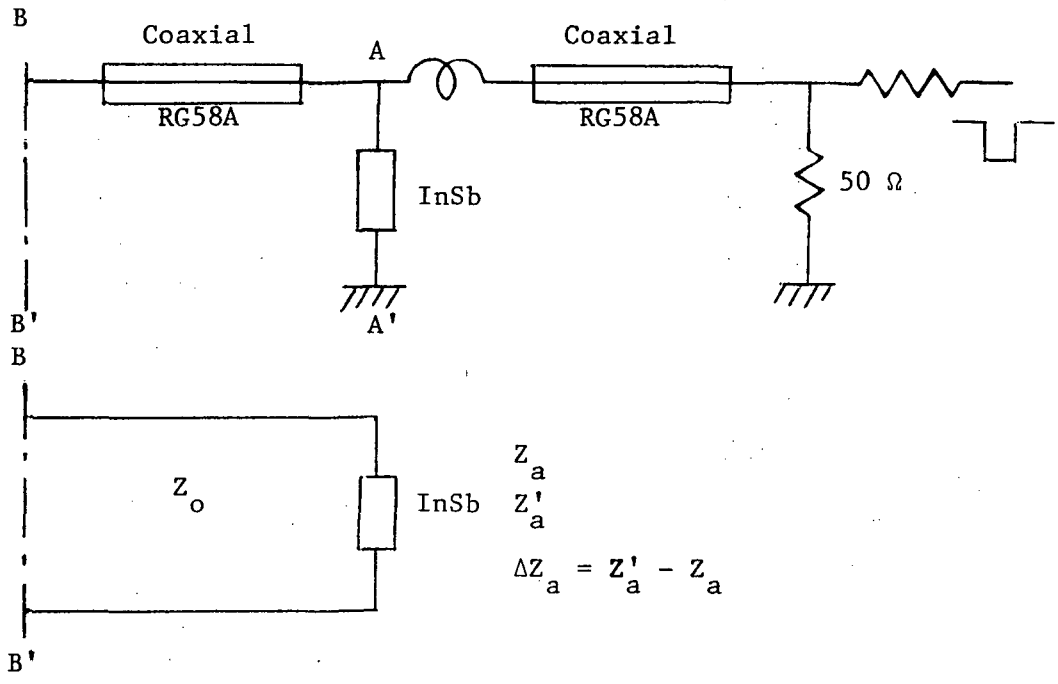

where

Z_a = impedance of InSb sample with no pulsed voltage across (AA')

Z_b = impedance of Z_a at the unknown terminal of the RF bridge (BB')

Z'_a = impedance of sample with voltage across

Z'_b = impedance of Z'_a measured at BB'

ΔZ_a = impedance difference at AA'

$\Delta Z_b = Z'_b - Z_b$

Fig. 5.18. RF equivalent circuit.

5.3.2 Procedure of Impedance Measurement

Indirect Method

When the desired pulsed voltage is applied to the InSb sample, the impedance difference ΔZ_b, due to the pulsed voltage, can be measured by following the bridge manual. We first balance the bridge outside the 2 μs pulsed period. When a balance is reached, the detector shows a waveform of Fig. 5.19. The initial readings on the

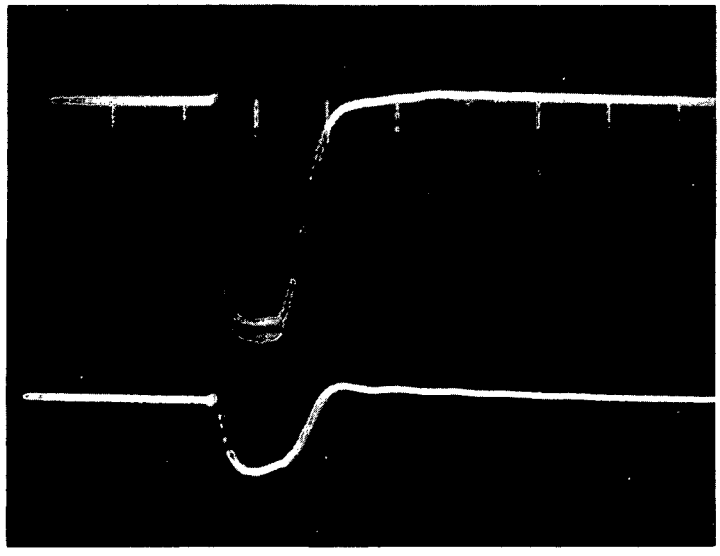

Fig. 5.19. Detecting waveform when an initial balance is reached.

dials are recorded. The ripple during the 2 μs period indicates the impedance difference due to the 2 μs pulsed voltage. Then the bridge is rebalanced during the 2 μs period. When a rebalance is reached, the detector shows a waveform of Fig. 5.20. The final readings on the

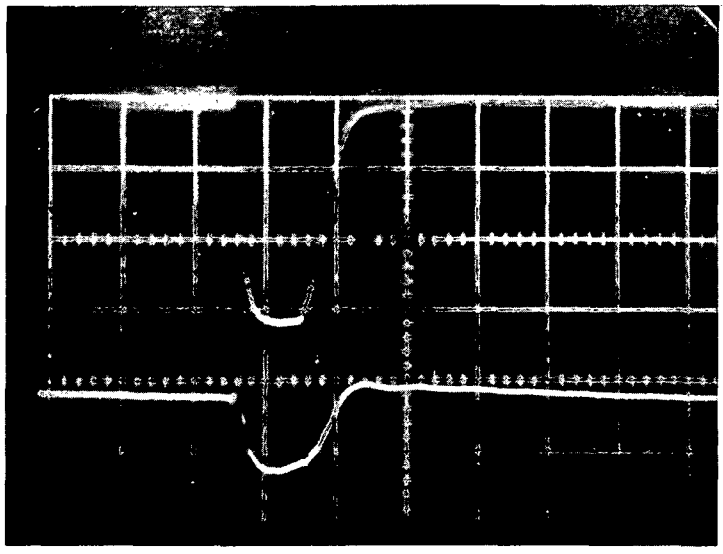

Fig. 5.20. Detecting waveform when a final balance is reached.

dial are recorded. The difference on the dial readings will give the resistance difference and the reactance difference due to the drifting field. The various impedance readings can be obtained from the different signal frequency and different pulsed voltage.

If the InSb sample is replaced by a dummy sample (pure resistance), and the pulsed voltage is applied, the ripple at the 2 μs period will not be seen. This indicates the linearity of our dummy sample, and agrees with our expectation.

The Z_a and Z_b can be measured easily by an HP 4815 RF vector impedance meter.† Once Z_a, Z_b, ΔZ_b are measured, Z_a' and ΔZ_a can easily

† Z_a and Z_b can also be measured by an RF bridge, if they have low reactance value, since an RF bridge can measure maximum reactance about 5000/XMC.

be obtained by using a Smith chart or by calculating from the transmission circuit theory.

Direct Measurement Method

The indirect method described above emphasizes the impedance difference due to the drifting pulsed current. The actual impedance can be obtained by the further step of superimposing and transformation as shown above. This is quite inconvenient and complicated. A more convenient method is proposed to help to fill the gap.

First the BB' terminal is shorted and the initial reading recorded. Next the InSb impedance is measured with the coaxial cable connection at BB' terminal by balancing the ripple during the 2 μ sec period. The impedance is transformed from BB' to AA', then we obtain the actual impedance of the InSb sample under a pulsing condition. The impedance of the InSb sample without an electric field across it can also be obtained by the same procedures.

Due to the effectiveness of the direct method, we prefer to adopt this method for our measurement. However, the indirect measurement still is a good technique and worthy of mention.

In the radio-frequency range, the effect of the inductive copper post and the gold wire lead on the impedance measurement cannot be neglected. They must be added to the equivalent circuit as part of the geometrical circuit impedance. The equivalent circuit of Fig. 5.18 must be modified as shown in Fig. 5.21.

Each geometrical reactance of one sample post is different from

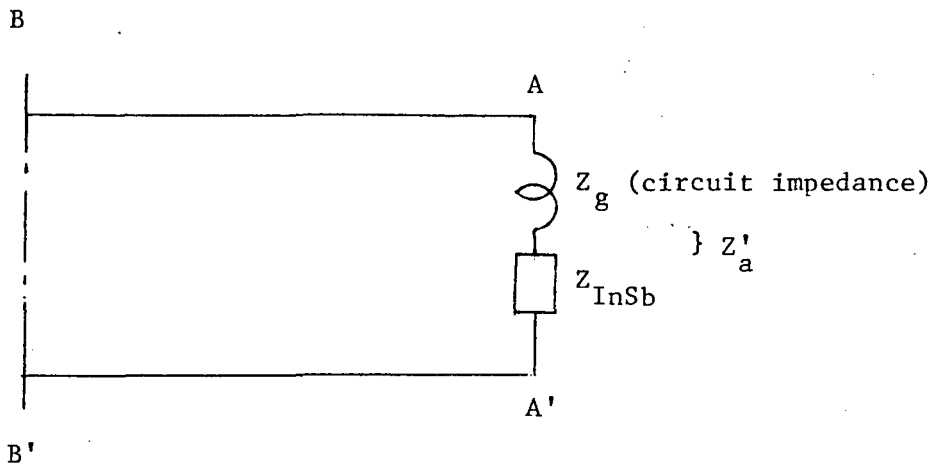

Fig. 5.21. The equivalent circuit of the InSb sample.

the others. The reactance depends upon the dimension of the inductive post and the gold wire lead. So each geometrical reactance Z_g must be measured separately. A simple experimental evaluation of the geometrical reactance may be accomplished by measuring the sample post with the gold wire lead at room temperature where the conductivity of the InSb sample is so high that the internal impedance is negligible; i.e., $Z_{InSb} = 0$ at room temperature. This can be measured either by the RF bridge or directly by the vector impedance-meter. The results obtained by both methods agree with each other. One measurement for the geometrical reactance is plotted in Fig. 5.22. This shows that the geometrical reactance is almost a pure inductance and its magnitude is linearly proportional to the frequency. In this specific case, $L_g \simeq x/2\pi f \simeq 0.04$ μH.

Now the impedance bridge measurement will be summarized as follows:

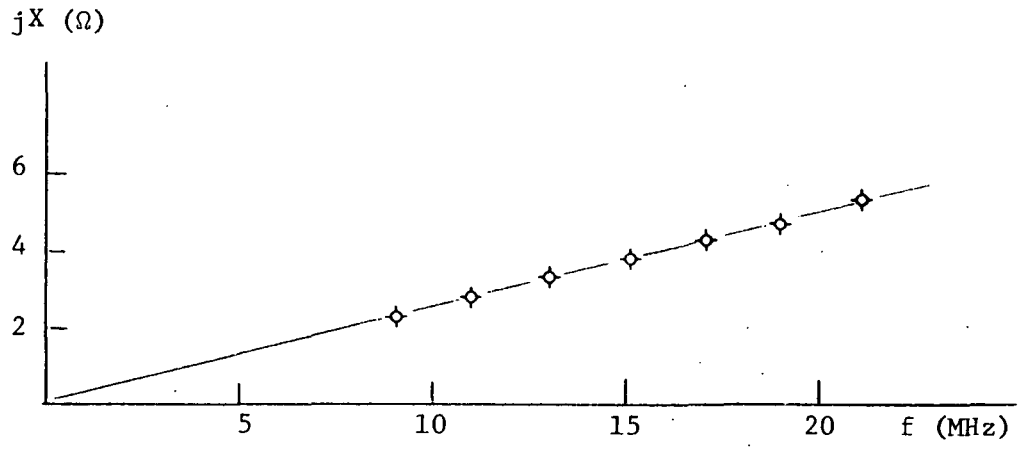

Fig. 5.22. The magnitude of geometrical reactance.

1. Measure Z_g' at BB' at room temperature and then transform Z_g' at BB' to Z_g at AA'.
2. Measure Z_b' at 77° K and plot Z_b' on a Smith chart.
3. Calculate Z_a' from Z_b' by the proper transformation.
4. Calculate Z_{InSb} from $Z_{InSb} = Z_a' - Z_g$.

5.3.3 Observations and Experimental Results

As shown in previous chapters, the theoretical impedance of an InSb sample based on carrier stream interaction is a function of n-type or p-type doping, external drifting electric field and magnetic field, and the applied frequency. Following the experimental procedure described above, the experimental impedance will be reported in the following sections.

n-type InSb Sample

When a pulsed electric current is applied to the n-type InSb

sample (Is59) with $n_e = 1.1 \times 10^{13}$ cm^{-3} and $\mu_e = 3.28 \times 10^5$ cm^2/Vs, the impedance change due to the pulsed current is too small (less than 1 Ω) to be detected. When a longitudinal magnetic field is applied, we obtain the same result. This means that the impedance of an n-type InSb sample is not a function of electric field.

p-type InSb Sample (Is56)

The observations in the p-type InSb samples are quite different from the n-type InSb samples. Sample No. 1 has the dimensions of .495 x .462 x .465 mm^3. First the I-V curve was measured as shown in Fig. 5.23, and then the geometric reactance Z_g was measured as shown in Fig. 5.24. The impedance expression can be measured in two ways -- changing either applied signal frequency or electric field individually.

At 9 MHz, the impedance of sample No. 1 was measured at different electric fields and the impedances Z_b''s (at BB') are plotted on a Smith chart as shown in Fig. 5.25. The impedance locus of Z_a' (at AA') can be obtained by properly transforming Z_b'; the transformations are also shown on the same Smith chart. Then the results of Z_a' and Z_{InSb} are plotted in a complex impedance plane as shown in Fig. 5.26.

At some specific field, the impedance Z_b' can also be measured at different signal frequencies.† The locus of Z_b' and Z_a' are shown in Fig. 5.27.

Changing the RF choke (LP filter) directly changes the frequency range of operation as mentioned. Using the same sample and a different

† The frequencies are chosen near the resonance frequency of RF choke.

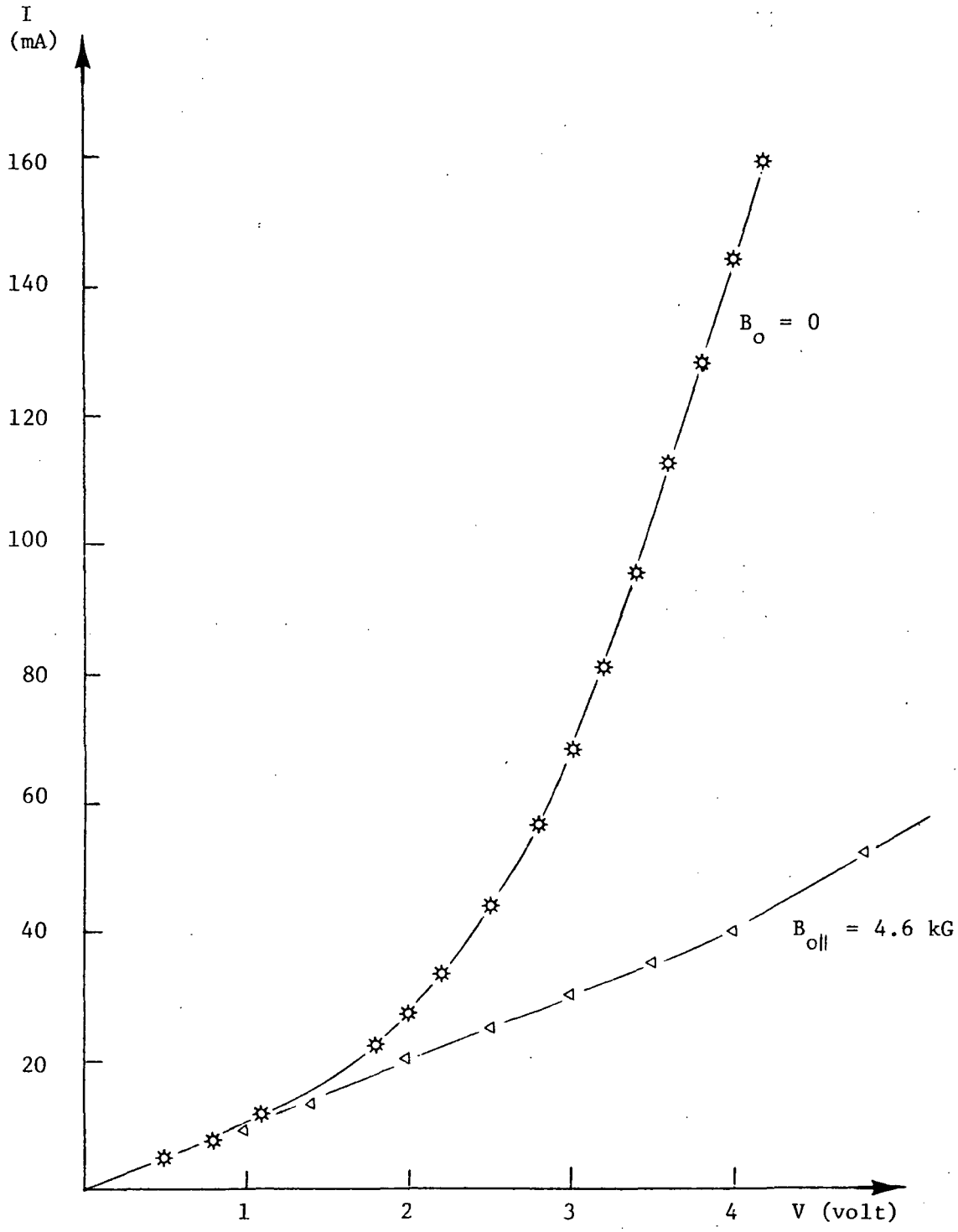

Fig. 5.23. I-V characteristics of sample No. 1.

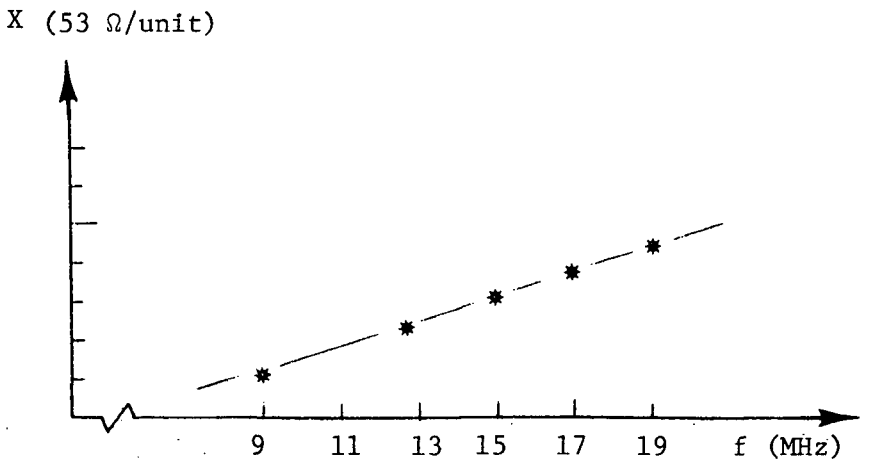

Fig. 5.24. The magnitude of geometric reactance Z_g of sample No. 1.

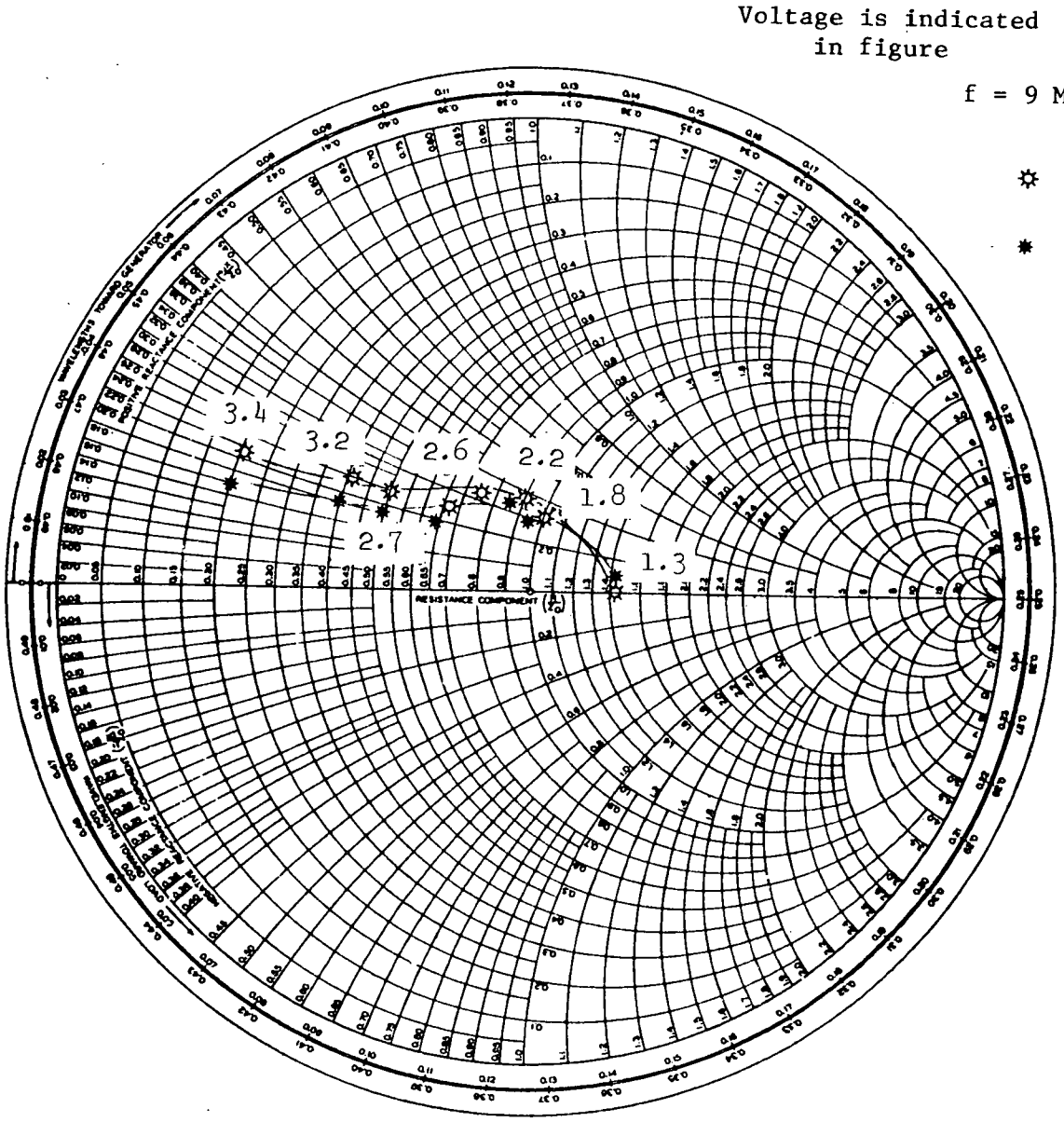

Fig. 5.25. The locus of Z'_b and Z'_a (see p. 116) with electric field as parameters.

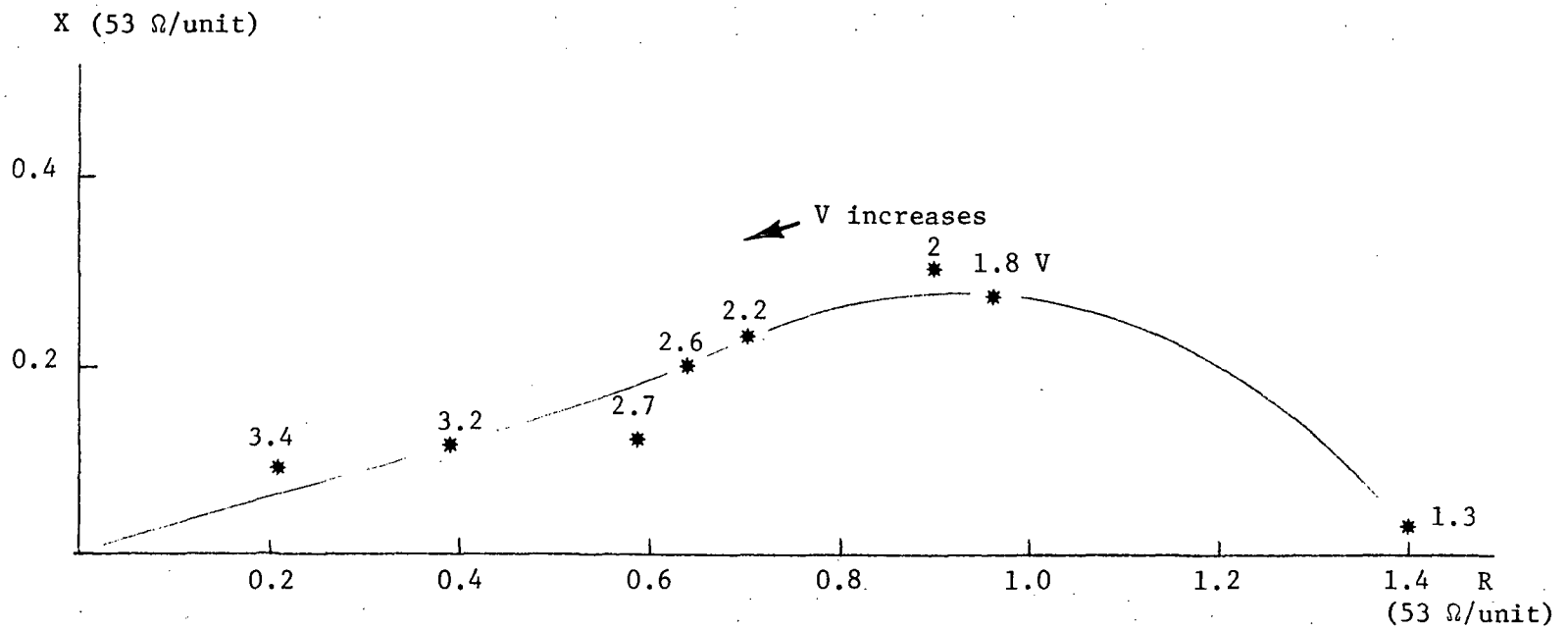

Fig. 5.26. The complex plot of Z_{InSb} with electric voltage as parameter.

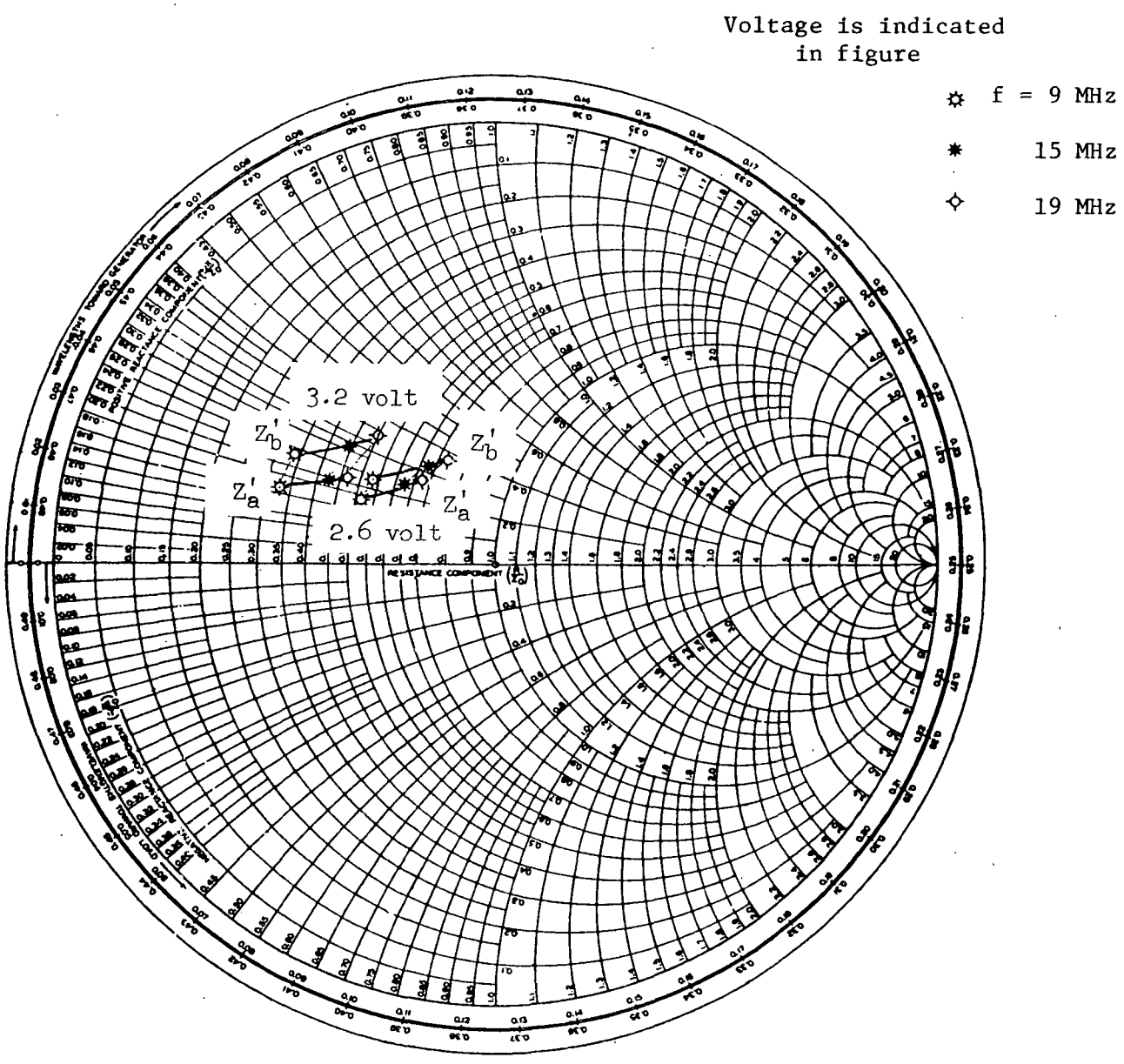

Fig. 5.27. The locus of Z_b' and Z_a' (see p. 116) with frequency as parameter.

choke (resonance at 21 MHz), we are able to measure the sample impedance at higher frequencies. The impedance results at 19, 21, and 23 MHz were measured and are plotted first on a Smith chart as shown in Figs. 5.28, 5.29, and 5.30, and then in a complex impedance plane as shown in Figs. 5.31, 5.32, and 5.33.

When a longitudinal magnetic field is applied to the sample, the I-V curve changes drastically as shown in Fig. 5.23. Due to the low frequency instability in the sample, the impedance can only be measured below the threshold electric field. The results are plotted in Figs. 5.34 and 5.35.

When a transverse magnetic field is applied, an impedance change due to a pulsed current is also observed. Since it is quite difficult to correlate to the theory as mentioned before, the data will not be recorded and studied.

The experiments have been performed many times for each individual sample. The experimental results are repeatable. Each different sample shows more or less the same impedance characteristics. The results can be summarized as follows:

A. The sample has to be cooled at 77° K in order to observe the impedance change effect. This cooling is necessary to keep the value of the thermal velocities low. At room temperature, no impedance change due to pulsed current is observed.

B. When no pulsed current is applied to the sample, the sample impedance approaches that of a lossy capacitor. Since V = 0,

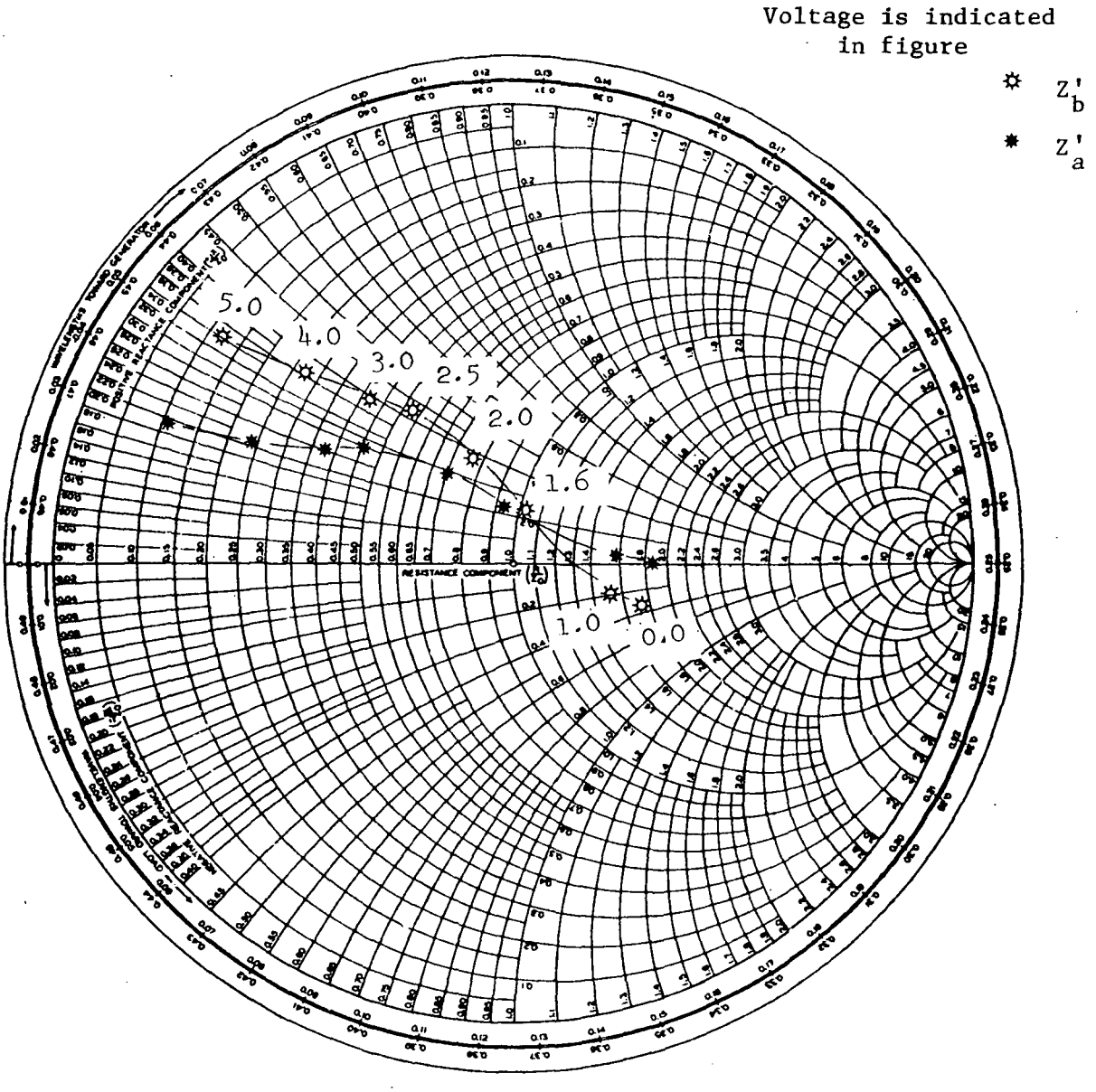

Fig. 5.28. The experimental impedance plot at f = 19 MHz and B_o = 0. (See p. 116 for definitions of Z'_a and Z'_b.)

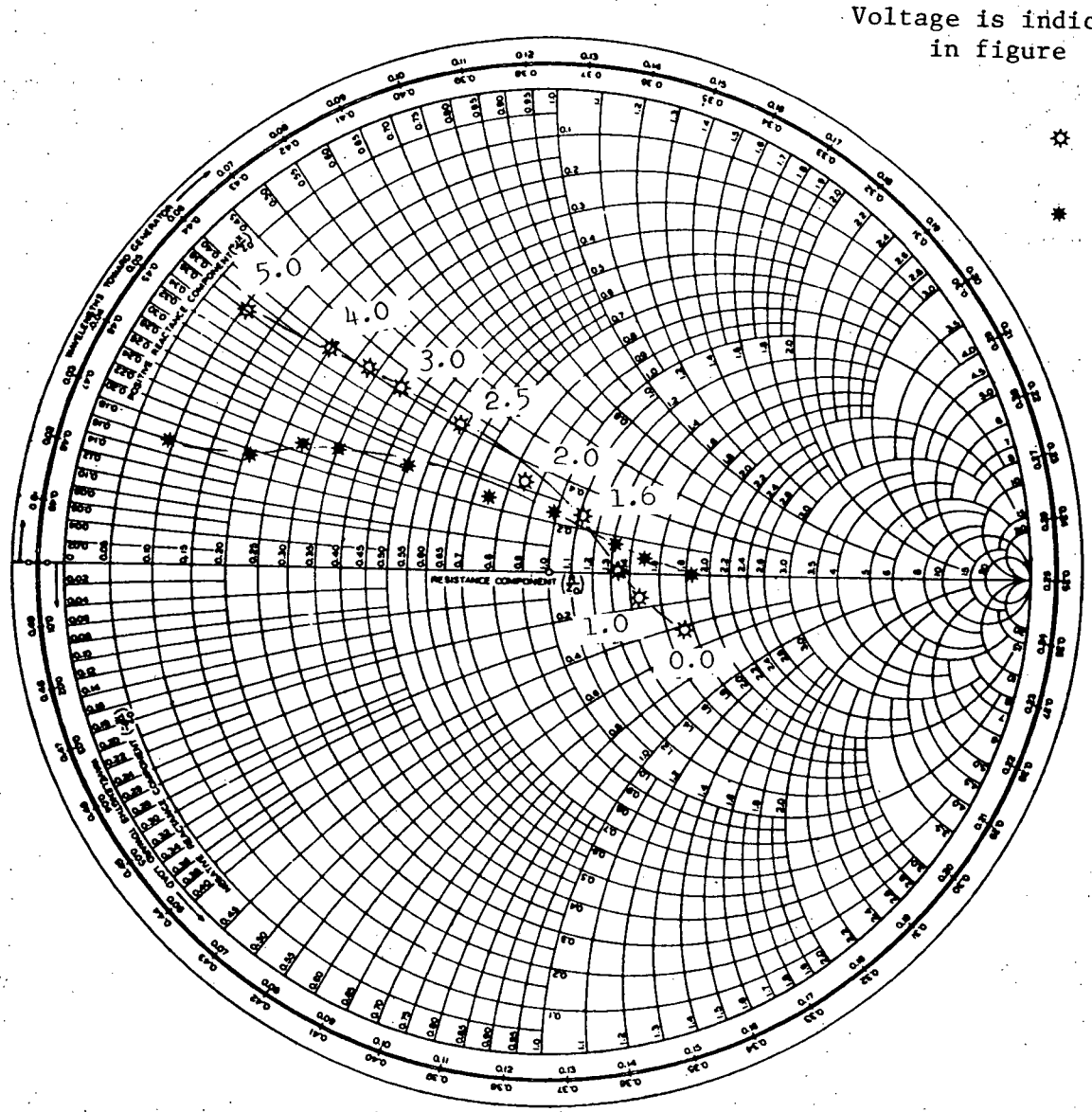

Fig. 5.29. The experimental impedance plot at f = 21 MHz and $B_o = 0$. (See p. 116 for definitions of Z'_a and Z'_b.)

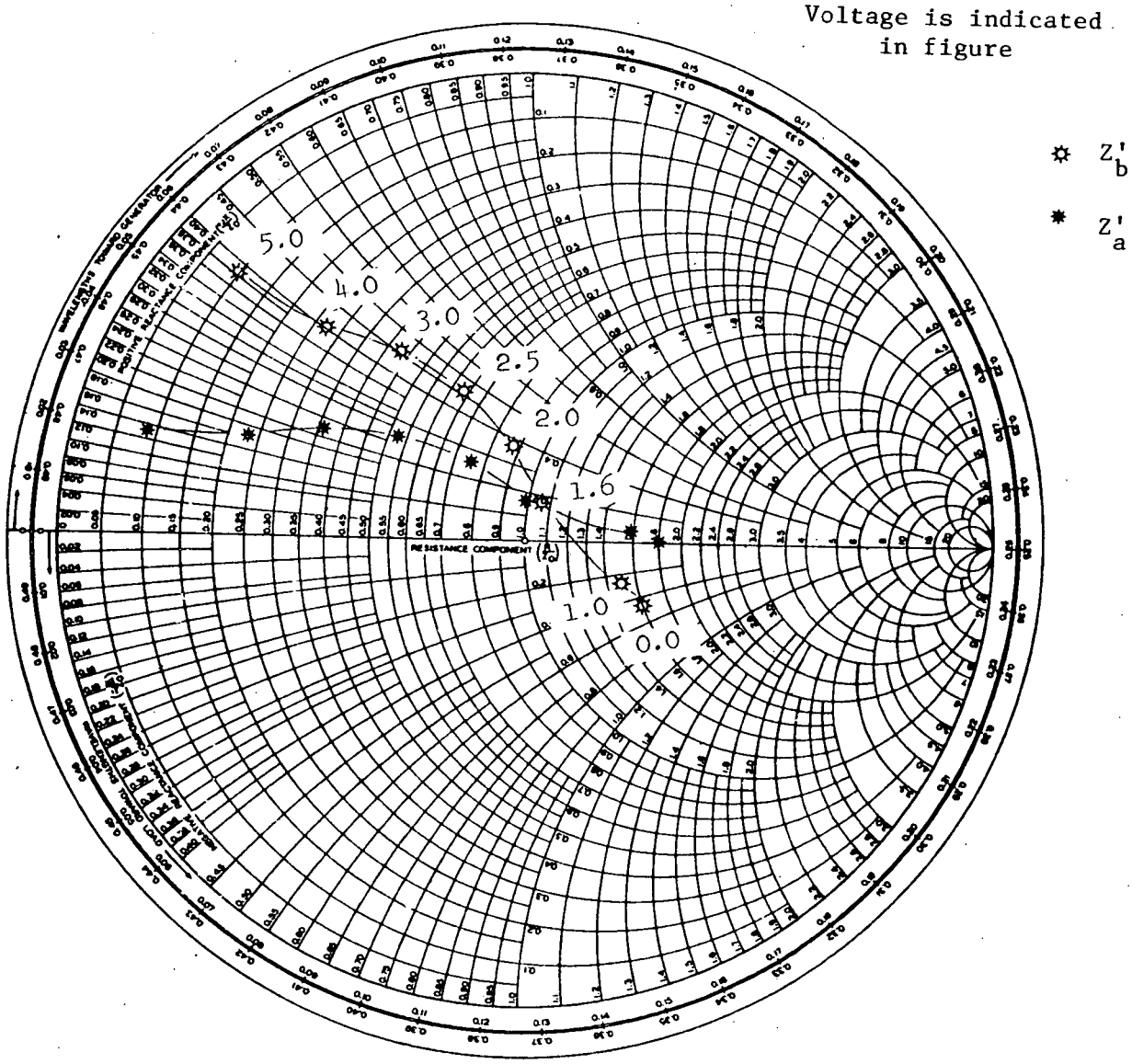

Fig. 5.30. The experimental impedance plot at f = 23 MHz and B_o = 0 kG. (See p. 116 for definitions of Z'_a and Z'_b.)

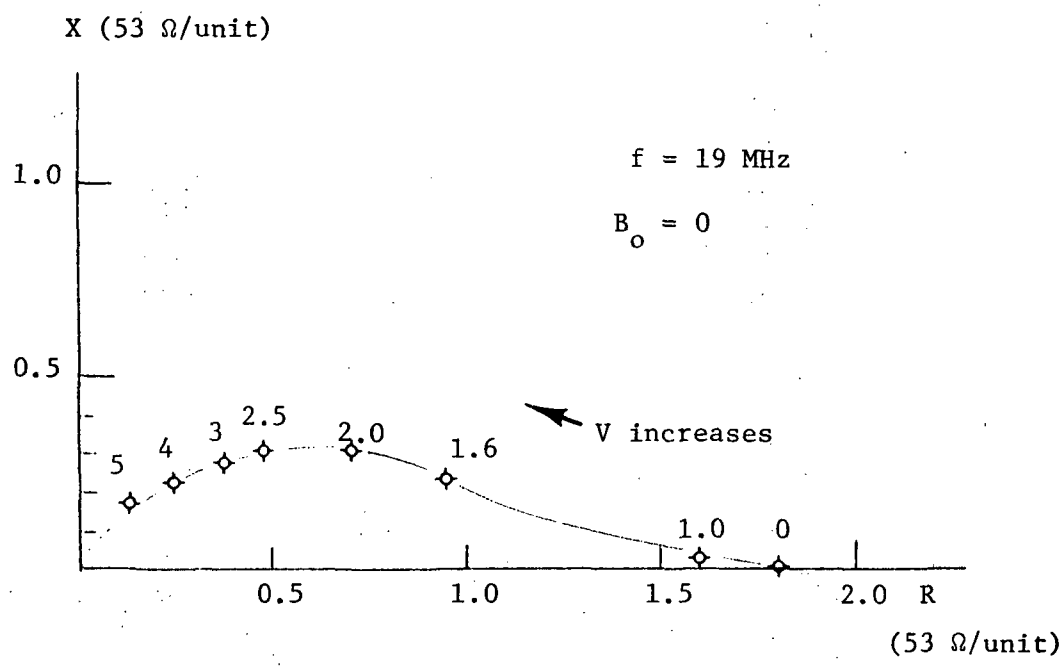

Fig. 5.31. The experimental impedance plot.

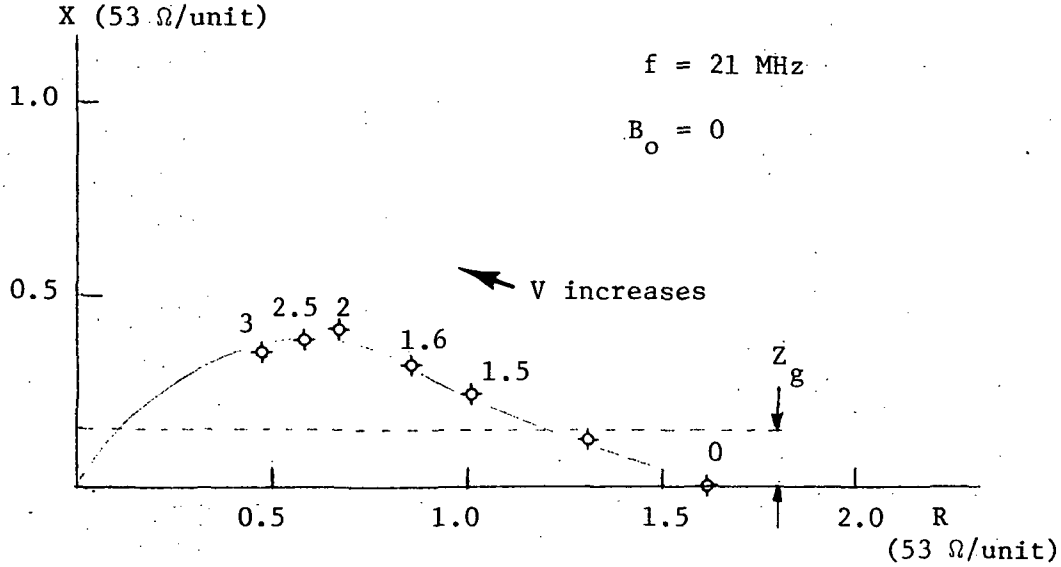

Fig. 5.32. The impedance plot of Z_a' with V as parameter. $Z_{InSb} = Z_a' - Z_g$.

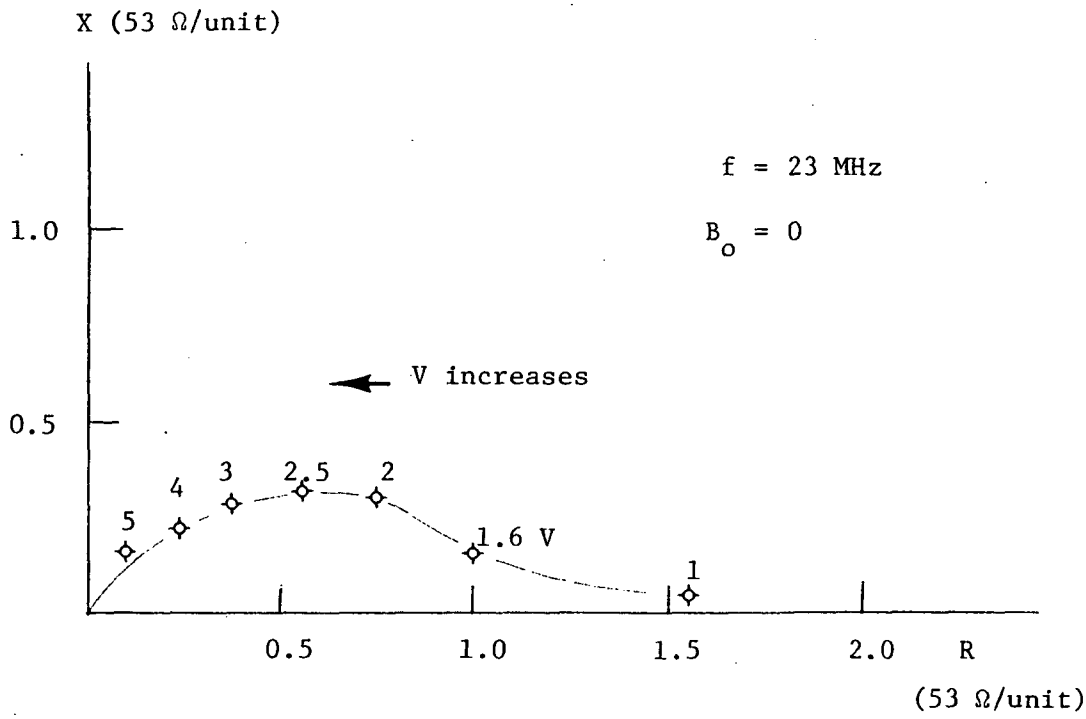

Fig. 5.33. The experimental impedance plot of Z'_a with no magnetic field.

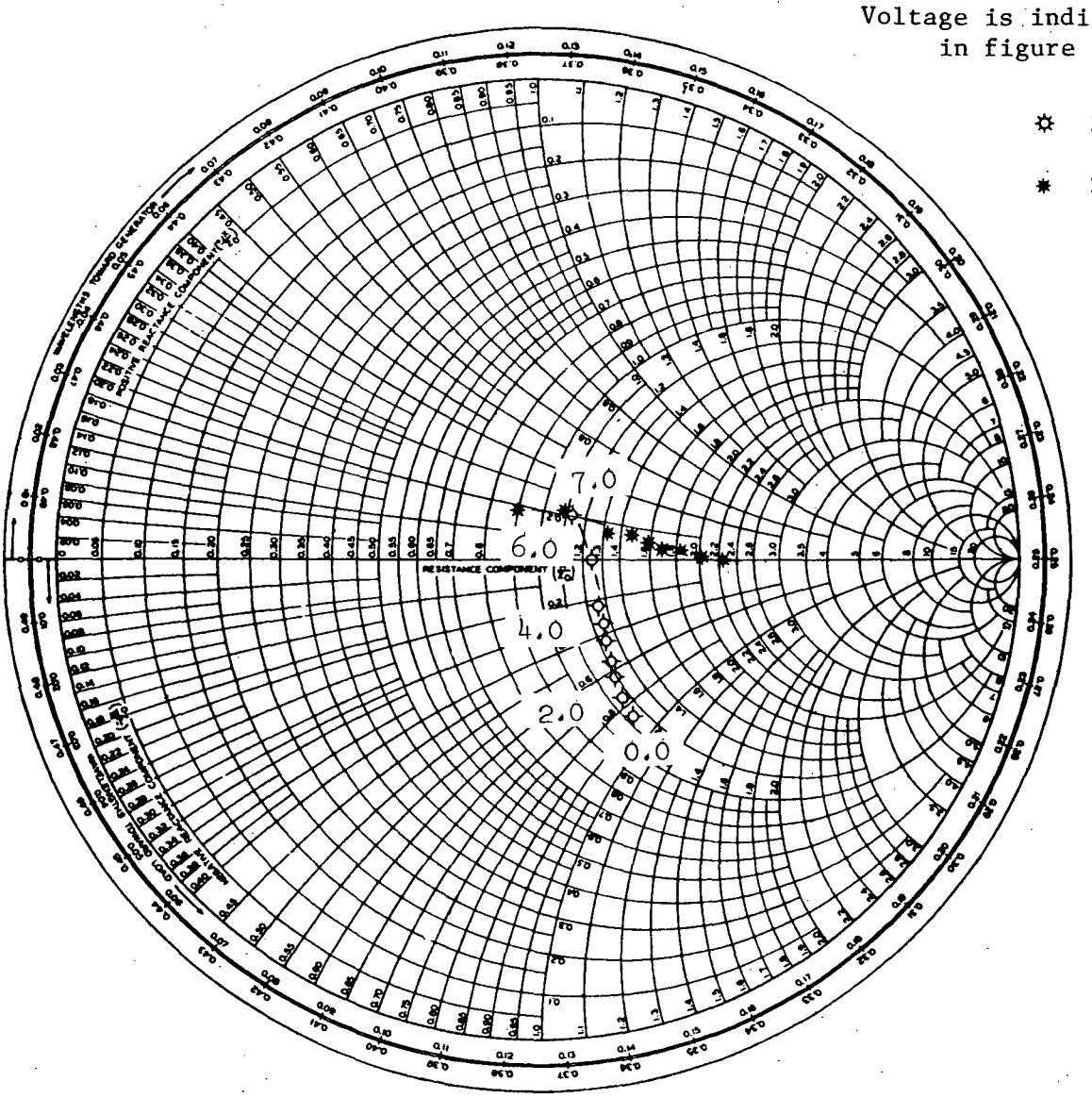

Fig. 5.34. The experimental impedance plot at 21 MHz and $B_{o\parallel} = 4.6$ kG. (See p. 116 for definitions of Z'_a and Z'_b.)

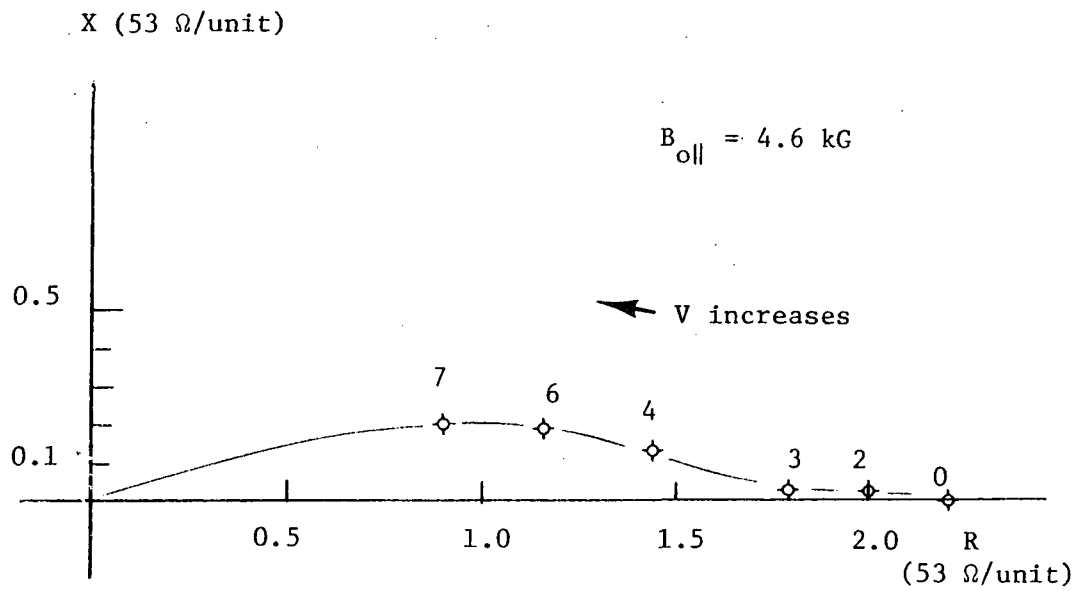

Fig. 5.35. The experimental impedance plot of Z_a' with a parallel magnetic field.

then $V_{oe} = 0$ and $k = \infty$, and the carrier wave effect is negligible in the impedance calculation.

C. When a high pulsed current is applied, the sample impedance approaches zero since n_e and n_h increase due to injection.

D. The resistance of the sample always decreases as pulsed current increases. The reactance of the sample increases first and then decreases to zero as the pulsed current increases.

E. The sample impedance changes due to different signal frequency under fixed pulsed voltage (as shown in Fig. 5.27).

F. The impedance measurement indicates that the longitudinal magnetic field does not change the impedance characteristics very much.

These observations can be interpreted as carrier stream interaction effects. To the author's knowledge, there is no other effect which can well explain these observations. A discussion and comparison between theory and experiment will be given in the next section.

5.3.4 Comparison and Discussion

A. The experimental impedances of n-type InSb are not influenced by the pulsed voltage in agreement with calculated one-carrier stream interaction impedances. This indicates that the electron carrier wave in n-type InSb is heavily damped and is not measurable. Therefore, the impedance of n-type InSb looks like a lossy capacitor or can be regarded as an inactive semiconductor as shown in Eq. 66.

B. The impedance of a semiconductor based on double stream interaction as derived in Chapter III can generally be written as

$$Z = \frac{d}{A\left[j\omega\varepsilon + \sum_i \sigma_i\right]} \left[1 - \frac{e^{-j\theta} - 1}{-j\theta}\right] \qquad (67)$$

where

$$\theta = kd$$

$$k = \frac{\omega}{V_{oe}} \left(1 + \frac{n_e\mu_e}{n_h\mu_h}\right) - j \frac{\omega}{V_{oe}} \frac{n_e\mu_e}{n_h\mu_h} \frac{\omega\nu_{ch}}{\omega_{ph}^2} - j \frac{\omega}{V_{oe}} \frac{V_{Te}^2}{V_{Th}^2} \frac{\omega}{\nu_{ce}}$$

$$\cdot \left(1 + \frac{n_e\mu_e}{n_h\mu_h}\right)^2$$

The theoretical impedances of sample No. 1 using different values of thermal velocities $\left(V_{Te} = 3, 6, 8 \times 10^5 \text{ m/s}\right)$ and with voltage as a parameter are computed and plotted in the complex impedance plane as shown in Figs. 5.36 to 5.39. The diffusion effects damp the propagating wave and depress the impedance curves as shown in the figures. This is physically reasonable.

The experimental impedances of p-type InSb (sample No. 1) only give a qualitative similarity with the theory; i.e., counter-clockwise changes in impedance as voltage increases.

C. The measurements significantly deviate from the theory quantitatively. The measured inductive component is far smaller than the calculated one. One possible explanation is that our assumed model is not

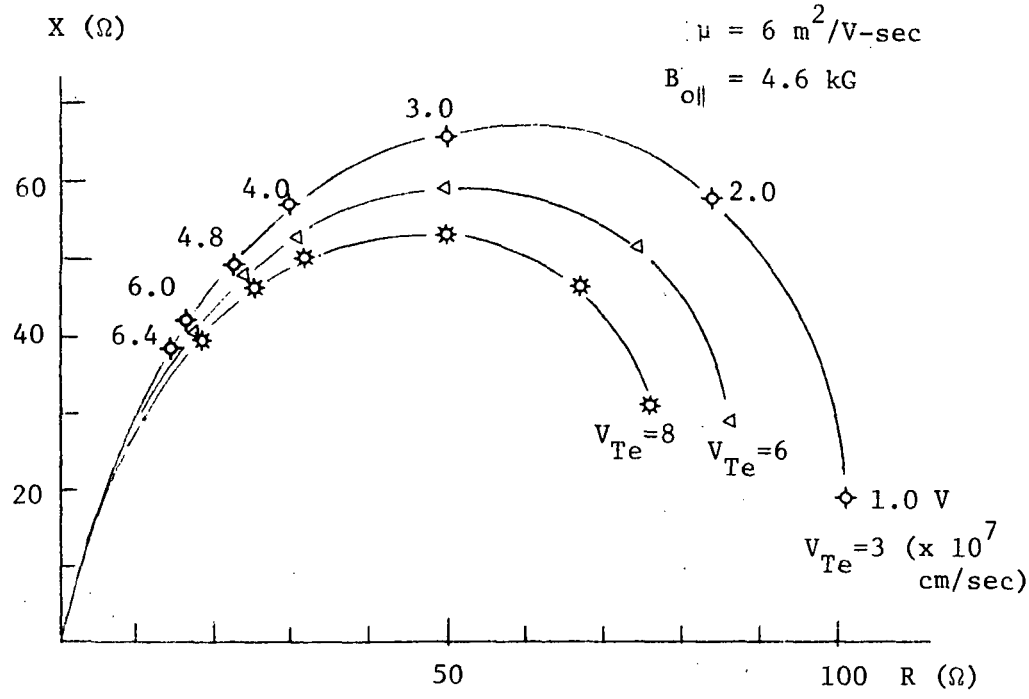

Fig. 5.36. Theoretical impedance plot for sample No. 1 for several values of thermal velocity V_{Te} with a parallel magnetic field.

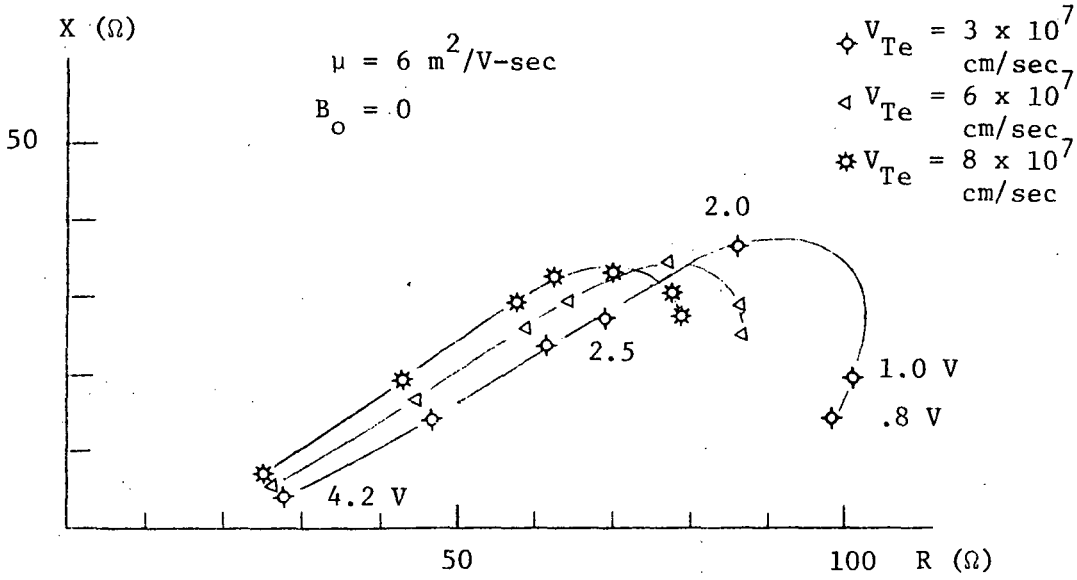

Fig. 5.37. Theoretical impedance plot for sample No. 1 for several values of thermal velocity V_{Te} with no magnetic field.

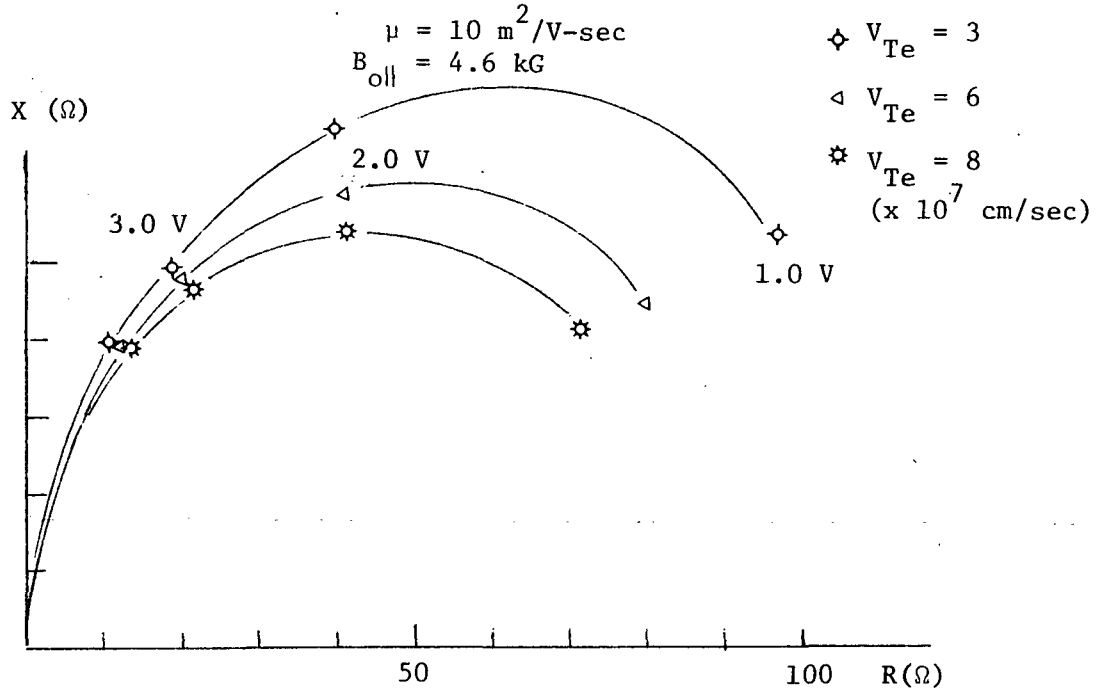

Fig. 5.38. Theoretical impedance plot for sample No. 1 for several values of thermal velocity V_{Te} with a parallel magnetic field.

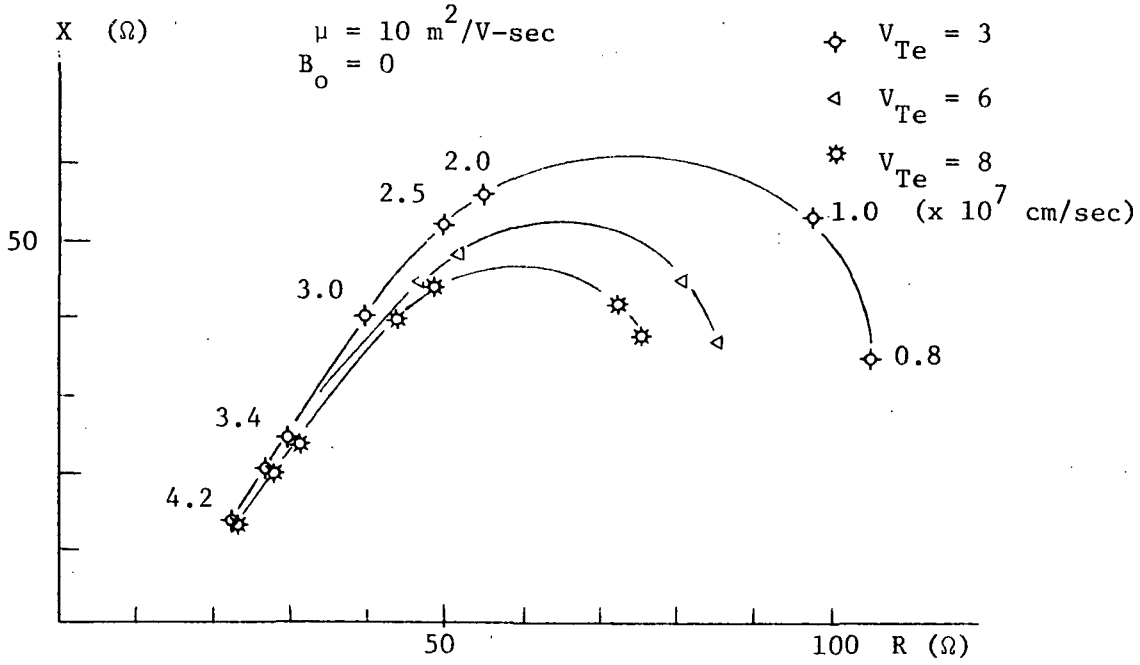

Fig. 5.39. Theoretical impedance plot for sample No. 1 for several values of thermal velocity V_{Te} with no magnetic field.

adequate because it is based on a uniform dc electric field across the sample. However, it is quite likely that the electric field across the sample is not uniform, and this might significantly affect the results. In addition, the interaction length and sample length can only be estimated, and may be quite different from what we assumed them to be. It is also possible that the two end regions of the sample are inactive semiconductor regions due to solder diffusion and other effects (e.g., charge depletion, accumulation, etc.). Therefore, the interaction region decreases and two passive resistances due to inactive semiconductor regions must be added. If this is the case, the equivalent circuit should be modified as shown in Fig. 5.40 where R_o is the parasitic

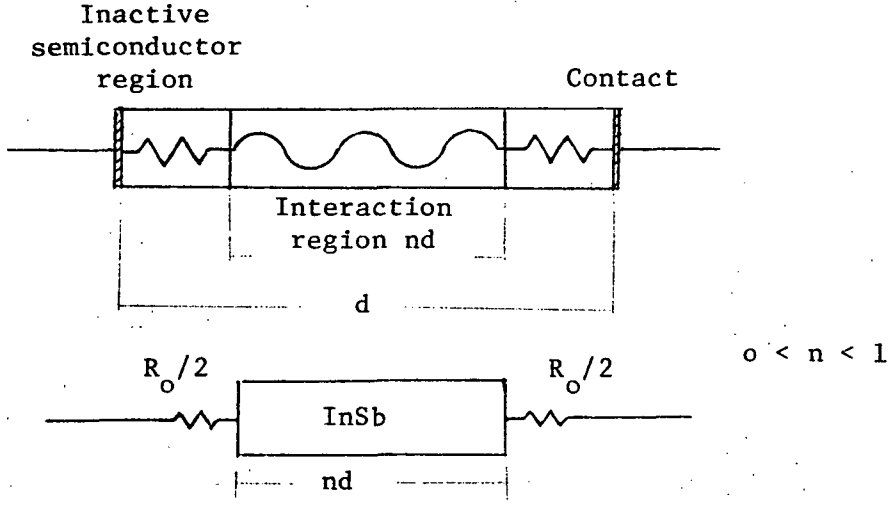

Fig. 5.40. The modified equivalent circuit of p-type InSb sample.

resistance of the inactive zone and n is a value between 0 and 1. This model[47] has been used to analyze Read diodes quite successfully, and it will be applied to our case. For the current work, we will choose n = 1/2, 1/3, and arbitrary R_o to get a closer comparison with the measured impedance. The results with n and R_o as indicated are plotted in Figs. 5.41 and 5.42. As shown in

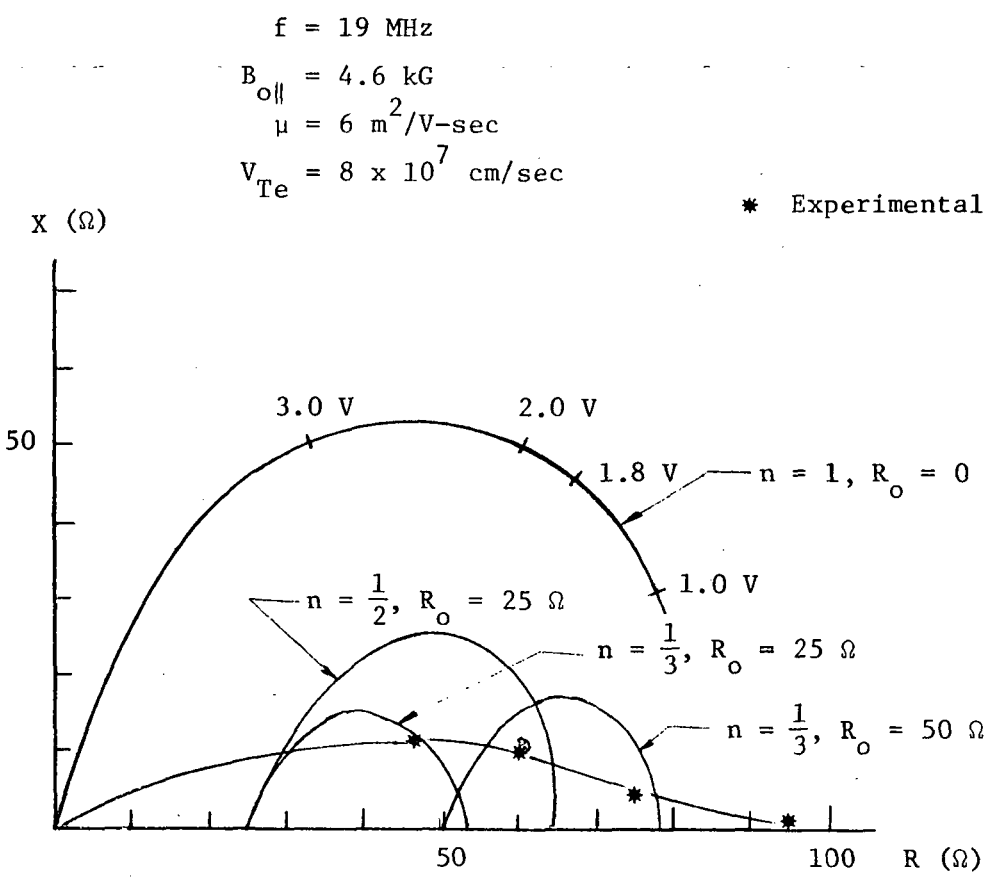

Fig. 5.41. Comparison between experimental curve and theoretical curves calculated using several values of the n and R_o shown in Fig. 5.40.

---

[47] M. Gilden and M. E. Hines, *op. cit.*

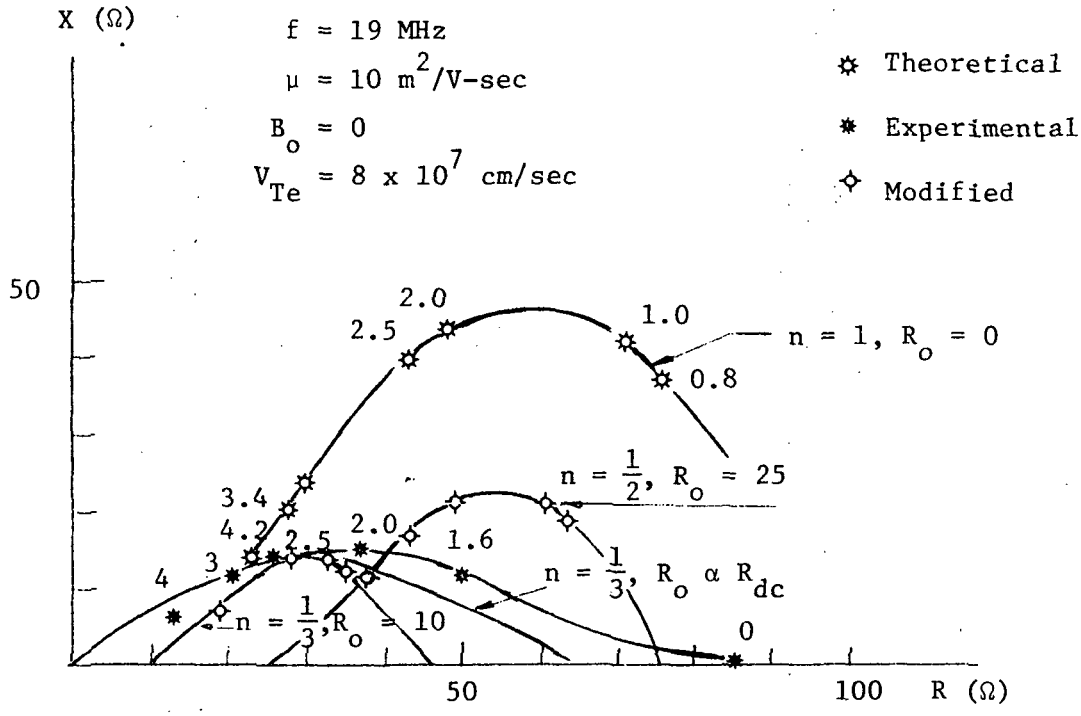

Fig. 5.42. Comparison between theory and experiment.

the figures, the magnitudes of the inductive component reduce drastically and become comparable with measured ones, although the curves still do not fit the experimental curves very well.

By comparison, the parasitic resistance is on the order of 10 to 50 ohms, about one half of the dc resistance, and the interaction length nd is about 1/2 to 1/3 of the sample length. The parasitic resistance seems to be a function of pulsed voltage, which is smaller in the high field region and larger in the low field region, while in our plots we assume that R_o is a constant which is independent of voltage. If we assume that R_o is proportional to dc resistance R_{dc}, which is physically reasonable

and possible, then R_o is no more a constant and is a function of dc voltage, as shown in Fig. 5.43. Under this assumption

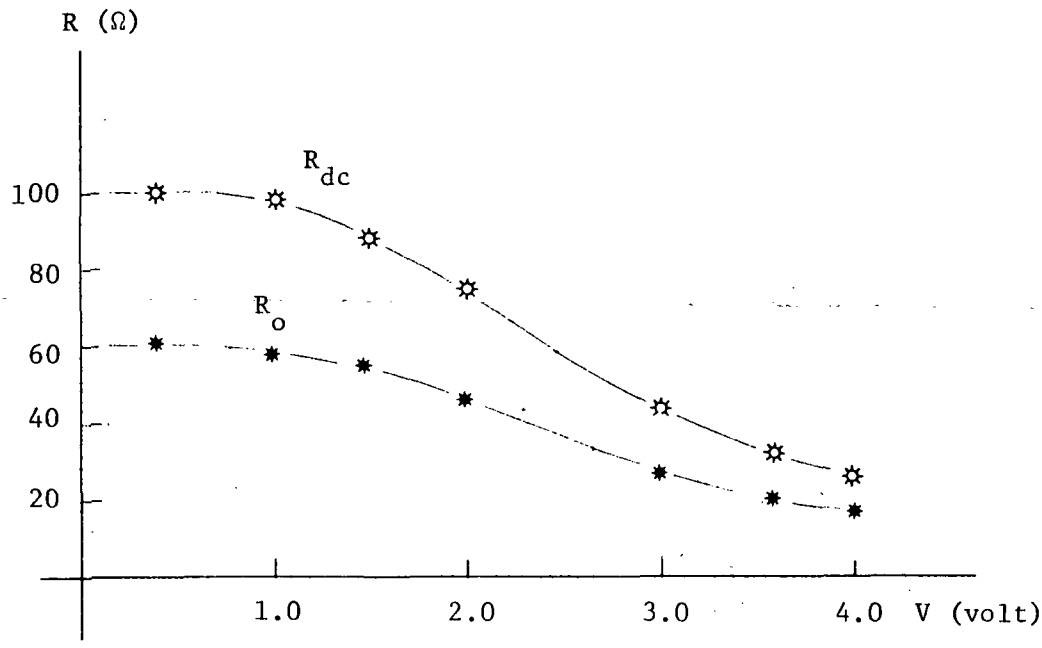

Fig. 5.43. Magnitudes of parasitic resistance R_o and dc resistance R_{dc}.

the calculated impedance should be remodified as shown in Fig. 5.42. Consequently it gives a much better correlation with the experimental curve. Further investigation of these aspects are needed.

D. To get good quantitative comparisons, presumably we need both an accurate model and precise determination of each quantity such as carrier mobilities, thermal velocities, electric field distribution, etc. However, using a simple model and reasonable assumptions, we have obtained qualitative agreement between measurement and theory,

and from this we conclude that the existence of space-charge wave effects can be established by impedance measurements.

E. The observed impedance of the sample is a lossy capacitor in some cases when no pulsed current is applied. This observation deviated a little from our prediction since the theory predicts an almost pure resistance when $V_{oe} = 0$, since $\omega\varepsilon << \sum_i \sigma_i$. This contradiction can probably be explained by the geometric structure of the contacts.

VI. SUMMARY AND CONCLUSIONS

In the previous chapters, the possibility of using impedance concepts to investigate the carrier wave behaviors in a semiconductor plasma has been studied both theoretically and experimentally. It is now appropriate to summarize some of the important results, and to draw some conclusions from this investigation.

1. Typical one-carrier and two-carrier stream interactions in solid-state plasmas have been analyzed using the one-dimensional hydrodynamic equations with small-signal approximations.
2. The impedance concept was introduced to study the carrier-wave behavior in a plasma. The theoretical impedances based on one-carrier and two-carrier stream interactions have been calculated. It is found that the impedance of a solid-state plasma based on one-carrier stream interaction is a passive leaky capacitance, and the impedance based on two-carrier stream interaction is

$$Z = \frac{d}{A\left[j\omega\varepsilon + \sum_i \sigma_i\right]} \left[1 - \frac{e^{-j\theta} - 1}{-j\theta}\right]$$

where

$$\theta = kd$$

$$k \simeq \frac{\omega}{V_{oe}} \left(1 + \frac{n_e \mu_e}{n_h \mu_h}\right)$$

3. The presence of a longitudinal magnetic field does change the

carrier number densities; however, it does not change the impedance expression. The presence of transverse magnetic field complicates the impedance expression due to the Suhl surface.

4. To the author's knowledge, this is the first attempt to use impedance concepts to describe and measure the carrier-stream interactions in semiconductors. The impedance concept has the advantage that the calculated quantities can also be measured.
5. We developed a bridge method for measuring the impedance in the radio-frequency range. The RF bridge measurement is a powerful tool for measuring the impedance of any nonlinear element subjected to a pulsed voltage. Sensitivity is high and reliable.
6. The theory of impedance analysis explains various experimental observed results; in particular:
   a. The impedance measurements of an n-type InSb sample indicate that the carrier waves in n-type InSb semiconductors are heavily damped in the low-electric field region, and consequently it can be described adequately by a one-carrier stream interaction model.
   b. The impedance measurements of p-type InSb samples indicate that the carrier waves in p-type InSb semiconductors are quite dominant and detectable. The damping term is heavy in the lower electric field region and decreases as electric field increases.
7. The inductive components of the measured impedance are much smaller than our theory predicts. The reason is still obscure. It may be due to the following factors:

a. The one-dimensional hydrodynamic model is too simple. The predicted results are too optimistic. The assumptions of the inactive zones in semiconductor were introduced to modify our simple model and make the theoretical results correspond more closely to the measured results.

b. The actual stream interactions are not strong, as expected. The lattice vibration, carrier velocity spread, and some other factors may decrease the interaction strength.

c. The transverse boundary is not included.

8. From our impedance measurement in p-type InSb material, we have demonstrated the existence of carrier waves in a semiconductor plasma; the effect is quite small, but detectable.

9. Since the carrier stream interaction is weak in InSb material, especially in the low electric field region, and cooling at liquid nitrogen temperature is needed, InSb is not likely to be useful in fabrication of microwave solid-state devices based on double-stream interaction.

APPENDIX I

IMPEDANCE OF SOLID-STATE DIELECTRIC DIODE

The solid-state dielectric diode impedance is

$$Z = \frac{d}{J\omega\varepsilon A}\left[\frac{1 - j\theta - e^{-j\theta}}{-j\theta}\right]$$

$$= \frac{d}{\omega\varepsilon A}\,\frac{(1 - \cos\theta) - j(\theta - \sin\theta)}{A}$$

Since

$$Y = \frac{1}{Z} = G + jB, \qquad \theta = \frac{\omega}{u_o}\,d$$

$$Y = \frac{\varepsilon A u_o}{d^2}\left[\frac{\theta^2(1 - \cos\theta) + j\theta^2(\theta - \sin\theta)}{(1 - \cos\theta)^2 + (\theta - \sin\theta)^2}\right]$$

then

$$G = \frac{\varepsilon A u_o}{d^2}\,\frac{\theta^2(1 - \cos\theta)}{(1 - \cos\theta)^2 + (\theta - \sin\theta)^2}$$

$$B = \frac{\varepsilon A u_o}{d^2}\,\frac{\theta^2(\theta - \sin\theta)}{(1 - \cos\theta)^2 + (\theta - \sin\theta)^2}$$

If θ approaches 0, then

$$G = \lim_{\theta \to 0} \frac{\varepsilon A u_o}{d^2} \frac{\theta^2 \left(1 - 1 + \frac{\theta^2}{2} - \ldots\right)}{\left(1 - 1 + \frac{\theta^2}{2} - \ldots\right)^2 + \left(\theta - \theta + \frac{\theta^3}{6} - \ldots\right)^2}$$

$$= \frac{2\varepsilon A u_o}{d^2}$$

$$C = \lim_{\theta \to 0} \frac{B}{\omega} = \lim_{\theta \to 0} \frac{d}{u_o} \frac{B}{\theta}$$

$$= \frac{A}{d} \lim_{\theta \to 0} \frac{\theta(\theta - \sin \theta)}{(1 - \cos \theta)^2 + (\theta - \sin \theta)^2}$$

$$= \frac{2}{3} \frac{\varepsilon A}{d}$$

which coincides exactly with Shao and Wright's formulas if $E_o(x)$ is assumed to be independent of x.

REFERENCES

1. B. Ancker-Johnson, "Microwave Emission from Magnetic Field-Free Electron-Hole Plasmas," *Applied Physics Letters*, Vol. 10, May 1967, pp. 279-280.

2. B. Ancker-Johnson, R. W. Cohen, and M. Glicksman, "Properties of Injected Plasmas in Indium Antimonide," *Physical Review*, Vol. 124, December 1961, pp. 1745-1753.

3. B. Ancker-Johnson and W. P. Robins, "Dynamic and Steady-State Injection of Electron-Hole Plasma in p-type InSb," *Journal of Applied Physics*, Vol. 12, February 1971, pp. 762-773.

4. T. Arizumi, T. Aoki, and K. Hayakawa, "Microwave Emission from Acoustoelectrically Oscillating n-InSb," *Journal of the Physical Society of Japan*, Vol. 23, December 1967, pp. 1251-1256.

5. W. H. Bennett, "Magnetically Self-Focusing Streams," *Physical Review*, Vol. 45, June 1934, p. 890.

6. J. Bok and P. Nozieres, "Instabilities of Transverse Waves in a Drifted Plasma," *Journal of Phys. Chem.Solids*, Vol. 24, 1963, pp. 709-714.

7. S. J. Buchsbaum, A. G. Chynoweth, and W. L. Feldmann, "Microwave Emission from InSb," *Applied Physics Letters*, Vol. 6, February 1965, pp. 67-69.

8. P. W. Chen, C. H. Durney, and R. W. Grow, "Theoretical and Experimental Investigation of Solid-State Mechanisms for Generating Coherent Radiation in the Ultraviolet and X-ray Regions," Final Report under Grant NGR 45-003-027, Microwave Device and Physical Electronics Laboratory, University of Utah, Salt Lake City, Utah, July 1969.

9. D. A. Christensen, C. H. Durney, and R. W. Grow, "An Exact Small-Signal Analysis of the Interaction of Two Electron Streams in a Finite Longitudinal Magnetic Field," *IEEE Transactions on ED*, Vol. ED-16, July 1969, pp. 615-624.

10. A. G. Chynoweth and A. A. Murray, "Pinch Effect in Indium Antimonide," *Physical Review*, Vol. 123, July 1961, pp. 515-516.

11. J. C. Eidson and G. S. Kino, "A New Type of Oscillation in InSb," *Applied Physics Letters*, April 1966, pp. 183-185.

12. R. W. H. Engelmann and C. F. Quate, "Linear or Small Signal Theory for Gunn Effect," *IEEE Transactions on ED*, Vol. ED-13, January 1966, pp. 44-52.

13. O. P. Gandhi and R. W. Grow, "Microwave Emission from InSb With and Without Magnetic Fields," *IEEE Transactions on ED*, Vol. ED-18, October 1971, pp. 853-865.

14. M. Gilden and M. E. Hines, "Electronic Tuning Effects in the Read Microwave Avalanche Diode," *IEEE Transactions on ED*, Vol. ED-13, January 1966, pp. 169-175.

15. M. Glicksman and W. A. Hicinbotham, "Hot Electrons in Indium Antimonide," *Physical Review*, Vol. 129, February 1963, pp. 1572-1577.

16. M. Glicksman and W. A. Hicinbotham, "Hall Drift Velocity at High Electric Fields in InSb," *Proceedings of the Symposium on Plasma Effects in Solids*, Paris, France, 1964; published by Dunod, Paris, 1965, pp. 137-146.

17. M. Glicksman and M. C. Steele, "Plasma Pinch Effects in Indium Antimonide," *Physical Review Letters*, Vol. 2, June 1959, pp. 461-462.

18. L. C. Goodrich and C. H. Durney, "A Small Signal Field Analysis of Double Stream Interactions in Finite Semiconductors," Ph.D. dissertation, University of Utah, 1969.

19. F. R. Holmstrom, "Stability and RF Behavior of Plasma Diode," Technical Report No. 0833-2, Stanford Electronics Laboratory, Stanford University, Stanford, California, August 1964.

20. M. Kawamura, S. Morishita, "A New Negative Resistance of Semiconductor Bulk," *Proceedings of the IEEE*, Vol. 56, July 1968, pp. 1213-1215.

21. C. Kittel, *Introduction to Solid State Physics*, Third Edition, John Wiley and Sons, Inc., New York, 1968, pp. 300-331.

22. R. Larrabee, "Microwave Impedance of Semiconductor Posts in Waveguides, Part I," *Journal of Applied Physics*, Vol. 36, May 1965, p. 1597.

23. R. D. Larrabee and W. A. Hicinbotham, "Observation of Microwave Emission from Indium Antimonide," *Proceedings of the Symposium on Plasma Effects in Solids*, Paris, France, 1964; published by Dunod, Paris, 1965, pp. 181-187.

24. F. B. Llewellyn and L. C. Peterson, "Vacuum-Tube Network," *Proceedings of the IRE*, Vol. 32, March 1944, pp. 144-166.

25. T. Misawa, "Negative Resistance in p-n Junctions Under Avalanche Breakdown Conditions, Part I," *IEEE Transactions on ED*, Vol. ED-13, January 1966, pp. 137-143.

26. D. Pines and J. R. Schrieffer, "Collective Behavior in Solid-State Plasma," *Physical Review*, Vol. 124, December 1961, pp. 1387-1400.

27. S. Ramo, J. R. Whinnery, and T. V. Duzer, *Fields and Waves in Communication Electronics*, John Wiley and Sons, New York, 1965, p. 296.

28. B. B. Robinson and G. A. Swartz, "Two-Stream Instability in Semiconductor Plasmas," *Journal of Applied Physics*, Vol. 38, May 1967, pp. 2461-2465.

29. J. Shao and G. T. Wright, "Characteristics of the Space-Charge-Limited Dielectric Diode at Very High Frequency," *Solid State Electronics*, Vol. 3, November 1961, pp. 291-303.

30. L. Spitzer, Jr., *Physics of Fully Ionized Gases*, Interscience Publishers, New York, 1956, p. 41.

31. K. Suzuki, "The Generation of Microwave Radiation from InSb," *Japanese Journal of Applied Physics*, Vol. 4, January 1965, pp. 42-52.

32. T. Suzuki, "Microwave Emission and Low Frequency Instabilities in InSb," *Japanese Journal of Applied Physics*, Vol. 4, September 1965, p. 700.

33. G. A. Swartz, "Coherent Emission from Indium Antimonide with Closely Spaced Coplanar Contacts," *Journal of Applied Physics*, Vol. 40, August 1969, pp. 5343-5349.

34. G. A. Swartz and B. B. Robinson, "Coherent Microwave Instabilities in a Thin-Layer Solid-State Plasma," *Journal of Applied Physics*, Vol. 40, October 1969, pp. 4598-4611.

35. A. H. Thompson and G. S. Kino, "Noise Emission from InSb," *IBM Journal of Research and Development*, Vol. 13, September 1969, pp. 616-620.

36. C. W. Turner, "The Role of Acoustic Wave Amplification in the Emission of Microwave Noise from InSb," *IBM Journal of Research and Development*, Vol. 13, September 1969, pp. 611-615.

37. B. Vural and M. C. Steele, "Possible Two-Stream Instabilities of Drifted Electron-Hole Plasmas in Longitudinal Magnetic Fields," *Physical Review*, Vol. 139, July 1965, pp. A300-A304.

38. R. K. Willardson and H. L. Goering, *Compound Semiconductors*, Vol. I, Reinhold Publishing Corporation, New York, 1962, p. 227.

39. A. van der Ziel, S. T. Hsu, "High-Frequency Admittance of Space-Charge-Limited Solid-State Diodes," *Proceedings of the IEEE*, Vol. 54, September 1966, p. 1194.

DISTRIBUTION LIST

ACTIVITIES AT WRIGHT-PATTERSON AIR FORCE BASE	No. of Copies
AVN	1
AVTL	1
AVWW	1
AVTA	3

OTHER DEPARTMENT OF DEFENSE ACTIVITIES

Air Force

Air University Library
Maxwell Air Force Base
Alabama 36112 — 1

AFCRL (CRR-CSA)
Att: Mr. Charles Ellis, Jr.
L. G. Hanscom Field
Bedford, Massachusetts 01731 — 1

BSD (BSYDF)
Attn: Captain Hyslop
Norton Air Force Base
California 92409 — 1

RADC (EMATE)
Attn: Mr. H. Chiosa
Griffiss Air Force Base
New York 13440 — 1

Navy

Chief, Bureau of Ships
Attn: Mr. C. C. Walker
Department of the Navy
Room 3337
Washington, D. C. 20360 — 1

Director, Naval Research Laboratory
Attn: Mr. H. D. Arnett, Code 5244
Washington, D. C. 20360 — 1

	No. of Copies
Commanding Officer and Director USNASL, Mr. P. J. Giardano U. S. Naval Base Brooklyn, New York 10001	1
Scientific Officer, Code 427 Office of Naval Research Washington, D. C. 20360	1
Director U. S. Naval Electronics Laboratory San Diego, California 92142	1
Chief, Bureau of Ordnance Department of the Navy, Code RE-9 Washington, D. C.	1
Chief, Bureau of Aeronautics Department of the Navy, Code EL-412.1 Washington, D. C. 20025	1
Mr. Jay Froman Office of Naval Research San Francisco Area Office 50 Fell Street San Francisco, California	1

Army

Commanding General U. S. Army Electronics Command Attn: AMSEL-KL-S (Dr. H. Jacobs) Fort Monmouth, New Jersey 07703	1
Commanding General U. S. Army Electronics Command Attn: AMSEL-TL-BM (Mr. Harold J. Hersh) Fort Monmouth, New Jersey 07703	1
Commander, U. S. Army Materiel Command Harry Diamond Laboratories Attn: H. W. A. Gerlach Connecticut and Van Ness Streets, N. W. Washington, D. C. 20025	1
Commanding Officer Attn: Technical Reference Division Ft. Huachuca, Arizona 85613	1

	No. of Copies
Commander, U. S. Army Missile Command Attn: Mr. W. D. McKnight, ORDXR-RBE Redstone Arsenal, Alabama 35809	1
Commanding Officer U. S. Army Mobile Equipment Research and Development Center Attn: Technical Documents Center Building 315, Vault Fort Belvoir, Virginia 22060	1

OTHER U. S. GOVERNMENT AGENCIES

DDC (TISIA) Cameron Station Alexandria, Virginia 22314	12
National Science Foundation Washington District of Columbia 20550	1
Dr. Royal E. Rostenbach Acting Program Director Engineering Energetics, Engineering Division National Science Foundation Washington, D. C. 20550	1
Advisory Group on Electron Devices Attn: Mr. H. N. Serig 201 Varick Street, 9th Floor New York, New York 10014	4
National Bureau of Standards Attn: Librarian Department of Commerce Washington, D. C. 20025	1
U. S. Atomic Energy Commission Division of Research Attn: Dr. Roy W. Gould Washington, D. C. 20545	1
Library U. S. Department of Commerce Environmental Science Services Administration Boulder Laboratories Boulder, Colorado 80302	1

NONGOVERNMENT INDIVIDUALS AND ORGANIZATIONS	No. of Copies
Amperex Electronic Corporation 230 Duffy Avenue Hicksville, New York 11804	1
Dr. Robert L. Arnold 335 Bowen Avenue Aptos, California 95003	1
Dr. J. Mark Baird 2974 Molly Court Newberry Park, California 91302	1
Dr. Paul Berrett 269 ELB Electrical Engineering Department Brigham Young University Provo, Utah 84601	1
Dr. Vladislav Bevc, L382 Lawrence Radiation Laboratory P. O. Box 808 Livermore, California 94551	1
Dr. Lawrence Bowman Hughes Research Laboratories Microwave Semiconductor Research Department 3100 West Lomita Boulevard Torrance, California 90509	1
Dr. C. Kent Bullock Naval Weapons Center Code 4081 China Lake, California 93555	1
Dr. W. Charles Carr 11 Karen Drive New Fairfield, Connecticut 06810	1
Dr. Edwin G. Chaffee Litton Industries Electron Tube Division Crossed-Field Devices, Dept. 180 960 Industrial Way San Carlos, California 94070	1
Dr. Su-Min Chou 9008 Willow Valley Drive Potomac, Maryland 20854	1

	No. of Copies
Dr. John C. Clark 8389 Vereda del Padre Goleta, California 93017	1
Cornell University Electrical Engineering Department Attn: Professor Lester F. Eastman 316 Phillips Hall Ithaca, New York 14850	1
Cornell University School of Electrical Engineering Attn: Dr. Joseph M. Ballantyne Ithaca, New York 14850	1
Dr. Maylin Dittmore 241 Helen Way Livermore, California 94550	1
EIMAC, A Division of Varian Associates Attn: Technical Library 301 Industrial Way San Carlos, California 94070	1
EIMAC, A Division of Varian Associates Attn: Dr. George Caryotakis 301 Industrial Way San Carlos, California 94070	1
Eitel-McCullough, Inc. Attn: Larry Hansen, Manager 1678 Pioneer Road Salt Lake City, Utah	1
General Electric Company Research Laboratories Attn: Dr. T. G. Mihran P. O. Box 1088 Schenectady, New York 12305	1
General Telephone and Electronics Physical Electronics Laboratory Attn: Dr. Louis R. Bloom Miss M. Franc, Documents Custodian 208-20 Willets Point Boulevard Bayside, New York 11361	1 1

	No. of Copies
Dr. Lewis C. Goodrich 181 Harbor Drive, No. 4 Claymont, Delaware 19703	1
Grumman Aerospace Corporation Attn: Mr. Paul H. Savet Research Department, Plant 35 Bethpage, New York 11714	1
Dr. David R. Gunderson Bell Telephone Laboratories 4B301 Holmdel, New Jersey 07733	1
Hughes Aircraft Company Attn: Dr. Donald C. Forster 3011 Malibu Canyon Road Malibu, California 90265	1
Dr. Vern R. Johnson Electrical Engineering Department University of Arizona Tucson, Arizona	1
Dr. Tai-wu Kao Electrical Engineering Department Loyola University of Los Angeles 7101 West 80th Street Los Angeles, California 90045	1
Dr. John H. Keller 7 Duchess Court Newburgh, New York 12550	1
Dr. Kenneth G. Leib, Research Engineer Grumman Aerospace Corporation Plant 35 Bethpage, New York 11714	1
Library of Congress Attn: Mr. Nathan R. Einhorn, Chief Exchange and Gift Division Washington, D. C. 20540	1
Dr. C. H. Ma P. O. Box 3894 University, Mississippi 38677	1

	No. of Copies
Alpheus Smith Laboratory Physics Library Ohio State University 174 West 18th Avenue Columbus, Ohio 94210	1
Raytheon Company Attn: Dr. W. C. Brown Microwave and Power Tube Division Building 1 Foundry Avenue Waltham, Massachusetts 02154	1
RCA Laboratories Attn: Dr. Stanley Bloom Member, Technical Staff Princeton, New Jersey 08540	1
S. F. D. Laboratories Attn: Dr. Farney 800 Rahway Avenue Union, New Jersey 07083	1
Dr. Richard L. Schriever 1365 Fairview Court Livermore, California 94550	1
Dr. Aris Silzars 901 Stony Hill Road Redwood City, California 94061	1
Sperry Rand Corporation Electron Tube Division Attn: Dr. Sutherland Gainesville, Florida 32601	1
Stanford University Plasma Physics Library Institute for Plasma Research Attn: Librarian Via Crespi Stanford, California 94305	1
Dr. Kenneth I. Talbot 582 Dublin Way Sunnyvale, California 94807	1

	No. of Copies
Tulane University Electrical Engineering Department Attn: James A. Cronvich New Orleans, Louisiana 70118	1
University of California Electronics Research Laboratory Attn: Professor J. R. Whinnery Berkeley, California 94704	1
University of California Lawrence Radiation Laboratory Attn: Verle Gilson Building 170C, Room 2597 Box 808 Livermore, California 94551	1
University of California Attn: Professor Glen Wade Santa Barbara, California 93107	1
University of Colorado Department of Electrical Engineering Attn: Professor Russell E. Hayes Boulder, Colorado 80304	1
University of Illinois Department of Electrical Engineering Attn: Professor Paul D. Coleman Urbana, Illinois 61801	1
University of Michigan Electrical Engineering Department Attn: Dr. Joseph Rowe, Chairman Ann Arbor, Michigan 48107	1
University of Utah Gifts and Exchanges Division 242 Marriott Library Salt Lake City, Utah 84112	1
University of Utah Solid Rocket Structural Integrity Information Center 4003 W Merrill Engineering Building Salt Lake City, Utah 84112	1
Utah Engineering Experiment Station University of Utah 207 Mines Building Salt Lake City, Utah 84112	1

	No. of Copies
Varian Associates, Inc. Attn: Technical Library 611 Hansen Way Palo Alto, California 94303	1
Watkins-Johnson Company Attn: Dr. O. T. Purl, Vice President 3333 Hillview Avenue Stanford Industrial Park Palo Alto, California 94304	1
Dr. David C. Watson Electromagnetic Systems Laboratory 495 Java Drive Sunnyvale, California 94086	1
Westinghouse Electric Corporation Defense and Space Center Aerospace Division Attn: H. W. Cooper, MS 129 Friendship International Airport Baltimore, Maryland 21203	1
Zenith Radio Corporation Attn: Dr. Robert Adler, Director of Research 6001 West Dickens Avenue Chicago, Illinois 60639	1
Dr. Larry L. Campbell 11627 Vantage Hill Road Reston, Virginia 22070	1
Dr. Krishna B. Verma Hewlett-Packard, Microwaves 1501 Page Mill Road Palo Alto, California 94304	1
Georgia Institute of Technology Price Gilbert Memorial Library Attn: Mrs. Helen Citron, Librarian Atlanta, Georgia 30332	1